POLITECNICO
MILANO 1863

SCHOOL OF INDUSTRIAL AND INFORMATION ENGINEERING
Master Degree in Materials Engineering and Nanotechnology

Development of a SERS technique for Therapeutic Drug Monitoring: Case Study on Perampanel

Supervisor: Prof. Matteo Tommasini
Co-Supervisor: Prof. Andrea Lucotti
Co-Supervisor: Prof. Paolo Ossi

Candidate: Nicolò Simone Villa
Matr.: 853098

Academic Year: 2017 - 2018

"And once the storm is over,
you won't remember how you made it through,
how you managed to survive.
You won't even be sure,
wether the storm is really over.

But one thing is certain.

When you come out of the storm,
you won't be the same person who walked in.

That's what the storm's all about."

- Haruki Murakami

Acknowledgements

University is not only a place of formation and study. Here everything converges to the center, moving fast, driven by a stormy wind. Life, happiness, sadness, past, present and future, friendship, love. Experiences lived in this time leave their trace forever. And nothing would have been the same without the people that walked inside this hurricane alongside me. My family and friends that stepped in with me at the start, the friends I met inside it. Nothing I did would have been possible without them. They accompanied me in every laugh, every tear, every trouble and joy of this journey. I learned something from every single one of them, and they are all part of who I am.

Mom, the strongest woman ever existing on earth, the person who taught me everything, the absolute essence of everything I am.

Dad, who taught me how to find a way to smile at everything comes to you.

My brother, who taught me to keep going whatever happens.

My grandma, the everlasting root of my life.

Andrea, Federico and Roberto, who taught me friendship knows no distance.

Simone, Matteo, Kevin, Stefano and Valeria, who taught me to enjoy life in all its ways and forms.

Gabriele, Simone, Silvia, Stefano, Marta, Federica and Linda, who taught me everyone is free to be who they are.

In this hurricane I was lucky enough to find love, and catch it while drifting with the wind: Feifei, who saved my soul, gave me future, and inspires me to get better every day. I love you.

My soul is bound to them forever. Wherever I am, whatever I do, they will be with me and I will be with them.

This thesis would never been possible without my mentors Andrea and Matteo, my colleague and "partner in crime" Federica. I need to thank Gabriele, Simone, Stefano and Moira, whose advice and help were fundamental.

Matteo, thank you for being the best mentor, you are an inspiring role model of the researcher and teacher I would be honoured to be in the future. I wish all professors and researchers out there would be even slightly like you.

Thank you all, from the deepest of my heart.

Abstract

In my master thesis, I used Au, Ag, and AuAg alloy substrates produced from colloidal suspensions and PLAL (Pulsed laser ablation in liquid) as SERS sensors for Therapeutic Drug Monitoring (TDM) of the Anti-Epileptic Drug (AED) Perampanel (PER), the Active Pharmaceutical Ingredient (API) of the drug available as Fycompa, nowadays important in the treatment of epilepsy. The relevance of this study is related with the possibility to offer complementary spectroscopic techniques for TDM of Perampanel, which nowadays employs more expensive and time consuming analytical methods.

In the first part of my thesis, Perampanel was characterized. The UV-Vis, Raman and SERS spectra of the drug were collected, and a qualitative vibrational analysis was performed.

In the second part of my thesis, I systematically analyzed the different experimental conditions that produce differences in the SERS spectra and I optimized the procedure of sensing Perampanel using SERS. Preparation of the solution, acid species employed, pH, and Raman setup conditions were carefully addressed.

Moreover, two types of Au and Ag metallic nanostructures were tested: The more traditional nanoparticles (NPs) produced by chemical methods and the more recently introduced nanostructures produced by Enza Fazio (Università di Messina), through Pulsed Laser Ablation in Liquid (PLAL).

Therefore, it was possible to setup a procedure for optimal SERS analysis of Perampanel, which could be extended to many other drugs with similar chemical properties (pKb) and other families of drugs as well. The results here presented are very promising and will be further investigated to extend their applicability. This is important because in a clinical environment is crucial to have a standardized procedure for the preparation of the samples and have quantitative and reliable results.

Finally, a new setup for SERS analysis which makes use of a spinning cell was tested, to decrease analyte photodamaging and provide a more repeatable measurements.

The results here presented pave the way for enstablishing a standard procedure for SERS in quality control of drug formulations and Therapeutic Drug Monitoring.

Contents

Acknowledgements i

Abstract ii

1 Introduction 1

2 Methods 3
- 2.1 Raman spectroscopy . . . 3
  - 2.1.1 Quantum description of RS . . . 4
  - 2.1.2 Resonance Raman spectroscopy (RRS) . . . 6
- 2.2 SERS - Surface Enhanced Raman Spectroscopy . . . 6
  - 2.2.1 Optical properties of materials . . . 6
  - 2.2.2 Electromagnetic enhancement . . . 9
  - 2.2.3 Chemical enhancement . . . 10
- 2.3 Instrumentation . . . 12
  - 2.3.1 Dispersive Raman LabRAM HR800 . . . 12
  - 2.3.2 Spectrophotometer UV-VIS JASCO V-570 . . . 12

3 SERS materials 15
- 3.1 Au/Ag substrates produced by chemical methods . . . 15
  - 3.1.1 Synthesis and deposition . . . 15
  - 3.1.2 UV-vis characterization of the colloidal substrates . . . 20
- 3.2 Au/Ag SERS substrates produced by PLAL . . . 21

4 Perampanel (PER) 27
- 4.1 Raman characterization . . . 28
- 4.2 UV-vis characterization of Perampanel . . . 33
  - 4.2.1 UV-vis of Perampanel in neutral MeOH solutions . . . 33
  - 4.2.2 UV-vis of Perampanel in HCl aqueuous solutions . . . 35
- 4.3 Stability . . . 38

5 SERS on colloidal nanoparticles substrates 40
5.1 Ag NPs substrates 40
5.1.1 Au NPs substrates 44
5.2 The role of the acid 47
5.2.1 HCl and sulphuric acid mix tests 48

6 SERS detection of PER on substrates made by PLAL 52
6.1 SERS of PER on ns-PLAL Ag substrates 53
6.2 SERS detection on ps-PLAL Ag substrates 55
6.3 SERS detection on ns- and ps-PLAL Au substrates 61
6.4 SERS detection on Ag/Au alloys substrates 64
6.5 SERS detection on irr-Ag/Au alloys substrates 67
6.6 Concluding remarks 70

7 Spinning Cell (SC) for improving SERS 72
7.1 Multiple-drops spinning cell (MDSC) 73
7.2 Single-centered drop spinning cell (SCDSC) 78
7.3 Statistical analysis 82
7.4 Concluding remarks 85

Conclusions 87

Bibliography 88

List of Figures

2.1 From left to right: Energy levels diagram for Rayleigh, Stokes and anti-Stokes scattering. 4
2.2 From left to right: Absorption, fluorescence, Rayleigh scattering, Stokes and anti-Stokes scattering, related to the vibrational and electronic energy levels of the molecule. In the case of RSS the close vicinity of the virtual energy levels the real ones leads to a sharp increase in the scattered intensity. 5
2.3 reference scheme for description of CEME 9
2.4 Schematic view of the total CEME, where the two contribution, Laser (L) and Stokes (S), act differently 10
2.5 The dispersive Raman LabRAM HR800 produced by Horiba Jobin Yvon 12
2.6 JASCO V-570 UV - vis spectrophotometer. 13
2.7 Optical scheme of the JASCO V-570 spectrophotometer. 13

3.1 Chemical structure of Trisodium Citrate (TSC). 16
3.2 Stabilization of the nanoparticles acted by trisodium citrate. 16
3.3 Silver colloid produced by following the Lee-Meisel method. 17
3.4 Gold colloid produced by following the Lee-Meisel method. 18
3.5 Chemically produced Ag nanoparticles deposited on a glass support. 19
3.6 Chemically produced Au nanoparticles deposited on a glass support. The coffee ring effect is shown on the substrates on the right. 19
3.7 UV-Vis absorption spectrum of chemically produced Ag colloids diluted in deionized water. In green the region of the surface plasmon resonance peak, while in cyan the region of the laser employed for the measurements are highlighted. 20
3.8 UV-Vis absorption spectrum of chemically produced Au colloids diluted in deionized water. In purple the region of the surface plasmon resonance peak is highlighted. 21
3.9 Optical micrograph image of the surface of a ns-Ag SERS substrate. 23
3.10 Optical micrograph image of the surface of a ns-Au SERS substrate. 23

3.11 Optical micrograph image of the surface of a ps-Ag SERS substrate. 23
3.12 Optical micrograph image of the surface of a ps-Au SERS substrate. 24
3.13 Optical micrograph image of the surface of a ps-AgAu 50/50 alloy SERS substrate. 24
3.14 Optical micrograph image of the surface of a ps-AgAu 75/25 alloy SERS substrate. 25
3.15 Optical micrograph image of the surface of an irradiated ps-AgAu 50/50 SERS alloy substrate. 25
3.16 Optical micrograph image of the surface of an irradiated ps-AgAu 75/25 SERS alloy substrate. 26

4.1 Chemical structure of perampanel (PER) 27
4.2 Raman spectra of solid PER. a) spectrum collected with 785 nm laser excitation, 10 mW power, 10 s exposition time (3 averages). and b) spectrum collected with 514 nm excitation, 10 mW power, 10 s exposition time (3 averages). The main vibrational modes are labelled. 28
4.3 Raman spectra of solid PER collected with 458 nm laser excitation, 0.1 mW power, 10 s exposition time (2 averages). The high fluorescence of the spectrum is clearly noticeable. 29
4.4 Zoom from 200 cm^{-1} to 950 cm^{-1} of the Raman spectra of solid PER collected with 785 nm laser excitation, 10 mW power, 10 s exposition time (3 averages). The main vibrational modes are labelled. 30
4.5 Zoom from 950 cm^{-1} to 1800 cm^{-1} of the Raman spectra of solid PER collected with 785 nm laser excitation, 10 mW power, 10 s exposition time (3 averages). The main vibrational modes are labelled. 31
4.6 Polymorph VII of PER, as stated in MAPI PHARMA LTD.'s patent (US 20140371273A1)[31] 31
4.7 Raman spectrum of PER obtained using 785 nm excitation, 10 mW laser power, 10 s exposure time (3 averages). Assigned with numbers are the main peaks of PER. Their assignment to the vibrational modes is provided in Tab.4.1. 32
4.8 *a*) UV-vis collected spectra of PER in methanol solutions at concentrations ranging from $5x10^{-5}$ to $5x10^{-6}$. *b*) Linear fit performed on the peak-height vs. concentration plot. $R^2 \simeq 0,97$. 34
4.9 UV-vis spectra of PER in acidic solutions at pH, which was set to vary between 0 and 5. 36
4.10 Most probable protonation sites of Perampanel. DFT B3LYP/6-31G(d,p) model was used (gaussian). 36

4.11 SERS spectra of a) PER dissolved in a solution of HCl at pH 6 and b) PER dissolved in a solution of HCl at pH 2. The spectra are obtained using 785 nm laser excitation, 0,1 mW laser power, 20 s exposure time (3 averages). 37

4.12 UV-vis absorption spectra of PER in aqueous solutions of hydrochloric and sulphuric acid at pH=2, taken at 0 days (black), 2 days (blue) and 8 days (red) after storage. 39

5.1 *a*) Raman spectrum of solid PER using 785nm excitation. *b*) SERS spectra of PER at pH 6 (red), 5(green), and 4(blue). *c*) SERS spectra of PER at ph 3(magenta), 2(green), 1(red) and 0(blue). All the SERS spectra are collected at the solid-liquid interface. 42

5.2 Comparison of the AgCl peaks heights in *a*) SERS spectrum obtained at pH 1 and *b*) SERS spectrum obtained at pH 2. Both SERS spectra are collected at the solid-liquid interface. 43

5.3 *a*) Raman spectrum of solid PER using 785nm excitation (1 mW power). *b* SERS spectrum using 785 nm excitation (0,1 mW power) of PER $10^{-5}M$ at pH 2. The spectrum was collected at the solid-liquid interface. 43

5.4 *a*) Raman spectrum of solid PER using 785nm excitation. *b*) SERS spectrum of PER at $10^{-4}M$ and *c*) SERS spectrum of PER at $10^{-5}M$, both collected using 785 nm excitation, 1mW power, 60 s exposure time (2 averages) 45

5.5 *a*) SEM image of the Ag nanoparticles substrate highlighting its rods structure and *b*) SEM image of the Au nanoparticles substrate showing its lack of a rods structure. The SEM images were collected as part of a parallel thesis work by the colleague Federica Iacoe. . . 46

5.6 SERS spectra of PER deposited from a pH 2 solution, which acidity was achieved through the exclusive use of HCl. *a*) Spectrum obtained at the time of deposition, *b*) spectrum obtained 15 minutes after deposition. The marked decrease in relative intensity of the PER signal is clearly shown. 47

5.7 SERS spectra of PER deposited from a pH 2 solution, where the acidic condition was achieved with the exclusive use of HCl. *a*) Spectrum obtained at the time of deposition, *b*) spectrum obtained 15 minutes after deposition. The sharp increase in intensity of the AgCl peak is clearly shown, going from about 1800 to almost 7000. 48

5.8 SERS spectra of PER $10^{-4}M$ using the hydrochloric and sulphuric acids mix. In red the spectrum obtained using a 1:9 hydrochloric/sulphuric ratio, in blue the spectrum collected using a 1:4 ratio. The spectra were collected using 785 nm excitation, 0,1 mW power, 10 s exposure time (3 averages). 50
5.9 SERS spectra of PER $10^{-5}M$ using the hydrochloric and sulphuric acids mix. In green the spectrum obtained using a 1:19 hydrochloric/sulphuric ratio, in blue the spectrum collected using a 1:4 ratio. The spectra were collected using 785 nm excitation, 0,1 mW power, 10 s exposure time (3 averages). 50
5.10 SERS spectrum of PER $10^{-5}M$ using the hydrochloric and sulphuric acids mix. In red the spectrum obtained using a 1:9 hydrochloric/sulphuric ratio. The spectrum was collected using 785 nm excitation, 0,1 mW power, 10 s exposure time (3 averages). 51
5.11 SERS spectrum of PER $10^{-4}M$ using the hydrochloric and sulphuric acids mix. In green the spectrum obtained using a 1:19 hydrochloric/sulphuric ratio. the spectrum shows similar features to the spectrum of sodium citrate[34], showing the similar features. The spectrum was collected using 785 nm excitation, 0,1 mW power, 10 s exposure time (3 averages). 51

6.1 SERS spectra of PER on nanosecond-PLAL Ag substrate. Spectra were collected using a 458 nm excitation (blue) focused with a 50x objective. 1mW laser power was employed with 30 seconds exposition time (2 averages). The spectra were collected at both the solid-liquid interface and at dry droplet. 54
6.2 a) SERS spectrum of PER on the solid-liquid interface of a nanosecond-PLAL Ag substrate collected using a 458 nm excitation (blue) focused with a 50x objective. 1mW laser power was employed with 30 seconds exposition time (2 averages). b) Raman spectrum of solid PER, collected using 785 nm excitation, 10 mW laser power, 10 s exposure time (3 averages). 55
6.3 SERS spectrum of PER on picosecond-PLAL Ag substrate. 458 nm excitation, 0,1 mW laser power, 100 seconds exposure time (5 averages). In green the two bands suggesting analyte photodamage are highlighted. 56
6.4 SERS spectrum of PER on picosecond-PLAL Ag substrate. 458 nm excitation, 1 mW laser power, 20 seconds exposure time (2 averages). In cian the two bands suggesting analyte photodamage are highlighted. 57

6.5 SERS spectrum of PER on picosecond-PLAL Ag substrate. 458 nm excitation, 10 mW laser power, 20 seconds exposure time (2 averages). The spectra were collected at increasing times for 40 minutes until the droplet was dry. 58

6.6 b) SERS spectrum of PER on the solid-liquid interface of a nanosecond-PLAL Ag substrate collected using a 458 nm excitation (blue) focused with a 50x objective. 10 mW laser power was employed with 20 seconds exposition time (2 averages). a) Raman spectrum of solid PER, collected using 514 nm excitation, 10 mW laser power, 10 s exposure time (3 averages). 59

6.7 SERS spectrum of PER on picosecond-PLAL Ag substrate. 458 nm excitation, 10 mW power, 20 seconds exposure time (2 averages). In orange the two bands suggesting analyte photodamaging are highlighted. 60

6.8 SERS spectrum of PER on picosecond-PLAL Ag substrate. 458 nm excitation, 10 mW laser power, 20 seconds exposure time (2 averages). In purple the bands suggesting the start of the analyte photodamaging process are highlighted. 60

6.9 SERS spectrum of PER detected on ns-Au substrate. 785 nm excitation, 0,1 mW power, 20 s exposure time (2 averages). 62

6.10 SERS spectrum of PER detected on ns-Au substrate. 785 nm excitation, 10 mW power, 20 s exposure time (2 averages). 62

6.11 SERS spectra of PER detected on ps-Au substrate. 785 nm excitation, 20 s exposure time (2 averages). a) spectrum detected with 1 mW laser power and b) spectrum detected with 10 mW laser power. In cian the fluorescent band is highlighted. 63

6.12 SERS spectrum of PER detected on a 50:50 Ag-Au alloy substrate using 514 nm laser excitation, 0,1 mW laser power, 20 seconds exposure time (3 averages). 64

6.13 SERS spectrum of PER detected on a 50:50 Ag-Au alloy substrate using 514 nm laser excitation, 1 mW laser power, 20 seconds exposure time (3 averages). 65

6.14 SERS spectrum of PER detected on a 75:25 Ag-Au alloy substrate using 514 nm laser excitation, 0,1 mW laser power, 20 seconds exposure time (3 averages). 66

6.15 SERS spectrum of PER detected on a 75:25 Ag-Au alloy substrate using 514 nm laser excitation, 1 mW laser power, 20 seconds exposure time (3 averages). 66

6.16 SERS spectrum of PER detected on an irradiated 50:50 Ag-Au alloy substrate using 514 nm laser excitation, 0,1 mW laser power, 50 seconds exposure time (3 averages). 68
6.17 SERS spectrum of PER detected on an irradiated 50:50 Ag-Au alloy substrate using 514 nm laser excitation, 1 mW laser power, 10 seconds exposure time (2 averages). 68
6.18 SERS spectrum of PER detected on an irradiated 50:50 alloy substrate using 514 nm laser excitation, 10 mW laser power, 10 seconds exposure time (2 averages). In green the bands suggesting analyte damaging are highlighted. 69
6.19 SERS spectrum of PER detected on an irradiated 75:25 Ag-Au alloy substrate using 514 nm laser excitation, 0,1 mW laser power, 50 seconds exposure time (3 averages). 69
6.20 SERS spectrum of PER detected on an irradiated 75:25 Ag-Au alloy substrate using 514 nm laser excitation, 1 mW laser power, 10 seconds exposure time (2 averages). 70

7.1 Au colloids deposited on the surface of the rotating disk. 24 droplets were deposited along a circumference 3,4 cm distant from the rotation axis. 73
7.2 SERS spectra of PER aquired in static mode using laser powers of increasing value from 0,1 mW to 100 mW. 10 s exposure time (2 averages). 74
7.3 Comparison between a) SERS sectrum of PER on Au aquired in static mode with 100 mW laser power, 10 s exposure time (2 averages) and b) spectrum of the DLC coating of the rotating disk. . . . 75
7.4 Microscope image of the Au substrate after irradiation with a 785 nm excitation at 100 mW incident power. 76
7.5 SERS spectra obtained in rotation mode using the MDSC configuration. 785 nm laser excitation, 25 mW power, 20 seconds exposure time (2 averages). 77
7.6 Au colloid droplet deposited on the axis of rotation of the device. . 79
7.7 Static mode SERS spectra. 785 nm laser excitation, 1 mW power, 10 s exposure time (2 averages). 80
7.8 Rotation mode SERS spectra using the SCDSC configuration. 785 nm laser excitation, 1 mW power, 10 s exposure time (2 averages). . 81
7.9 Static mode standard deviation graphs for the a-b) unreferenced values and c-d) AgCl-peak-referenced values 83
7.10 MDSC rotation mode standard deviation graphs for the a-b) unreferenced values and c-d) AgCl-peak-referenced values 84

7.11 SCDSC rotation mode standard deviation graphs for the a-b) unreferenced values and c-d) AgCl-peak-referenced values 84

Chapter 1

Introduction

Epilepsy is the most diffused among the neurological pathologies known and strikes the 0,6 - 1% of the world's population[1]. Epilepsy is a common health problem, occuring individually or as consequence of other diseases, such as Lafora Disease (LD) and other intellectual disabilities (ID)[2, 3]. In most scenarios, the treatment of epilepsy is a complicated task. Over the past few years, various anti-epileptic drugs (AEDs) featuring new modes of action have been developed and introduced. Perampanel is a newly developed AED. It is a non-competitive α-amino-3-hydroxy-5-methyl-4-isoxazole-propionic acid (AMPA) receptor antagonist. PER was approved in 2012 and since then its efficacy and safety has been analyzed. However, PER is a drug for which publications, studies and trials are still limited. In three randomized controlled trials[4–6], PER was reported to be fairly well tolerated with some mild side effects including somnolence, fatigue, dizziness, nausea and falls. The reported neuropsychiatric effects include aggression, depression and irritability[7]. Following studies reported PER efficacy and safety for treatment of patients with refractory epilepsy, although they are characterized by a *narrow therapeutic index* (TDI), i.e. a very limited range of dosage able to treat the patient without experiencing collateral effects. Patients who received a dosage exceeding the upper limit of this range will experience collateral effects, such as those already mentioned, while for those patients who received a dosage inferior than the lower limit of said range, epileptic crisis will not be controlled. More over, this range varies from patient to patient[8]. To avoid these issues, the possibility of providing a tailored treatment which requires a careful tuning of the drug dosage for every specific patient is of crucial importance.

For this purpose, a technique called *therapeutic drug monitoring* (TDM) is commonly employed. It consists in the constant determination of the drug concentration in biological fluids of the patient, such as blood plasma[9]. Major studies confirmed the correlation between the control of seizures and the drug concentration in the plasma[10, 11]. Therefore, to guarantee an effective treatment, it is

necessary that the amount of drug circulating in the patients body keeps a stable level inside its efficacy range, defined by the means of the TDM, patient by patient.

Routinely used techniques for TDM are High-Performance liquid chromatography (HPLC) and mass spectrometry (MS).[8, 12, 13] Although these techniques can guarantee a very high sensibility and reliability, they also come with high economic impact and excessively time-consuming laboratory procedures.[14] This keeps TDM away from being available for the treatment of every patient. Therefore, research literature is focusing on the development of complementary techniques able to speed up the process. Surface Enhanced Raman Spectroscopy (SERS), is certainly amongst the most promising ones.[14–16] SERS allows for the detection of very low-concentrated molecules adsorbed on metallic surfaces. By exploiting the properties of nanostructured metallic surfaces, it is possible to obtain a great electromagnetic enhancement when the nanostructure is irradiated with a laser. If the analyte molecule is present on the surface, its Raman signatures will be raised in intensity through the plasmonic enhancement process, allowing their detection.[17]

The aim of my thesis is to understand the phenomena underlying SERS activity of PER to develop a basic procedure for its systematic detection. The metallic nanostructures used are composed by gold and silver nanoparticles, which are amongst the most efficient materials for SERS detection.[18] To investigate SERS thoroughly, I employed chemically produced (i.e. by reduction of solutions of Ag/Au cations) Au and Ag nanoparticles. Furthermore, through the collaboration with prof. Enza Fazio (Università di Messina) I have been able to test the sers action of nanostructured films formed by Ag/Au colloids prepared by Pulsed Laser ablation in Liquid (PLAL) and sprayed on Si supports. PLAL features a low production yield.[19] Therefore, PLAL fabricated substrates can only be produced in small numbers. PLAL currently appears to be the most versatile technique for Au/Ag NPs because of its ability to control the growth process through manipulating the process parameters such as irradiation time, energy density, duration, wavelength and so on.[20]

This research has been formulated in conjunction with a parallel thesis, carried on by the colleague Federica Iacoe. Moreover, some experiments are done with the collaboration of bachelor degree's group 31[1]. Shared and borrowed data will be mentioned.

[1]Bachelor students of group 31: Federico Olla, Maria Teresa Caporaso, Nicola Melis, Francesco Tuccillo, Martina Golini and Matteo Danieli.

Chapter 2

Methods

2.1 Raman spectroscopy

Raman spectroscopy (RS) is a technique based on the inelastic scattering of radiation (usually in the visible) by a sample which can be solid, liquid or a gas. It is named after Sir C.V. Raman who first observed the physical phenomenon: When light is scattered from a sample, an intense light at the same wavelength of the impinging radiation is observed, which is due to elastic (Rayleigh) scattering. In addition to that, a small fraction of light with a different frequency is also observed. The energy of the incoming photon gets modified by inelastic interaction with the quantum vibrational states of the sample. This allows to probe vibrational states, and the technique is considered complementary to infrared (IR) spectroscopy.[21]

Early RS had many technical limitations. For instance, phenomena like fluorescence strongly compete with inelastic scattering, which hinders the effectiveness of the technique. It was then noticed that the Raman signal can be increased by several orders of magnitude thanks to a phenomenon called resonance: The smaller the difference between the incoming photon energy and one electronic transition of the sample, the more intense is the response. This situation brought to Resonance Raman Spectroscopy (RRS). Nowadays RS has developed into a mature technique for chemical analysis in a broad range of areas.[22]

The applicability of RS further increased thanks to the discovery of lasers and to the fact that metallic surfaces can interact with the molecules to enhance the Raman scattering by several orders of magnitude.[22]

Nanostructured metallic materials have since then been used, showing high sensitivity and selectivity. These properties are unique for the molecules analyzed with this technique, and may be considered as the analyte fingerprint.

Considering the incoming radiation composed by isoenergetic photons (i.e. with same frequency), we can distinguish three types of scattering phenomena

involved in the Raman process:

1. **Rayleigh scattering,** characterized by elastic collisions with the sample, therefore the incoming photon energy is completely conserved;

2. **Stokes scattering,** characterized by inelastic collision exchanging energy in the form of vibrational quanta, resulting with an outgoing radiation that is red-shifted (i.e. has a lower energy than the incoming radiation);

3. **Anti-Stokes scattering,** characterized by the same energy exchange mechanism of Stokes scattering, but the outgoing radiation is blue-shifted (i.e. has a higher energy than the incoming radiation). This is because the sample, after interacting with the photon, goes into a lower vibrational state.

An important feature of Raman scattering is that it is dependent on the physical-chemical conditions of the targeted molecule. Hence, the Raman Spectra will carry information on the molecule composition and structure, together with its interactions with the environment.

2.1.1 Quantum description of RS

Taking for the sake of simplicity a diatomic molecule, its potential energy can be described by the Morse potential, which can be further simplified through the harmonic approximation: The potential energy is then described by a parabolic function dependent quadratically by the nuclei relative distance(i.e. normal coordinates). This quantum oscillator only features quantized energy levels, meaning

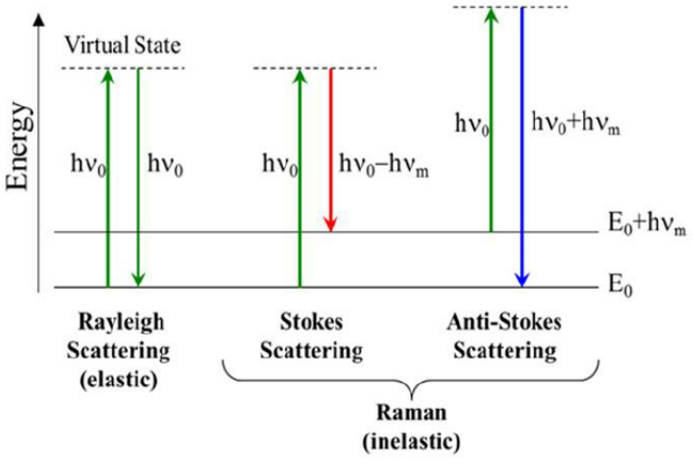

Figure 2.1: From left to right: Energy levels diagram for Rayleigh, Stokes and anti-Stokes scattering.

that the energy eigenvalues are discrete and labelled by a quantum number m (m=0,1,2...). Solving the Schroedinger's equation using the harmonic approximated potential, an expression for the eigenvalues is found:

$$E_m = \hbar\omega(m + \frac{1}{2}) \tag{2.1}$$

Considering the energy levels of the target molecule and the fact that a vibrational excitation happens when a photon interacts with the sample.

To describe RS, the concept of virtual states has to be introduced. The excitation brings the molecule to a state which is unstable and virtual states are reached when the excitation energy itself isn't enough to promote the state to a stable one. When this situation is achieved, the state relaxes to a lower state, scattering the photon without a real absorption. The relative positions of initial and final relaxation states determine if the scattering is elastic or inelasting and further if it is Stokes or anti-Stokes. This process can be easily understood from Fig. 2.1, depicting the different intensities of the phenomena.

The anti-Stokes scattering requires for the initial state to be at higher energy than the final state, thus is less probable due to the lower density of population of higher states. This phenomena are always in competition with photon absorption and subsequent fluorescence, as shown in Fig. 2.2.

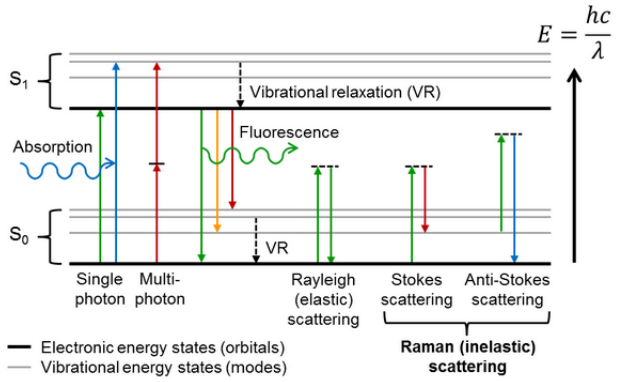

Figure 2.2: From left to right: Absorption, fluorescence, Rayleigh scattering, Stokes and anti-Stokes scattering, related to the vibrational and electronic energy levels of the molecule. In the case of RSS the close vicinity of the virtual energy levels the real ones leads to a sharp increase in the scattered intensity.

The intensities of the two inelastic scattering processes can be shown to be dependent by the derivative of the polarizability of the molecule and in the case of anti-Stokes scattering, also by the Boltzmann distribution of population factor.

$$I_{stokes} \approx I_0(\upsilon_0 - \upsilon)^4(\frac{\partial\alpha}{\partial q})^2 \tag{2.2}$$

$$I_{stokes} \approx I_0(\upsilon_0 - \upsilon)^4(\frac{\partial\alpha}{\partial q})^2 e^{\frac{-h\upsilon}{k_b T}} \tag{2.3}$$

2.1.2 Resonance Raman spectroscopy (RRS)

In this setup, the excitation energy is much closer to the real excitation energies of the targeted system. This leads to a sharp increase of the Raman excitation cross-section and the output signal rises up to five orders of magnitude.

There are two notable differences between fluorescence and RSS:

1. The lifetime of the excited states for the two processes is remarkably different: For fluorescence this is of the order of $10^{-8}s$ to $10^{5}s$, while for RSS this is of the order of $10^{-14}s$.

2. The intrinsic mechanisms are also completely different: The photon is absorbed and then emitted for the case of fluorescence. In RSS the photon is inelastically scattered, hence not absorbed.

2.2 SERS - Surface Enhanced Raman Spectroscopy

Surface enhanced Raman Scattering (SERS) was firstly observed in 1974 by Martin Fleischmann (together with Patrick J. Hendra and A. James McQuillan) at the department of Chemistry of the university of Southampton. His idea was to enhance the signal produced from an analyte using a metallic rougher surface for the interaction. The attempt succeded, but the real reasons why the signal was enhanced were still unknown.[23] Three years later two independent groups, namely David L. Jeanmarie with Richard P. Van Duyne and M. Grant Albreicht with Alan Creighton managed to reproduce the effect, giving two different interpretations: The first group proposed that the enhancement was due to an electric field intensification at the metallic surface, while the other noticed a modification of the molecular electronic levels introducing a new condition for resonance acted by the metallic surface itself.[24]

Nowadays we know that both mechanism can act separately or in conjunction. These mechanisms are named electromagnetic and chemical enhancement, respectively. The net result obtained is a strong intensification of the signal up to fifteen orders of magnitude, at the very best conditions.

2.2.1 Optical properties of materials

To understand how SERS mechanism works, the concept of Surface Plasmon (SP) and its related phenomena, has to be introduced. Lorentz gave a first analysis,

interpreting the motion of electrons around the nuclei under the effect of an external time-dependent electric field as a damped oscillator driven by the external electric field itself. Neglecting the magnetic contribution:

$$\bar{E} = \bar{E}_0 e^{i(kr-\omega t)} \tag{2.4}$$

This acts as a driving force for the electrons around the nuclei, therefore there will be a spatial displacement χ around the equilibrium. Recalling the approximation made for the explanation of RS, we can model the force acting between nuclei and electrons with a spring characterized by a force constant k. The possibility of scattering events is embedded in the damping constant of the motion Γ. We can then write the Lorentz fundamental equation for this motion:

$$m\frac{d^2\chi}{dt^2} + m\Gamma\frac{d\chi}{dt} + m\omega_0^2\chi = -e\bar{E} \tag{2.5}$$

In which $\omega_0 = \frac{k}{m}$ is the resonance frequency of the oscillator and we can introduce $\omega_d = \frac{\Gamma}{m}$ as the damping frequency of the system. The solution of the equation can be easily found:

$$\chi = \frac{e}{m}\frac{\bar{E}}{\omega_0 - \omega - i\Gamma\omega} \tag{2.6}$$

This result has a very deep meaning considering that the dipole moment of the system is $p = e\chi$ and the macroscopic polarization is $P = N_e p$ (with N_e being the electron density.) is related to the dielectric constant of the material:

$$\epsilon = 1 + \frac{P}{\epsilon_0} \tag{2.7}$$

$$\epsilon = \epsilon(\omega) = 1 + \frac{N_e e^2}{m\epsilon_0}\frac{1}{\omega_0^2 - \omega^2 - i\Gamma\omega} \tag{2.8}$$

The term $m\omega_0^2$ can be considered as the spring constant, when considering insulators or semiconductors. Considering metals, the electrons are free and don't feel any restoring force. This can be represented assuming the spring constant to be null. This assumption is introduced in the Drude model. Since we are analyzing metals, Eq. 2.8 becomes:

$$\epsilon(\omega) = 1 - \frac{\omega_p}{\omega^2 + i\Gamma\omega} \tag{2.9}$$

Where:

$$\omega_p = \sqrt{\frac{N_e e^2}{m\epsilon_0}} \tag{2.10}$$

Is the so called *plasma frequency* of the system.

It can be also seen that the dielectric constant is complex. This under the Drude model assumptions gives us information on the behavior of the material once irradiate with an electromagnetic wave with a characteristic frequency ω. Considering both real and imaginary parts of the dielectric function:

$$Re[\epsilon(\omega)] = \epsilon'(\omega) = 1 - \frac{\omega_p^2}{\omega^2} = n^2 + k^2 \tag{2.11}$$

$$Im[\epsilon(\omega)] = \epsilon''(\omega) = \frac{\omega_p^2}{\omega^3}\Gamma = 2nk \tag{2.12}$$

This results tell us the following information:

1. $\omega > \omega_p$**:** The propagation of light within th material and its absorption are determined by the imaginary part of the dielectric constant. This is called *"normal"* behaviour.

2. $\omega < \omega_p$**:** The real part of the dielectric constant is negative. Therefore, n (refractive index) is imaginary. The light can propagate in the metal with an intensity that decays exponentially as the penetration depth increases. We also have the phenomenon of "evanescent" fields. This is called *"anomalous"* behaviour.

3. $\omega = \omega_p$**:** All the electrons are oscillating collectively at the same frequency, in which there is excitation of harmonic oscillators that simultaneously vibrate at the plasma frequency. This phenomenon is characterized by quanta called *plasmons*.

Plasmons can be both found in the bulk of the material (bulk plasmons) or at the surface, hence the name *surface plasmons* (SP), with their own dispersion relations. Making use of the Maxwell's equations we can find that SP are bound modes only possible at the interface between the surface of a metal and another dielectric material and they are characterized by a frequency:

$$\omega_{sp} = \frac{\omega_p}{\sqrt{1 + \epsilon_{dielectric}}} \tag{2.13}$$

Now we can consider what happens in presence of metallic nanoparticles (NP). The electronic cloud of the NP oscillates in presence of the external field, generating an oscillating dipole. In turn this dipole generates a local electric field, such that the total field becomes:

$$\bar{E_{TOT}} = \bar{E_0} + \bar{E_{sp}} \tag{2.14}$$

Considering the NP's dimensions to be sub-wavelenght, we can suppose the total field $\bar{E_{TOT}}$ to be electrostatic, allowing us to make use of classic electrostatics to fing the NP's external and internal field, potentials and polarizability.

$$\bar{E_{IN}} = \frac{3\epsilon_{medium}}{\epsilon - 2\epsilon_{medium}} \bar{E_0} \tag{2.15}$$

$$\alpha \propto \frac{\epsilon - \epsilon_{medium}}{\epsilon - 2\epsilon_{medium}} r^3 \tag{2.16}$$

In which r is the characteristic dimension of the NP and ϵ is the dielectric constant of the metal. It can be noticed that both have a resonance condition when $\epsilon + 2\epsilon_{medium} = 0$. When can then find the frequency of the Localized Surface Plasmon (LSP) for which the resonance condition is set.

$$\omega_{lsp} = \frac{\omega_p}{\sqrt{1 + \epsilon_{medium}}} \tag{2.17}$$

The presence of the LSP can be checked via UV-vis spectroscopy, being its spectrum closely related to the polarizability and being a function of the NP's dimensions. The scattering cross-section depends from it as r^6 while the absorption cross-section as r^3.

2.2.2 Electromagnetic enhancement

To evaluate the classical electromagnetic enhancement (CEME) given by the generation of LSP we begin taking into consideration the polarizability α and the polarization induced by an external field. The electric field generated this way by the LSP is then:

$$\bar{E_{lsp}} = \bar{E_0} r^3 \frac{\epsilon - \epsilon_{medium}}{\epsilon + 2\epsilon_{medium}} \frac{1}{(r+d)^3} \tag{2.18}$$

In Eq. 2.18 r and d are the dimension of the NP and the reference distance of a molecule from its surface, respectively. We will then take the intensification factor

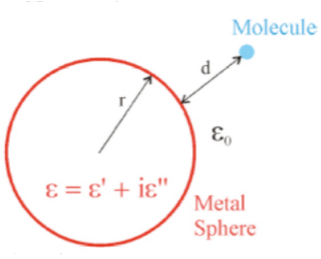

Figure 2.3: reference scheme for description of CEME

as follows:

$$A(\omega) \approx \frac{\bar{E_{lsp}}}{\bar{E_0}} = \frac{\epsilon - \epsilon_{medium}}{\epsilon + 2\epsilon_{medium}} \frac{r^3}{(r+d)^3} \tag{2.19}$$

Where we assumed $\bar{E_{lsp}} \gg \bar{E_0}$. Then the intensity enhancement factor will be:

$$I(\omega) = |A(\omega)|^2 \sim \left| \frac{\epsilon - \epsilon_{medium}}{\epsilon + 2\epsilon_{medium}} \right|^2 \frac{r^6}{(r+d)^6} \tag{2.20}$$

Here we can notice the tight relation between enhancement and the distance between NP and analyte. The final enhancement factor for CEME is:

$$I_{SERS}(\omega_S) = |A(\omega_S)|^2 |A(\omega_L)|^2 \sim \left| \frac{\epsilon(\omega_S) - \epsilon_{medium}}{\epsilon(\omega_S) + 2\epsilon_{medium}} \right|^2 \left| \frac{\epsilon(\omega_L) - \epsilon_{medium}}{\epsilon(\omega_L) + 2\epsilon_{medium}} \right|^2 \frac{r^{12}}{(r+d)^{12}} \tag{2.21}$$

Where S stands for Stokes contribution and L for Laser contribution.

NP arrays or aggregates can originate so called *hot spots*, in which very closely packed plasmonic interactions can produce a further intensification of the EM field, allowing single molecules to be detected if they are present in these regions.

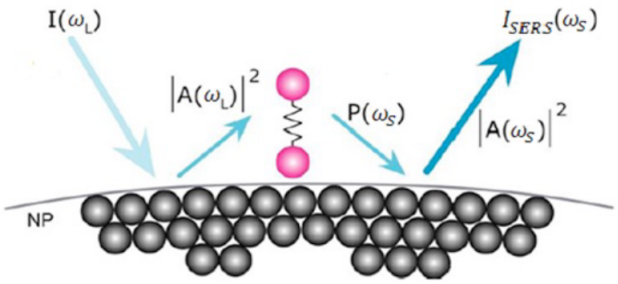

Figure 2.4: Schematic view of the total CEME, where the two contribution, Laser (L) and Stokes (S), act differently

2.2.3 Chemical enhancement

In RS, the enhancement induced on the electric field may also stem from a chemical process. This is due to the fact that the raman spectrum is strongly affected by the chemical nature of the analyte. In SERS, the analyte interaction with the metal must be considered. The electronic distribution of the analyte can be perturbed by the metal's presence and the whole raman spectrum is thus modified. In Chemical Enhancement (CE) the principal effect to be considered is the Charge Transfer (CT). Which can be involved in three different ways:

1. **Type I mechanism:** This acts on not-bonded analyte molecules. The metal perturbates the electronic structure of the analyte leading to an improved Raman efficiency on certain vibrational modes;

2. **Type II mechanism:** Acting on *surface complexes*, which can be formed by direct bond or by bridging from electrolyte ions. The molecular orbitals of the two components overlap and new electronic states provide a resonance condition that can be exploited.

3. **Type III mechanism:** Also named *photo-driven CT*, occurs when the formation of a complex provides a HOMO-LUMO gap which is matched by the laser employed.

The fundamental mechanisms from which the different CT types and CE itself stems, as proposed by Otto (mettere reference)are:

1. Excitation of the electrons at the metal HOMO-LUMO gap throug laser annihilation;

2. Excitation of electrons that propagate to the adsorbate to a charge transfer energy level;

3. Jahn-Teller distortion of the adsorbate electronic configuration;

4. Electrons relaxate and Stokes photons are generated.

To simplify, we can identify CE as the generation of resonant energy levels due to the interaction between the analyte with the nanostructured metallic surface. The molecule nature strongly affects the resonances induced with this process. Other effects should be mentioned as they give an important contribution, such as adsorption site location, molecule orientation, surface coverage and analyte concentration. The analyte-metal relative geometry affects the polarizability of the analyte itself, activating or deactivating certain modes. Finally, a crucial point for application of SERS to TDM is that the entity of the CE is proportional to the number of the adsorbed molecules and to the Raman cross-section of the adsorbate. Thus, we can write:

$$I(\omega_S)_{CE} \propto C_{ads} N_{ads} \tag{2.22}$$

In which C stands for cross-section and N stands for molecules density (or concentration).

2.3 Instrumentation

2.3.1 Dispersive Raman LabRAM HR800

The reference instrument used to collect the Raman spectra presented in my thesis has been the Horiba Jobin Yvon LabRAM HR800 (Fig. 2.5).

Figure 2.5: The dispersive Raman LabRAM HR800 produced by Horiba Jobin Yvon

This instrument is equipped with an Olympus BX41 microscope which allows micro-Raman measurements with different kinds of objectives. Three laser radiations were used: (i) 458 nm and 514 nm from an argon ion laser (Stabilite 2017, Spectra Physics) in the study of solutions; (ii) 633 nm from a HeNe laser in the study of solids and (iii) 785 nm (NIR) from a solid-state laser (Laser XTRA, Toptica Photonics) in SERS experiments. The laser radiation is initially filtered by an interference filter that can remove the spurious line coming from the laser. A series of filters with different optical densities can be used to modify the effective laser power at the sample. Once the light-sample interaction occurs, we obtain a backscattered light thanks to the RS effect. An edge filter is used to remove the Rayleigh component of the scattered light (the notch filter was used only for the 785 nm excitation). The Stokes and anti-Stokes radiations are dispersed through a grating (600 or 1800 line/mm) to finally arrive at the Peltier cooled CCD detector were the Raman signal is accumulated and processed by the electronics of the instrument.

2.3.2 Spectrophotometer UV-VIS JASCO V-570

The instrument features two deuterium and halogen lamps which cover the whole spectral range of measurement, emmitting radiation on UV and VIS-NIR, respec-

Figure 2.6: JASCO V-570 UV - vis spectrophotometer.

tively. A spherical mirror selects the source that then illuminates the entrance slit of the monochromator, sending the radiation on a plane mirror that further leads the light on the filters. The two slits are variable in width and height and the Czerny-Turner monochromator exploits two disperding gratings with a switch at 800-900nm to cover the whole spectral range. The optical scheme of the instrument is in Fig. 2.7

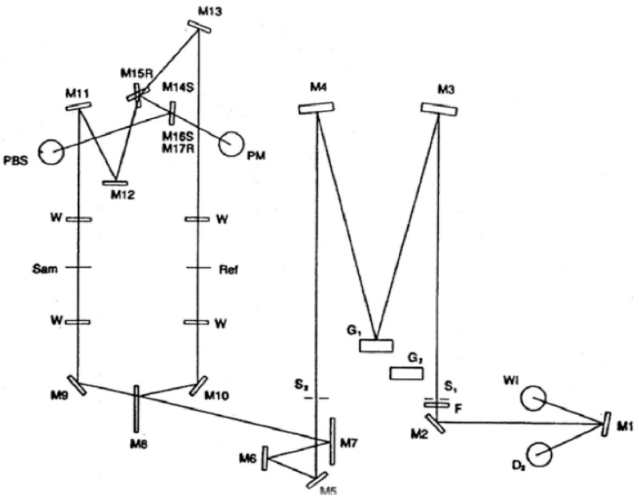

Figure 2.7: Optical scheme of the JASCO V-570 spectrophotometer.

Then the radiation is reflected to reach a splitter that separates it in two components that will intecept the sample and the reference. Than the radiation is collected and reaches the detector, which is a photomultiplier for UV or PbS for NIR. The detector see in succession the sample signal, then the reference and

the dark which are subtracted. The signal is then elaborated by the software to give the requested information (absorbance, trasmittance, reflectance...). For the colloids and analyte solutions, quartz cells of 1cm width have been used, changing the reference sample properly.

Chapter 3

SERS materials

Nanostructures made of gold (Au) and silver (Ag) find nowadays widespread use in optics and spectroscopy, thanks to their plasmonic resonances that allow for remarkable enhancement of local electromagnetic fields.[17] Fabrication of such nanoparticles can be achieved in different ways. Here chemical fabrication involving colloids and physical fabrication by pulsed laser ablation in liquid (PLAL) will be described, as these methods were used to produce the substrates employed in SERS experiments.

3.1 Au/Ag substrates produced by chemical methods

3.1.1 Synthesis and deposition

The synthesis process[1] starts with the dissolution of the Ag or Au metal salt in deionized water, followed by the release of metallic ions. Subsequently a reducing agent is added and the metal ions are neutralized. These progressively start agglomerating forming nanoparticles, which are then stabilized by the same reducing agent. The reducing agent used was trisodium citrate (TSC, fig.3.1) which has good stabilizing properties, although it promotes the reduction process of metal ions only at temperatures close to boiling.

The oxydation of TSC catalyzes the growing process of the nanoparticles. When this is completed, there is nanoparticle stabilization due to the unreacted bicarboxylic acid and citrate (fig.3.2). These two molecules adhere on the nanoparticles creating a charged shell which hinders their aggregation, reducing their superficial energy.

[1]Work done in collaboration with the bachelor students of group 31: Federico Olla, Maria Teresa Caporaso, Nicola Melis, Francesco Tuccillo, Martina Golini and Matteo Danieli.

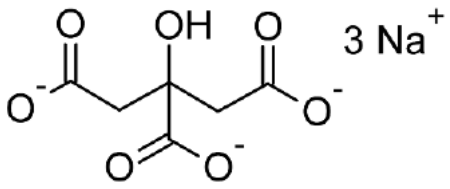

Figure 3.1: Chemical structure of Trisodium Citrate (TSC).

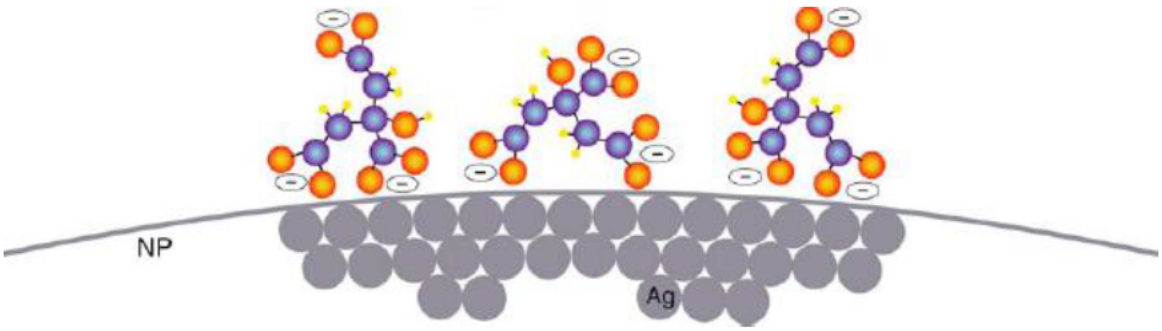

Figure 3.2: Stabilization of the nanoparticles acted by trisodium citrate.

Ag colloids

The production of the Ag colloidal nanoparticles was done following the Lee-Meisel method[25]:

1. 72 mg of silver nitrate are dissolved in 400 mL of deionized water.
2. 80 mg of TSC are dissolved in 8 mL of deionized water.
3. both solutions are heated up to boiling point into a conical flask, then mixed.
4. The solution is kept at boiling point for one hour and agitated through a magnetic agitator for an hour.
5. The solution is then cooled while keeping the agitation.

A thorough cleaning of the flask with nitric acid before starting the preparation is required, to avoid the formation of nanoparticles on the glass surfaces which would act as an heterogeneous nucleation site, altering the whole process.

Au colloids

For the synthesis of the Au colloidal nanoparticles the Turkevich[26] method was followed:

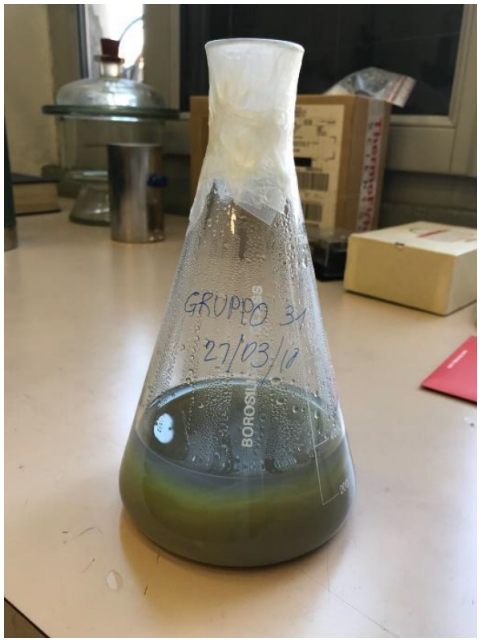

Figure 3.3: Silver colloid produced by following the Lee-Meisel method.

1. 180 mL of a $10^{-3}M$ solution of $HAuCl_4$ in deionized water is prepared.
2. 9,6 mg of TSC are dissolved in 9,6 mL of deionized water.
3. both solutions are heated up to boiling point into a conical flask, then mixed.
4. The solution is kept at boiling point and agitated through a magnetic agitator for one hour.
5. The solution is then cooled keeping the agitation.

Also on this case the careful cleaning of the flask with nitric acid before the synthesis process is required.

Deposition of the colloids

The production of the SERS substrates starting from the prepared colloid can be summarized in the following steps:

1. Centrifugation of the colloid: this operation allows for the heavier nanoparticles and aggregates to concentrate on the bottom of the vials.
2. Removal of the surnatant containing a low concentration of nanoparticles.

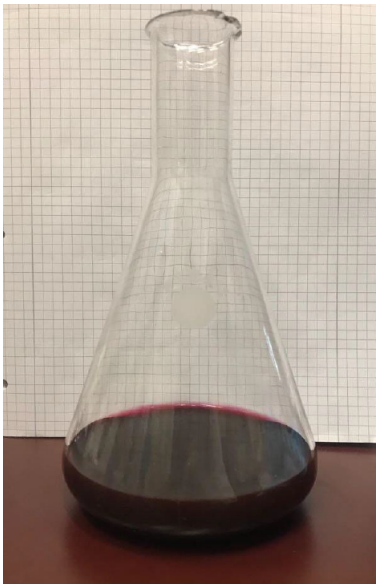

Figure 3.4: Gold colloid produced by following the Lee-Meisel method.

3. Glass supports preparation using toluene.

4. Deposition of 2-10 μL of concentrated colloidal droplets on the glass (fig.3.5 and 3.6).

5. Evaporation of the water from the deposited colloidal droplet.

When depositing the colloid by drop casting, a phenomenon known as *coffee stain effect* can occur. Its effect is to create an annulus-shaped substrate which leaves the center uncovered. It has been noticed that by depositing smaller drops (2μL or lower) the effect can be reduced. Moreover, the cleaning step of the glass supports with toluene contributes to reduce the effect.

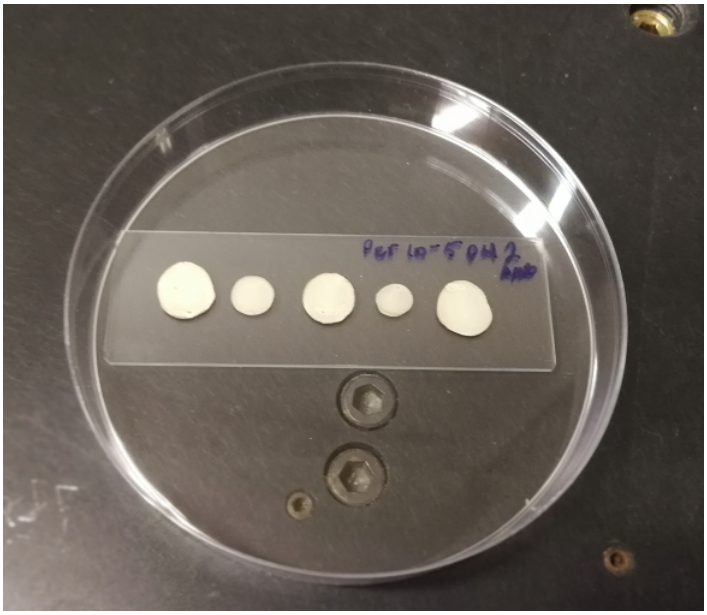

Figure 3.5: Chemically produced Ag nanoparticles deposited on a glass support.

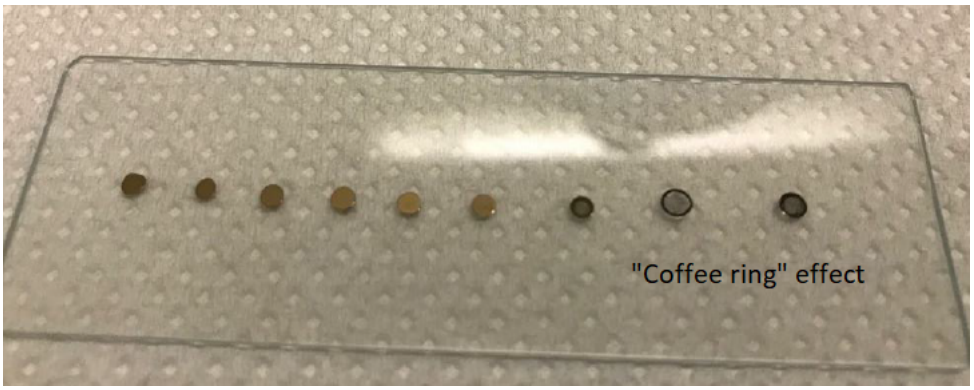

Figure 3.6: Chemically produced Au nanoparticles deposited on a glass support. The coffee ring effect is shown on the substrates on the right.

3.1.2 UV-vis characterization of the colloidal substrates

Both colloids were characterized for the means of a parallel thesis, authored by the colleague Federica Iacoe. Here the final results are briefly reported below as a reference for my SERS experiments discussed later in this thesis. UV-vis spectroscopy allows to obtain the position of the plasmonic frequency of the colloids. This peaks at 416 nm for the Ag substrates (Fig.3.7), while for the Au colloid it peaks at 522 nm (Fig.3.8). It is well worth notice that the UV-vis done for the Ag substrates shows that the peak is significantly enlarged, reaching regions as far as 700-800 nm. This allow us to choose a 785 nm laser for SERS detection, greatly lowering the risk of damaging the analyte.

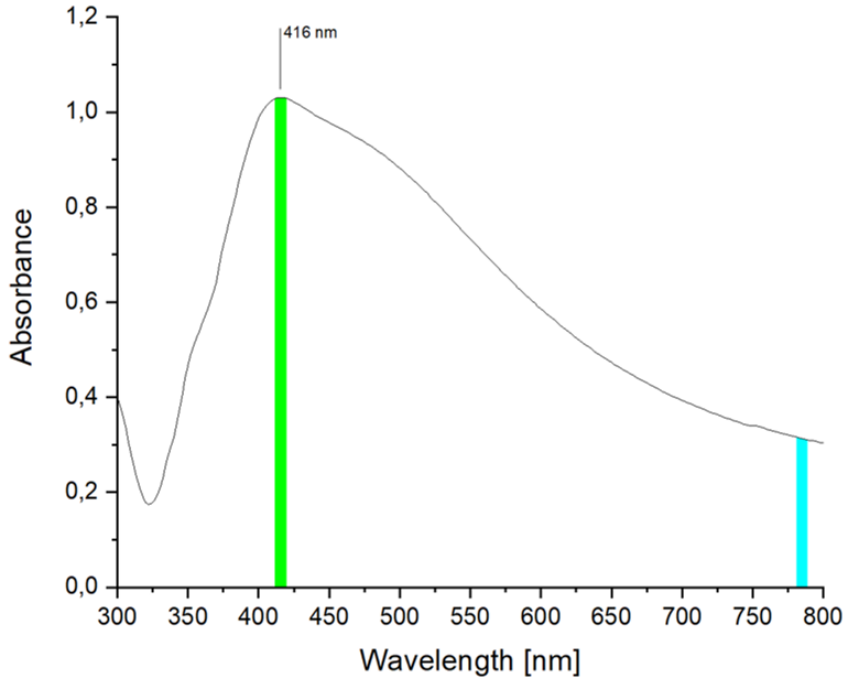

Figure 3.7: UV-Vis absorption spectrum of chemically produced Ag colloids diluted in deionized water. In green the region of the surface plasmon resonance peak, while in cyan the region of the laser employed for the measurements are highlighted.

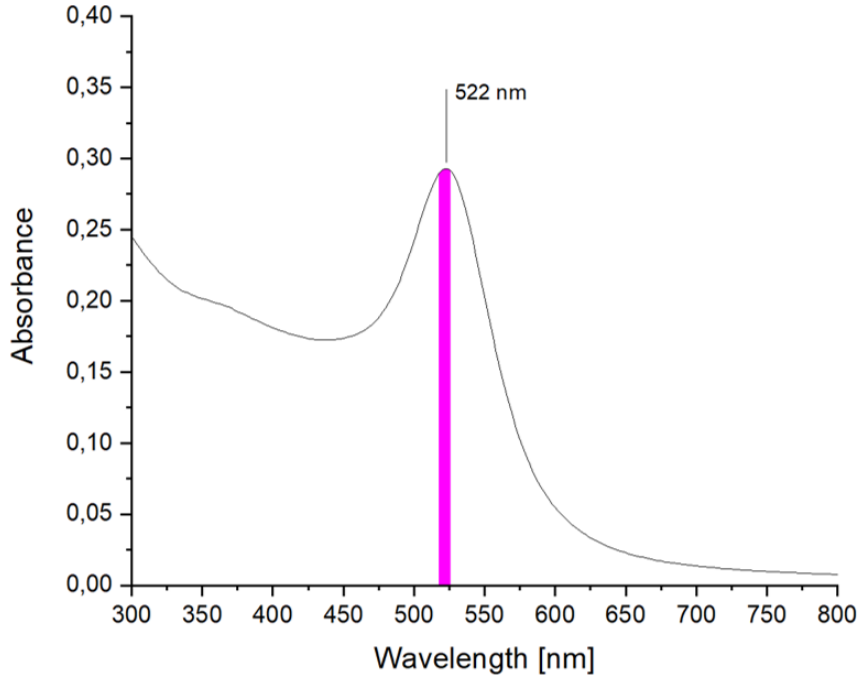

Figure 3.8: UV-Vis absorption spectrum of chemically produced Au colloids diluted in deionized water. In purple the region of the surface plasmon resonance peak is highlighted.

The absorbance of the colloid deposited on glass supports will differ considerably from the absorbance of the diluted colloid, due to the aggregation of the nanoparticles which will broaden the plasmonic resonance, as well as shifting it towards 750-800 nm region and beyond. Therefore, the choice of using a 785 nm excitation to carry the SERS experiments is not unreasonable.

3.2 Au/Ag SERS substrates produced by PLAL

The PLAL-made nanoparticles (NP) used in the experiments have been produced by Prof. Enza Fazio of the university of Messina using a 532 nm laser radiation to ablate pure(99.9%) gold and silver targets[17, 27] submerged in a pure water environment. The radiation is provided by (i) the second harmonic of a pulsed Nd:YAG source with a 10 Hz repetition rate and pulse witdh of 6 ns as well as by (ii) an ultra-fast Nd:YVO_4 source with repetition rate of 100 kHz and pulse width of 6-8 ps.[17, 27]

Changing the two sources the fabricated substrate will feature different structural and morphological properties, leading to different surface plasmon reso-

nance.[27] The polar water environment allows for surface-charged NPs surrounded by a shell of dipolar molecules (water) which are stable against agglomeration.[28] The ablation parameters were fixed in order to obtain tailored size distributions and concentrations nanoparticles. Finally, highly stable and chemically pure NPs, with average size ranging from 5 to 30 nm were synthesized.[27] Two types of substrates were obtained depending on the laser source used:

1. **ns-PLAL** nanostructures were obtained with the nanosecond laser source, with ablation time of 20 minutes and laser fluence of 1.5 Jcm^{-2};[27]

2. **ps-PLAL** nanostructures were obtained using the picosecond laser source, with ablation time of 10 minutes for Ag and 5 minutes for Au. The laser fluence adopted was the same of ns-PLAL.[17, 27]

The full synthesis and characterization of the nanostructures is treated on the relative articles published.[17, 27, 29]

PLAL fabrication technique counters many of the disadvantages that chemical production features, being a remarkably simpler process requiring a single-step rather than being multi-step.[28] The timescale of the process is of the order of minutes instead of hours/days. Finally, the NPs obtained are surfactant-free and no stabilizing agent is needed.[27] Using the Olympus BX41 microscope integrated in the Horiba Jobin Yvon LabRAM HR800, images of the substrates surfaces, obtained by spraying the colloids on Si or glass supports, could be taken to analyze their morphological structure. ps-PLAL favours a more homogeneous distribution of NPs with respect to ns-PLAL. Moreover, the irradiation imposed on AuAg alloys enhanced homogeneity even better.

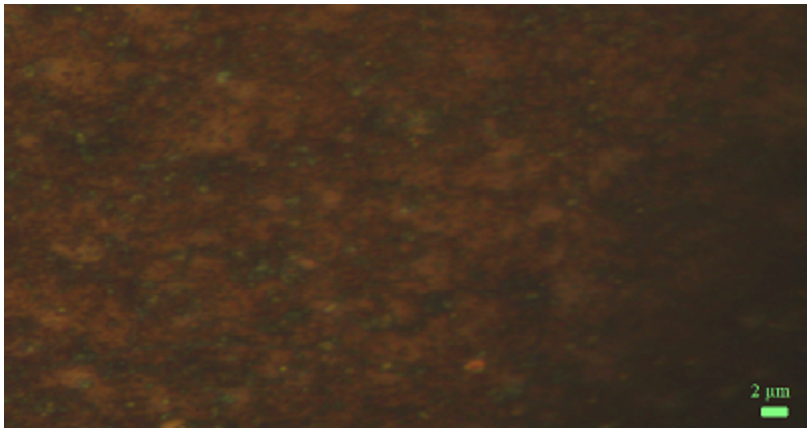

Figure 3.9: Optical micrograph image of the surface of a ns-Ag SERS substrate.

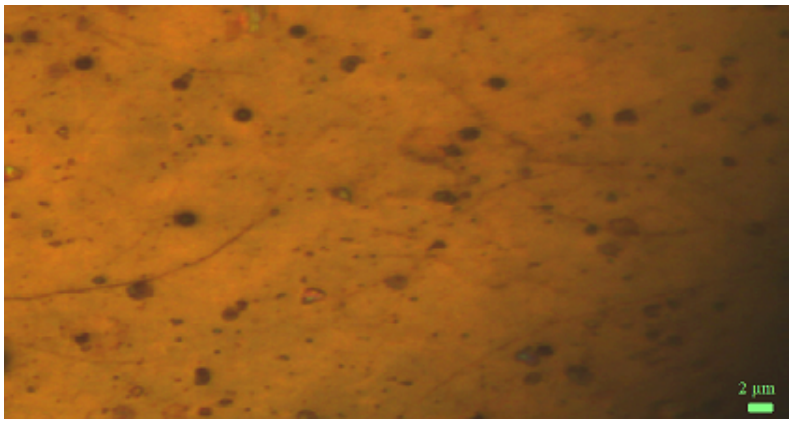

Figure 3.10: Optical micrograph image of the surface of a ns-Au SERS substrate.

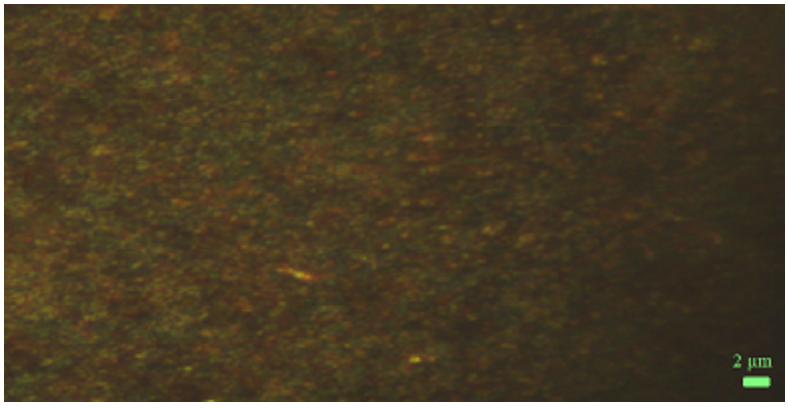

Figure 3.11: Optical micrograph image of the surface of a ps-Ag SERS substrate.

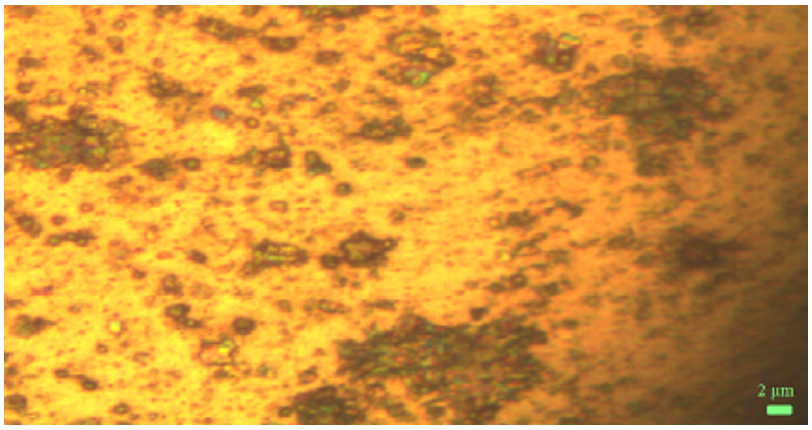

Figure 3.12: Optical micrograph image of the surface of a ps-Au SERS substrate.

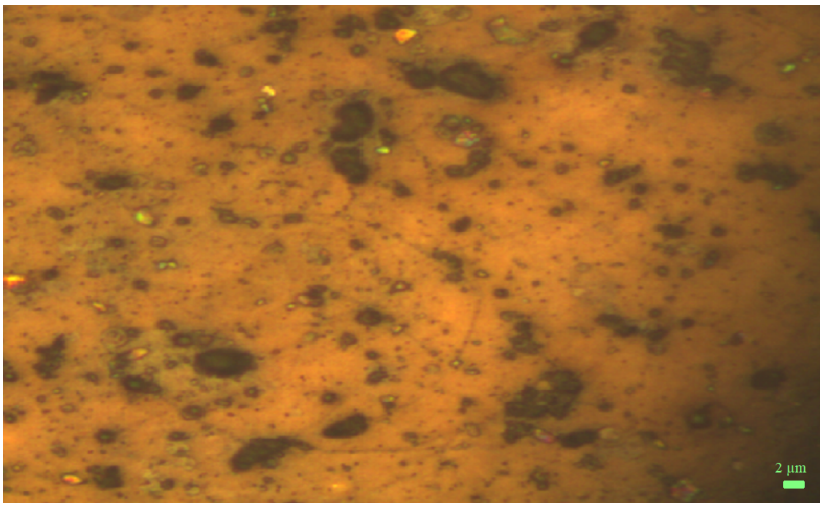

Figure 3.13: Optical micrograph image of the surface of a ps-AgAu 50/50 alloy SERS substrate.

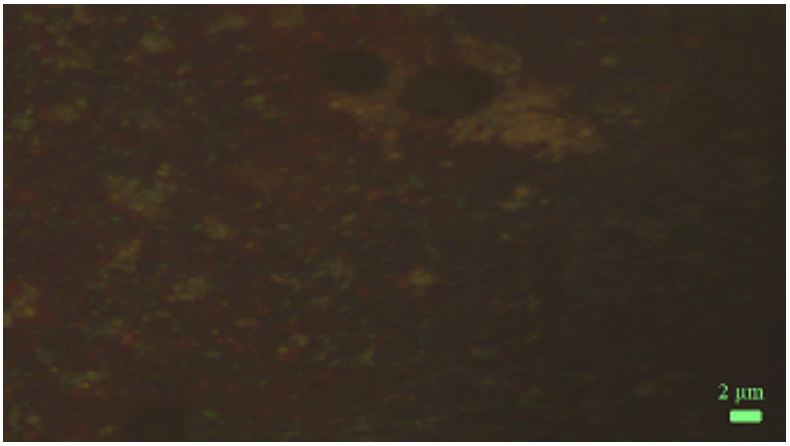

Figure 3.14: Optical micrograph image of the surface of a ps-AgAu 75/25 alloy SERS substrate.

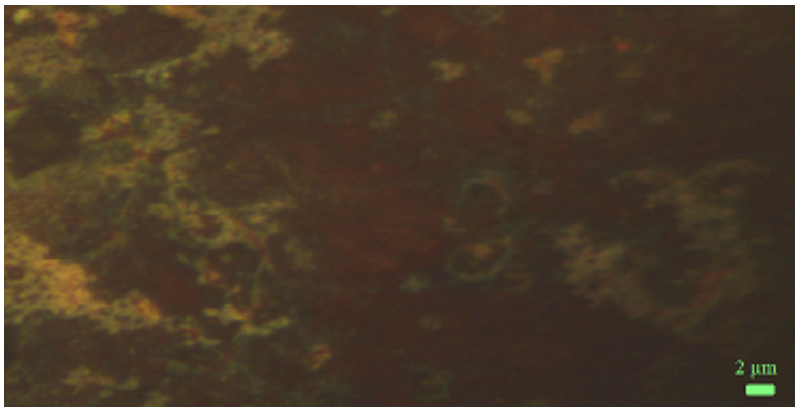

Figure 3.15: Optical micrograph image of the surface of an irradiated ps-AgAu 50/50 SERS alloy substrate.

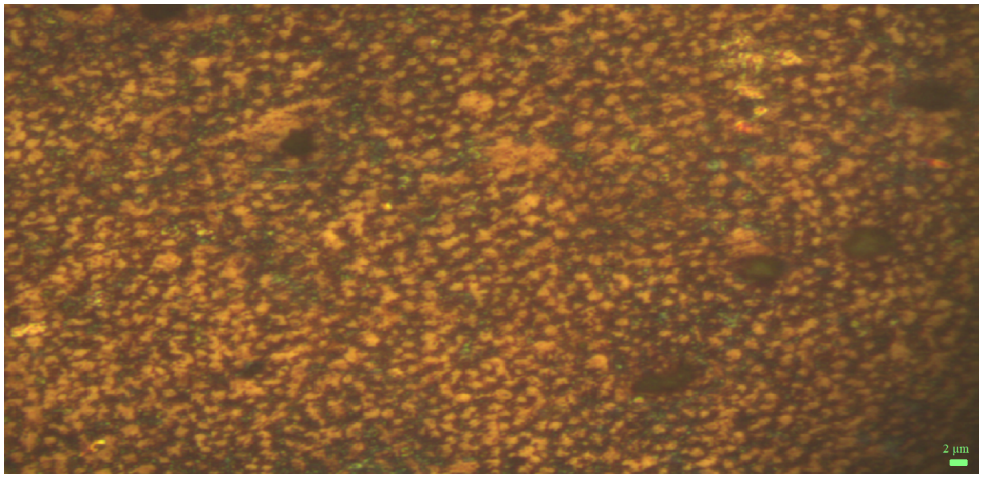

Figure 3.16: Optical micrograph image of the surface of an irradiated ps-AgAu 75/25 SERS alloy substrate.

Chapter 4

Perampanel (PER)

Perampanel is a novel, highly selective, orally active, non-competitive AMPA receptor antagonist used for treatment of epileptic seizures. It was identified via a focused discovery program at Eisai Research Laboratories.[30] Powder of pure PER was purchased from Cayman Chemical (Item No. 23003; CAS 380917-97-5) and used as received. The chemical structure of PER is shown in fig.4.1. In order to carry on the SERS experiments, assessing the Raman spectrum of the molecule is crucial. Thus, Raman spectroscopy is used, to probe PER vibrational modes, frequencies and relative Raman intensities.

Section 4.2 aims at investigating protonation of PER to favour its deposition on the surface of the substrates, improving their electromagnetic enhancement. Therefore, the SERS experiments will be pH-dependent. To verify the efficiency of the protonation process and give an estimate of the most likely protonated sites of the molecule, UV-Vis spectroscopy was carried out. Finally, in section 4.3 UV-Vis spectroscopy was used to test the stability of PER in acid solutions. This data is crucial for the setup of a clinical procedure, setting the time range in which

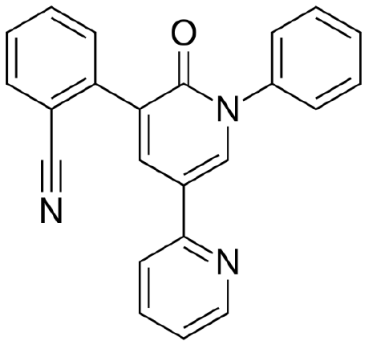

Figure 4.1: Chemical structure of perampanel (PER)

the measurements can be considered reliable, as well as giving instructions on the storage of the samples to be analyzed.

4.1 Raman characterization

Three Raman spectra are collected on solid PER powder, focusing it with 3 different laser wavelengths the dispersive LabRAM HR800 is equipped with: 458 nm, 514 nm and 785 nm. The SERS spectra are reported on Fig. 4.2 and 4.3. It can be easily noticed how in spectrum obtained with the 458 nm laser fluorescence dominates the spectrum. Therefore only the other two spectra are analyzed to find and label the main vibrational modes.

The characterization and assignment of Raman active modes of PER is carried out considering the spectrum obtained using the 785 nm excitation wavelength, as the same excitation will be used for the majority of the following experiments. Furthermore, as expected, the same Raman lines are also present on the spectrum obtained at 514 nm.

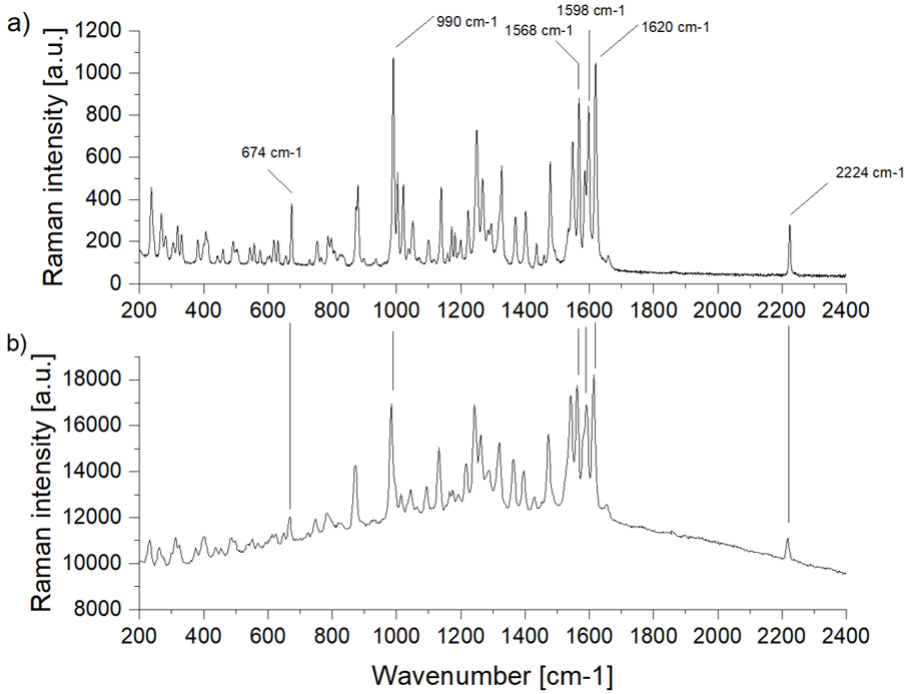

Figure 4.2: Raman spectra of solid PER. a) spectrum collected with 785 nm laser excitation, 10 mW power, 10 s exposition time (3 averages). and b) spectrum collected with 514 nm excitation, 10 mW power, 10 s exposition time (3 averages). The main vibrational modes are labelled.

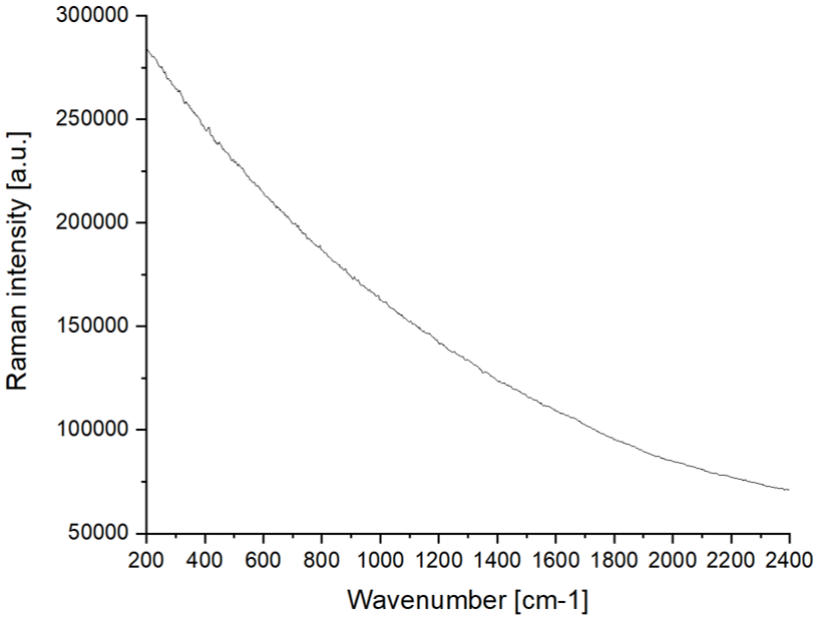

Figure 4.3: Raman spectra of solid PER collected with 458 nm laser excitation, 0.1 mW power, 10 s exposition time (2 averages). The high fluorescence of the spectrum is clearly noticeable.

Comparing the region at low wavenumbers (Fig. 4.4), more sensitive to crystalline field effects, with the FT-Raman spectra provided in MAPI PHARMA LTD.'s patent (US 20140371273A1) regarding PER, there is a correspondence, even if with some discrepancies, with the polymorph VII (Fig. 4.6).[31]

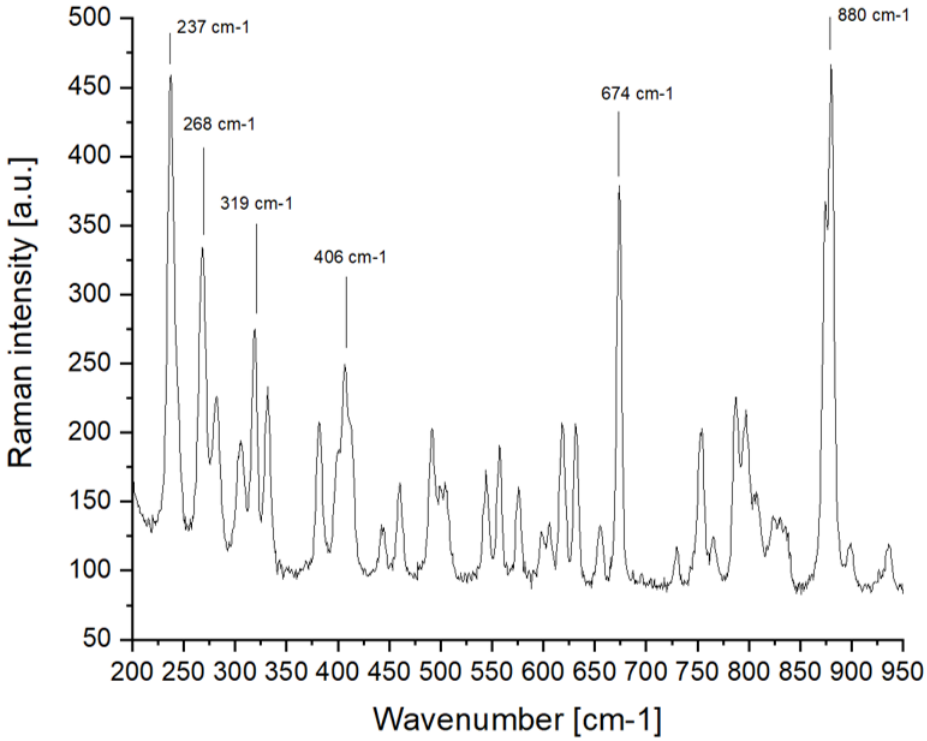

Figure 4.4: Zoom from 200 cm^{-1} to 950 cm^{-1} of the Raman spectra of solid PER collected with 785 nm laser excitation, 10 mW power, 10 s exposition time (3 averages). The main vibrational modes are labelled.

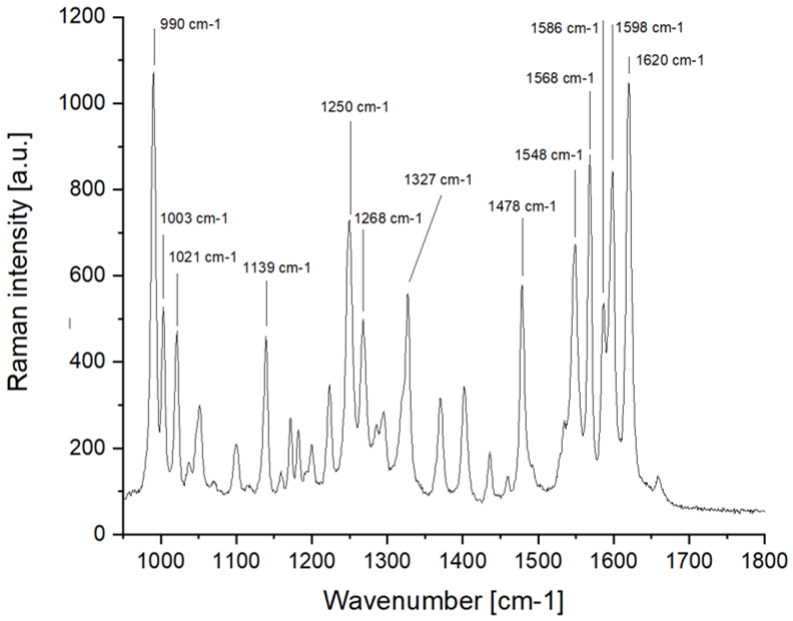

Figure 4.5: Zoom from 950 cm^{-1} to 1800 cm^{-1} of the Raman spectra of solid PER collected with 785 nm laser excitation, 10 mW power, 10 s exposition time (3 averages). The main vibrational modes are labelled.

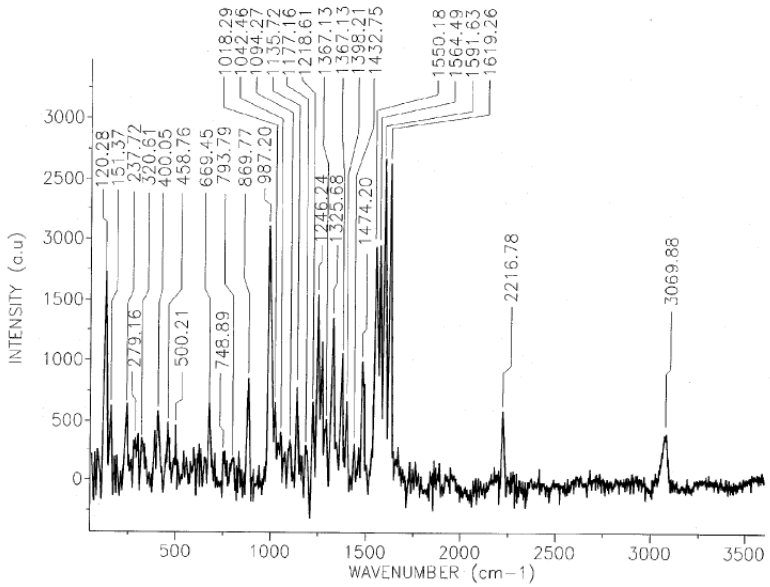

Figure 4.6: Polymorph VII of PER, as stated in MAPI PHARMA LTD.'s patent (US 20140371273A1)[31]

Even without a detailed quantum mechanical modelling of the vibrational states, which would entirely describe the molecule and provide an accurate analysis of the vibrational modes, a qualitative description can be carried out, based on empirical correlations[32](Fig.4.7). The assignation of the main Raman active modes is shown in Tab. 4.1.

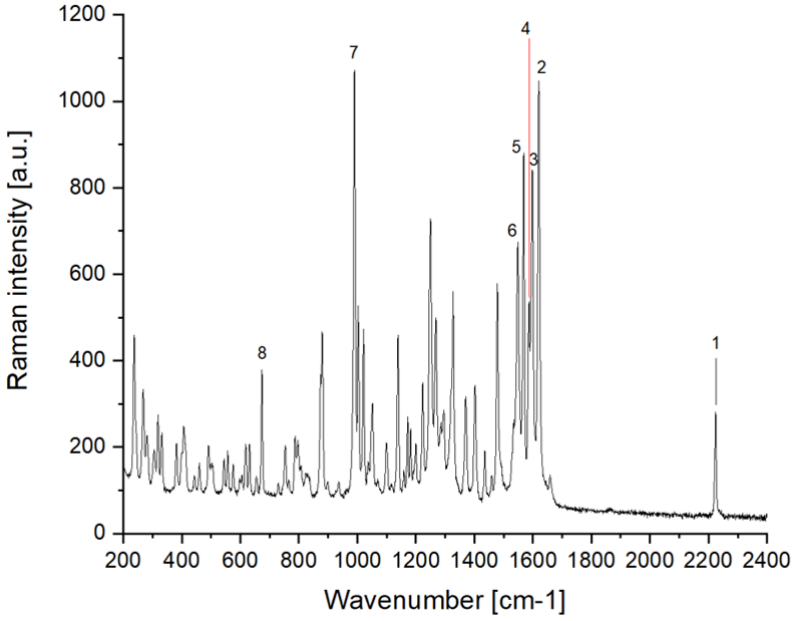

Figure 4.7: Raman spectrum of PER obtained using 785 nm excitation, 10 mW laser power, 10 s exposure time (3 averages). Assigned with numbers are the main peaks of PER. Their assignment to the vibrational modes is provided in Tab.4.1.

Label	Wavenumber (cm-1)	Mode
1	2224	CN bond stretching
2, 3, 4, 5, 6	1620, 1598, 1586, 1568, 1548	Aromatic ring stretching modes
7	990	Ring breathing
8	674	Aromatic ring deformation

Table 4.1: List of the main vibrational modes of PER with qualitative assignation.

4.2 UV-vis characterization of Perampanel

Firstly, UV-vis tests on PER dissolved in neutral solution, secondly, UV-vis test on PER dissolved in acidic solutions as a function of pH. The aim of the tests was to find the molar extinction coefficient and in the case of acidic solutions, find the correct pH in which the molecule is stably protonated. This in order to perform simulations in the future and to find the most likely protonation sites of the molecule.

4.2.1 UV-vis of Perampanel in neutral MeOH solutions

SERS analysis on PER dissolved in neutral solutions haven't given out satisfactory results so far. The hypothesis is that to enhance the adsorbation on the SERS nanoparticles an electrostatic interaction is necessary. Therefore, protonation of PER appears to be of crucial importance. Moreover, the action of the negative charged ion particles that are present in the solution could favour the adsorbation of PER attaching to the nanoparticles and bridging the protonated molecules to the metallic structures through their charge. HCl was chosen due to the great affinity of Cl^- ions towards silver and gold nanoparticles.

For this test the solutions were prepared by initially mixing 3 mg of PER in 8,58 mL of methanol, subsequently agitated for 30 minutes, obtaining complete dissolution. The concentration of PER obtained is $10^{-4}M$. After the preparation of the first solution, other concentrations were obtained by dilution in the proper amount of methanol. This way I obtained solutions with concentration of $1x10^{-4}M$, $5x10^{-5}M$, $2.5x10^{-5}M$, $1.25x10^{-5}M$, $1x10^{-5}M$ and $5x10^{-6}M$. A UV-vis spectrum was collected for each of the concentrations.

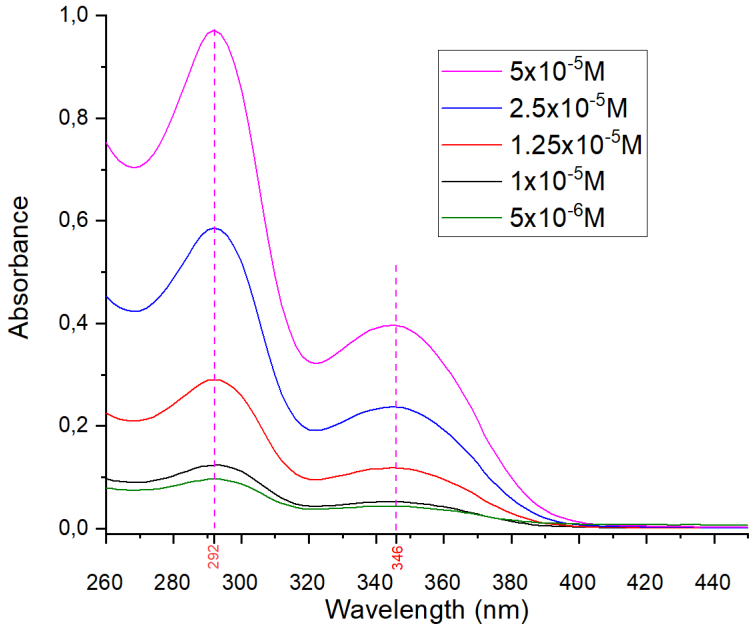

(a)

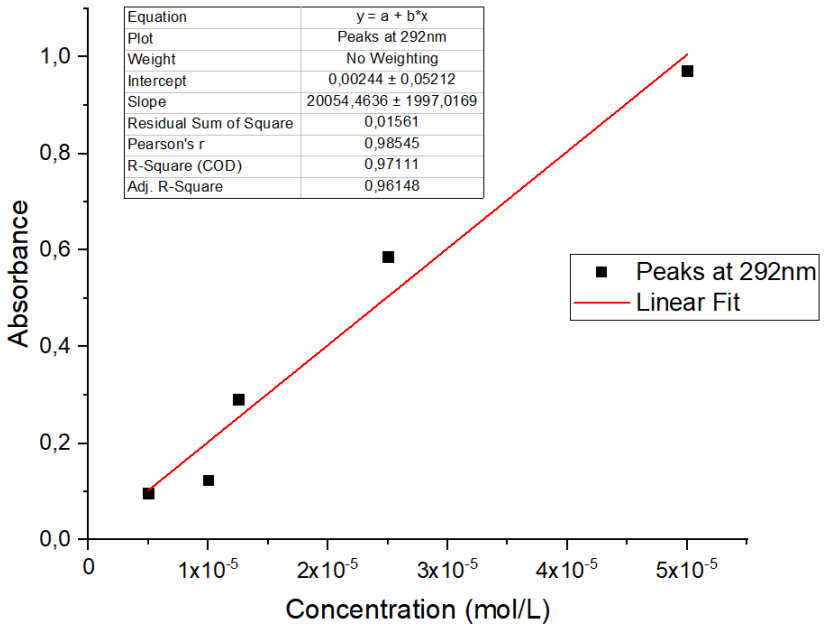

(b)

Figure 4.8: *a*) UV-vis collected spectra of PER in methanol solutions at concentrations ranging from $5x10^{-5}$ to $5x10^{-6}$. *b*) Linear fit performed on the peak-height vs. concentration plot. $R^2 \simeq 0,97$.

The spectra were collected through the JASCO V-570 spectrophotometer, and they are shown in fig.4.8a.

The absorption peaks in UV-vis are found at 292 nm and 346 nm. It is then safe to assume electronic absorption will not be reached during SERS analysis, in which the wavelengths employed are considerably higher.

The peak at 292 nm was used to perform the calculation of the molar extinction coefficient. The height of the peak was measured for every concentration and put on a peak height-concentration correlation graph. Then a linear fit was performed (Fig. 4.8b). The coefficient of the linear fit will be then proportional to the molar extinction coefficient being:

$$A = \epsilon_\lambda Cl \tag{4.1}$$

Which is the well-known Lambert-Beer relation. ϵ_λ is the molar extinction coefficient and its S.I. dimensions are cm^2/mol. From the calculation it resulted that $\epsilon_\lambda = 1,9x10^7 cm^2/mol$ (or $1,9x10^4 Lmol^{-1}cm^{-1}$). The linearity of the absorbance with the concentration shows that aggregation is not present in this concentration range.

4.2.2 UV-vis of Perampanel in HCl aqueuous solutions

Aqueous HCl solutions of 3 mL each were prepared, starting from 2,7 mL of HCl in water ranging from 0 to 5 in pH. The pH was checked each time before adding the drug. Subsequently, 0,3 mL PER from methanol solution, originally $5x10^{-4}M$, was added to achieve a concentration of PER of $5x10^{-5}M$ in each acidic solution. Therefore in this test the concentration was fixed, to see the changes in spectrum due to the variation of acidity of the solution. The results showed that the spectra systematically depends on the pH of the solution, with the protonation process starting at $pH = 3$ (Fig 4.9).

The possible protonation sites have been investigated by density functional theory (DFT) B3LYP/6-31G(d,p) modelling, without considering the solvent's effect for the sake of simplicity, as a model considering a solvent would have been inconvenient for the means of a thesis. The protonation energy and electrostatic charge of suitable spots have been calculated. The final result shows that the most probable spots for protonation are found on the N and O sites, as shown on Fig. 4.10. Based on the experimental results shown, the best acidic conditions for SERS appear to be reached when the pH of the solution is lower than 3.

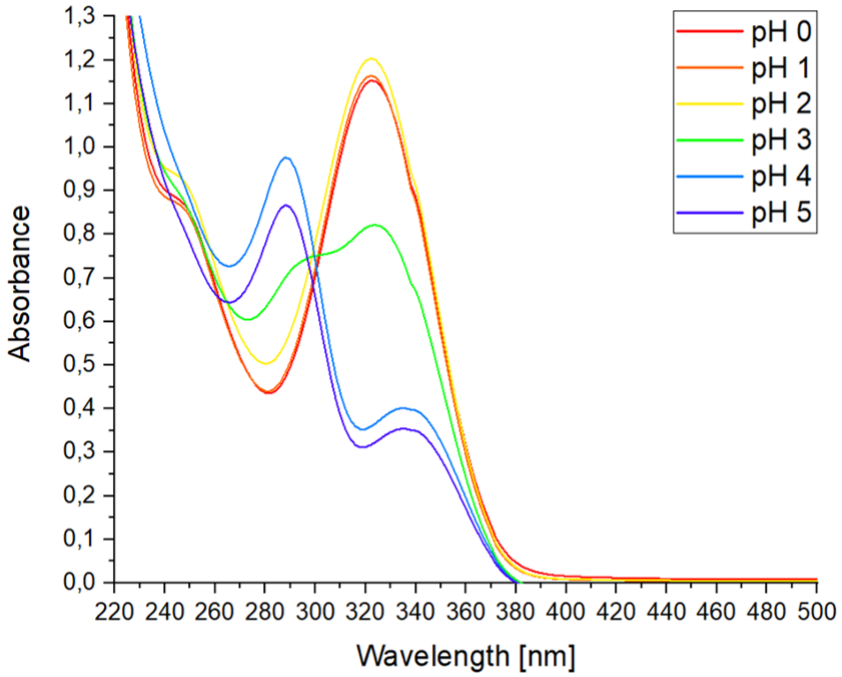

Figure 4.9: UV-vis spectra of PER in acidic solutions at pH, which was set to vary between 0 and 5.

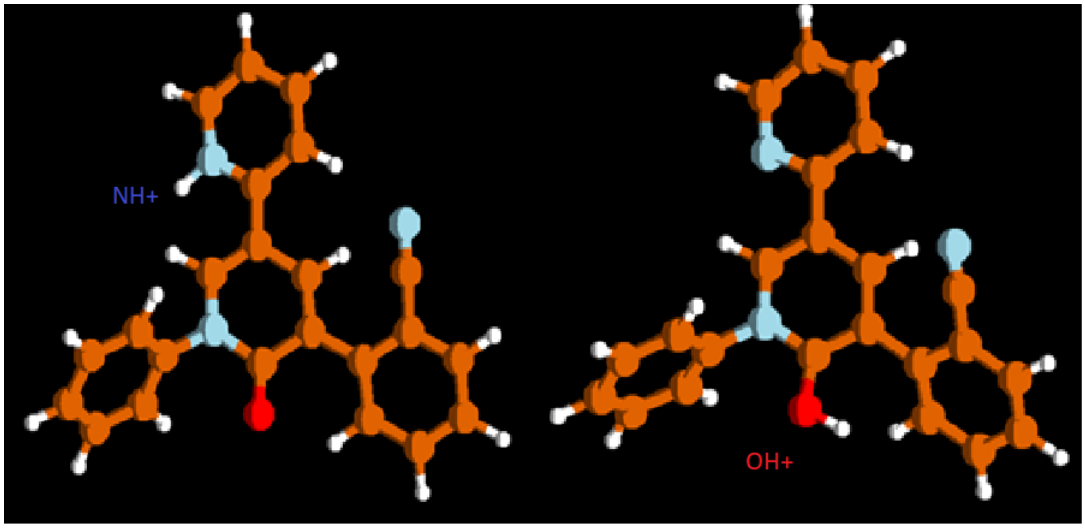

Figure 4.10: Most probable protonation sites of Perampanel. DFT B3LYP/6-31G(d,p) model was used (gaussian).

To further confirm the hypothesis that protonation of PER is necessary for its SERS detection, a SERS spectrum of PER dissolved in a pH 6 solution is compared with a SERS spectrum of PER dissolved in a pH 2 solution (Fig. 4.11). It can be noticed that the spectrum of PER is only detected in the acid case. These results will be analyzed in depth in Ch. 5.

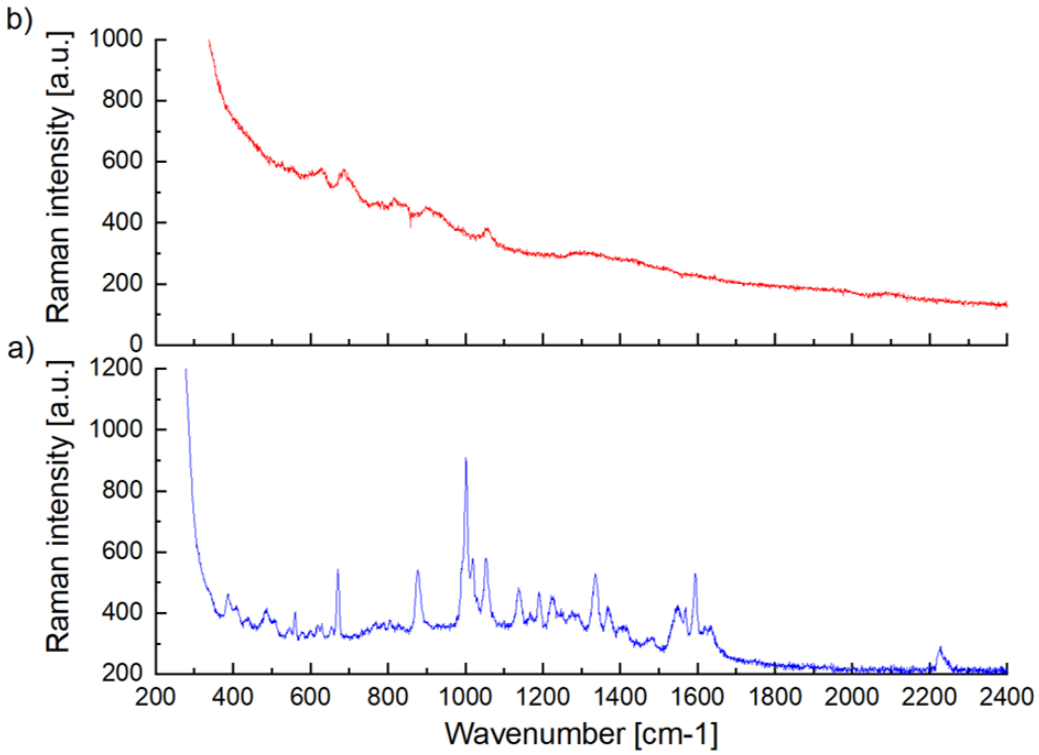

Figure 4.11: SERS spectra of a) PER dissolved in a solution of HCl at pH 6 and b) PER dissolved in a solution of HCl at pH 2. The spectra are obtained using 785 nm laser excitation, 0,1 mW laser power, 20 s exposure time (3 averages).

4.3 Stability

Due to the nature of the processing of the molecule needed for the application in the techniques that are going to be described, it is crucial to know the stability of PER, in this case being the time needed for the molecule to be possibly degraded in an acidic environment. For reasons that are going to be explained in the next chapters, the analyte is supposed to be stored in an acidic solution of hydrochloric acid and sulphuric acid in a molar concentration ratio of 1:9, at pH 2. To address the stability in the specific, UV-vis spectroscopy was used, to spot the changes in the spectrum with time and give a rough estimate of the time to degradation. As a time range, 8 days are considered as a wide enough duration, as it would be very unlikely to store samples for a longer time.

Experimental setup

The instrument used was the JASCO V-570 spectrophotometer. 5 aqueous solutions of hydrochloric and sulphuric acid in a molar concentration ratio of 1:9 at pH 2 were prepared, for a total volume of 3 mL each. For 3 out of the 5 solutions, in each one 0,3 mL were substituted with 0,3 mL of a solution of PER $10^{-4}M$ dissolved in methanol, to reach a total concentration of $10^{-5}M$. The remaining 2 solution were used as reference and for calibration of the instrument. UV-vis meaurement were taken at the day of preparation, 2 and 8 days after, one for each of the 3 solutions containing PER.

Results

As shown in Fig. 4.12, the UV-vis spectrum doesn't feature relevant change in the observed time duration. This is a satisfactory result, meaning that PER samples can be stored for at least one week in the conditions described without damage, ensuring safe measurements during this time range. As an added note, the measurement serves also the purpose of verifying the protonation process in this mixed acids solution. Indeed, comparing the spectrum with the UV-vis spectra obtained in the neutral solution the phenomenon is easily confirmed.

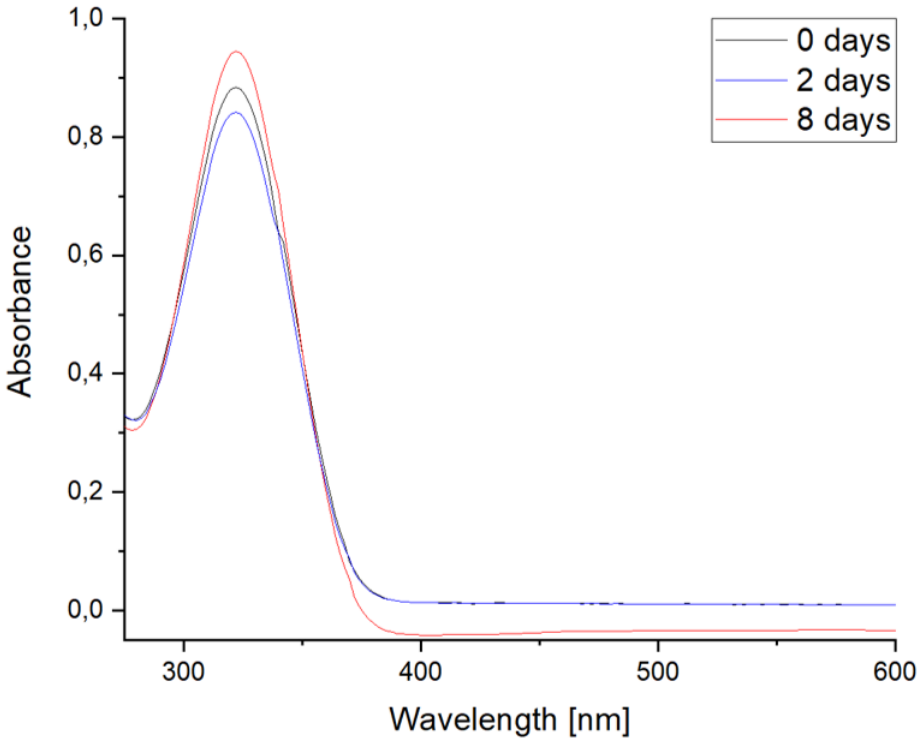

Figure 4.12: UV-vis absorption spectra of PER in aqueous solutions of hydrochloric and sulphuric acid at pH=2, taken at 0 days (black), 2 days (blue) and 8 days (red) after storage.

Chapter 5

SERS on colloidal nanoparticles substrates

As described in Ch. 4, the SERS of PER is pH-dependent. Acidic conditions, reached by adding HCl, lead to good-quality SERS spectra. The aim of this chapter is to find the best conditions (pH, acidic solution, substrate composition and type, optical settings) to achieve a strong SERS signal. SERS was performed using chemically produced Au and Ag substrates. On Ag the test was performed at different acidic pH and the optimal condition was identified. Therefore, SERS spectra were collected on Au substrates using only the optimal procedure determined.

5.1 Ag NPs substrates

Experimental setup

Aqueous solutions of PER were produced, as described for the pH-dependent UV-vis analysis. Briefly. The solutions were made by mixing 2,7 mL of aqueous HCl prepared at pH ranging from 0 to 6 (1 pH step) with 0,3 mL of PER dissolved in methanol. The pH was checked every time before adding PER. The final concentration of PER is $10^{-4}M$. This concentration is low enough to ensure that normal Raman from PER is too weak to be detected. Thus, the spectra recorded in the following can be safely inscribed to SERS. 20 μL droplets of the solution were deposited on the SERS substrates. It has to be noted that all spectra have been collected when the droplet of solution deposited on the Ag nanoparticles surface was yet to be dry. When the droplet dries, no spectrum can be collected, and a sharp increase of the AgCl peak (xxx cm^{-1}) is observed, due to the full coverage of the nanoparticles by a layer of Cl^{-}. This will be discussed in details shortly after in section 8.2. The spectra were recorded using a 785 nm laser excitation, 0,1 mW power, 20 seconds exposure time (3 averages). To focus the radiation on

the substrate a 50x microscope objective with $NA = 0,75$ was used. Later, the same preparation and optical setup was employed to collect a SERS spectrum of PER at a concentration of $10^{-5}M$ at pH 2.

Results

The SERS spectra collected from the seven solutions of PER at varying pH are shown in Fig. 5.1. The results are consistent with the UV-Vis analysis described in Ch. 4 and the protonation of PER. At pH equal to 4, 5 and 6 there's no trace of the molecule's signal, which parallels the fact that PER is not protonated. When the acidity of the solution reaches pH 3 or lower, PER gets protonated and its signal starts appearing in the spectra. At pH equal to 3 the spectrum appears to be similar to the spectrum at pH 4 with some features of PER sightly showing off. At pH 2 and 1 the spectrum of PER is clearly visible, showing the majority of its features, while at pH 0 the signal is again lost. In this very acidic conditions is very likely that the presence of an excessive amount of Cl^-. ions may form a negatively charged shell on the NPs, which then will repel the coupled analyte-Cl^-, impairing PER from reaching the metal surface.

Looking at the candidates for optimal acidity, leading to the best quality of SERS (pH 1 and 2), it can be seen in Fig. 5.2 that the AgCl peak (244 cm^{-1}) is much higher at pH 1. This is due to the presence of greater amounts of Cl^- ions. The height of the AgCl peak is likely to be the cause of the lost signal at pH 0, as it is granted that the analyte is indeed protonated at such low pH (see also Ch. 4). Therefore pH 2 seems to be a more suitable condition due to its lower content of Cl^- and the ability to promote a good SERS signal from the analyte.

After choosing pH 2 as the best acidic condition, SERS spectra were recorded for a lower concentration of PER. The spectrum of PER at a concentration of $10^{-5}M$ is shown in Fig. 5.3, and all the PER features can be reliably observed.

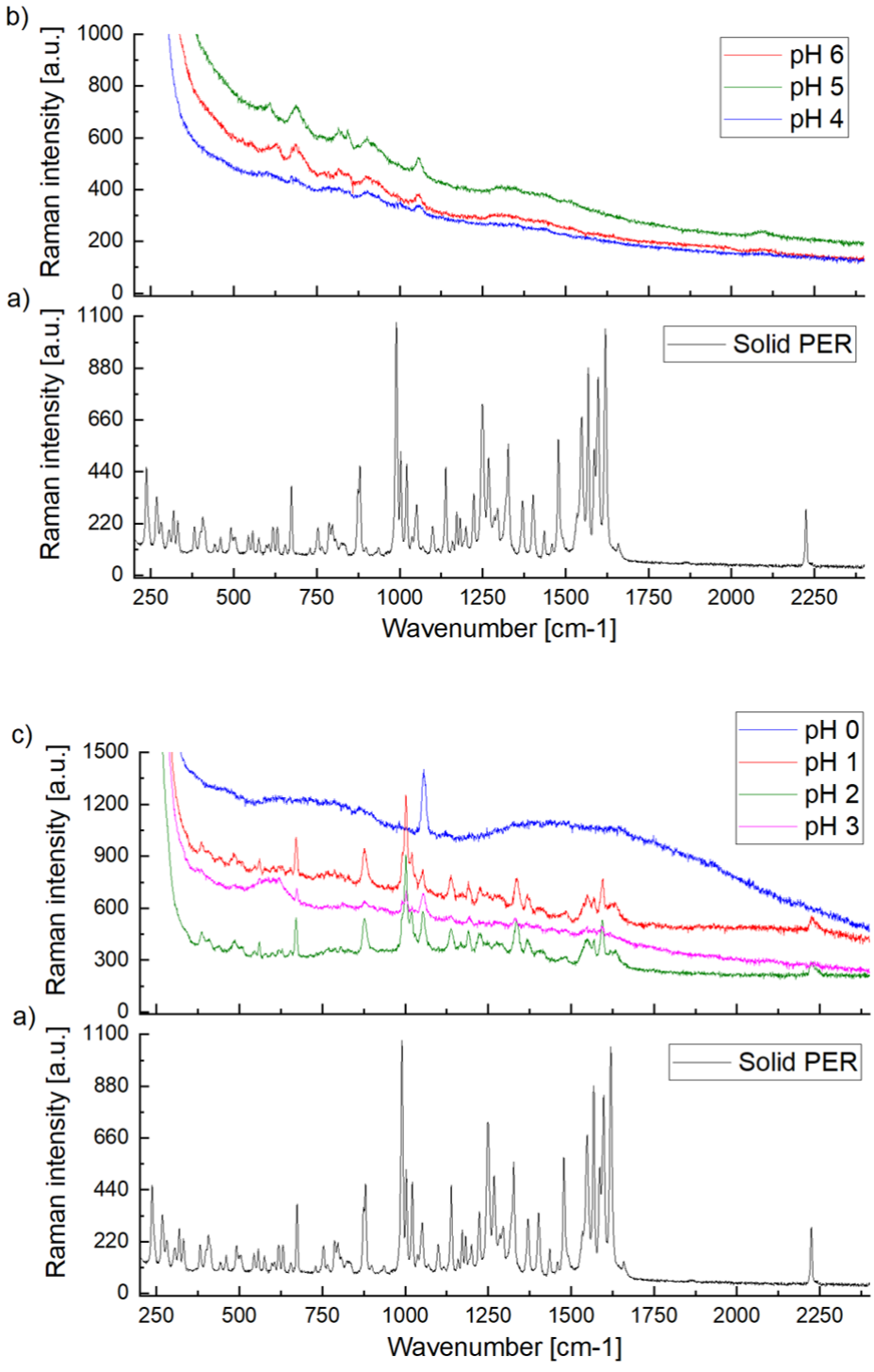

Figure 5.1: *a*) Raman spectrum of solid PER using 785nm excitation. *b*) SERS spectra of PER at pH 6 (red), 5(green), and 4(blue). *c*) SERS spectra of PER at ph 3(magenta), 2(green), 1(red) and 0(blue). All the SERS spectra are collected at the solid-liquid interface.

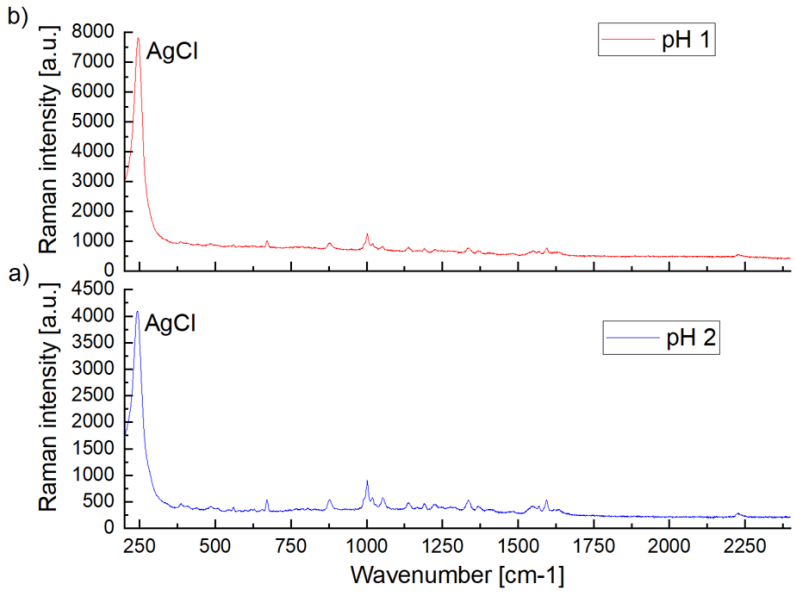

Figure 5.2: Comparison of the AgCl peaks heights in *a*) SERS spectrum obtained at pH 1 and *b*) SERS spectrum obtained at pH 2. Both SERS spectra are collected at the solid-liquid interface.

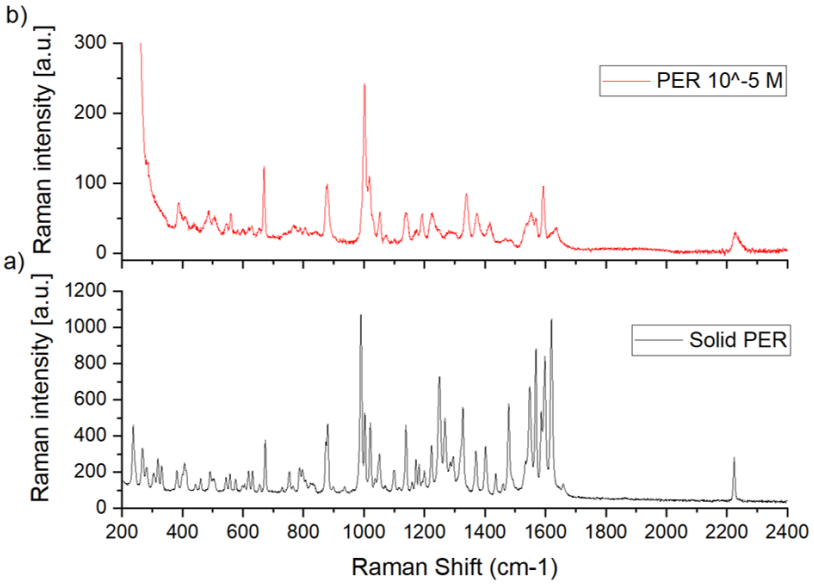

Figure 5.3: *a*) Raman spectrum of solid PER using 785nm excitation (1 mW power). *b* SERS spectrum using 785 nm excitation (0,1 mW power) of PER $10^{-5}M$ at pH 2. The spectrum was collected at the solid-liquid interface.

5.1.1 Au NPs substrates

Experimental setup

The SERS spectra on Au substrates were collected at pH2, which was the optimal value determined on Ag substrates. The spectra were collected for both $10^{-4}M$ and $10^{-5}M$ PER and the sample prepared in the same way as for the SERS measurements on Ag substrates. The spectra were recorded using a 785 nm laser excitation, 1 mW power, 60 seconds exposure time (2 averages). To focus the radiation on the substrate a 50x microscope objective with $NA = 0,75$ was used.

Results

The results of the SERS measurements are shown in Fig. 5.4. The features of PER are still noticeable in both spectra, but the relative intensities are much decreased with respect to the spectra collected on Ag. Hence, the Au nanoparticles appear to be less performant than the Ag nanoparticles. The reason might be that the plasmon of the Au NPs substrate is less matched with the laser radiation at 785 nm. This might be simply due to morphological features in Ag nanoparticles might favour the interaction with the radiation with respect to Au nanoparticles.

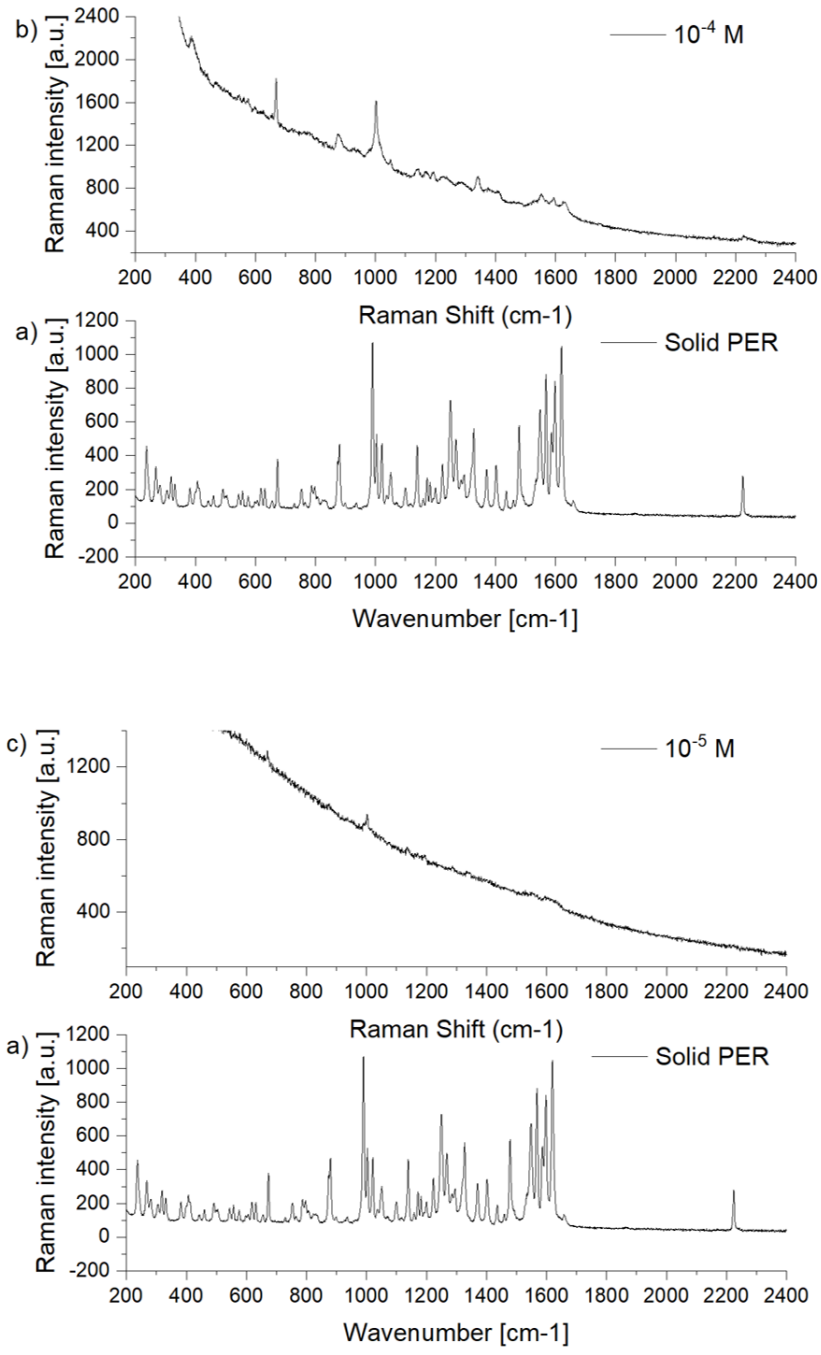

Figure 5.4: *a*) Raman spectrum of solid PER using 785nm excitation. *b*) SERS spectrum of PER at $10^{-4}M$ and *c*) SERS spectrum of PER at $10^{-5}M$, both collected using 785 nm excitation, 1mW power, 60 s exposure time (2 averages)

To verify the situation, SEM micrographs of the colloids deposited on Si supports were analyzed (Fig. 5.5). As expected, the micrographs reveal a substantial difference in morphological features. In addition to spherical nanoparticles, the Ag structure feature a rods structure, which introduces new plasmonic modes (one transversal and one longitudinal), that increase the resonance at longer wavelengths (longitudinal plasma resonances) and amplifies the electromagnetic enhancement at the basis of SERS.

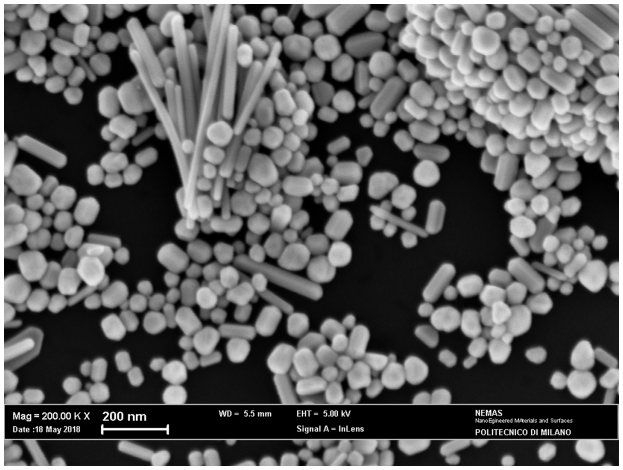

(a)

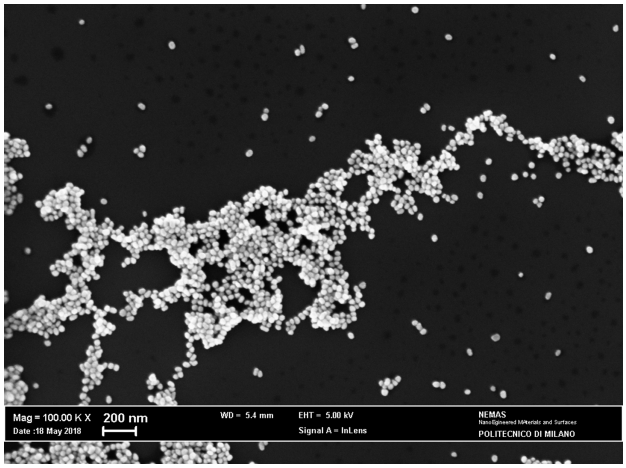

(b)

Figure 5.5: *a*) SEM image of the Ag nanoparticles substrate highlighting its rods structure and *b*) SEM image of the Au nanoparticles substrate showing its lack of a rods structure. The SEM images were collected as part of a parallel thesis work by the colleague Federica Iacoe.

5.2 The role of the acid

The issue about the change of SERS spectra between dry and wet droplets has been highlighted earlier. Upon drying on the surface, the spectra of PER becomes slowly less visible until it is not anymore detected when the droplet has completely dried. This is probably due to the mentioned excess of Cl^- ions in the droplet, which modifies the dielectric environment of the nanoparticles and shifts the plasma resonance. To confirm this observation, the SERS spectrum of PER was collected at increasing time since the deposition of the droplet. The results are shown in Fig. 5.6. It can be seen that the signal of PER disappears upon drying, as just 15 minutes after the deposition the signal has decreased significantly.

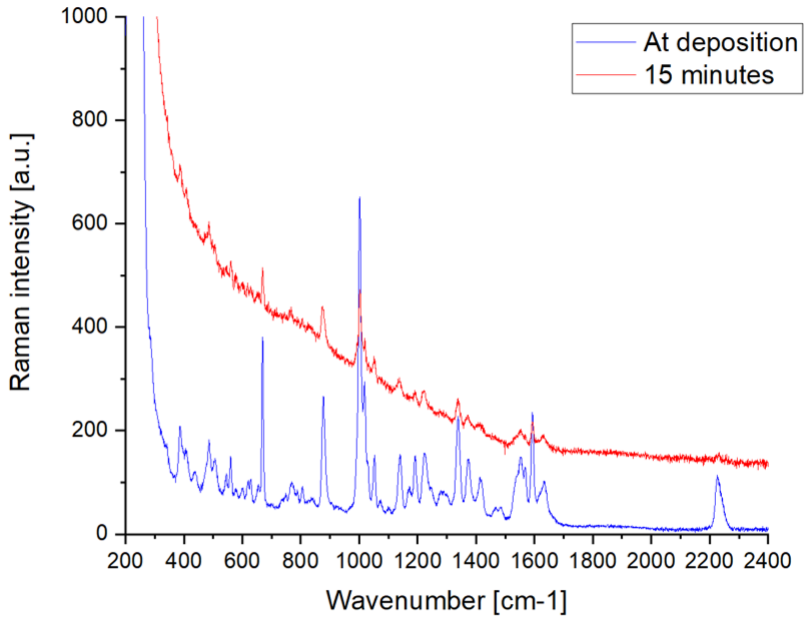

Figure 5.6: SERS spectra of PER deposited from a pH 2 solution, which acidity was achieved through the exclusive use of HCl. *a*) Spectrum obtained at the time of deposition, *b*) spectrum obtained 15 minutes after deposition. The marked decrease in relative intensity of the PER signal is clearly shown.

At the same time the AgCl peak sharply increases, as shown in Fig. 5.7. Although pH 2 is the best condition for SERS sensing of PER, the experiment just described shows that excess of Cl^- leads to detrimental effects on the SERS signal of PER. Hence, for a better measurement conditions, I have used a mixture of hydrochloric acid and sulphuric acid to reach the desired pH, in such a way that the number of chlorine ions would be limited. Sulphuric acid was selected due to

the reduced affinity of HSO_4^- with Ag with respect to Cl^-, as sulphuric acid metal salts dissolve readily in aromatic hydrocarbons[33].

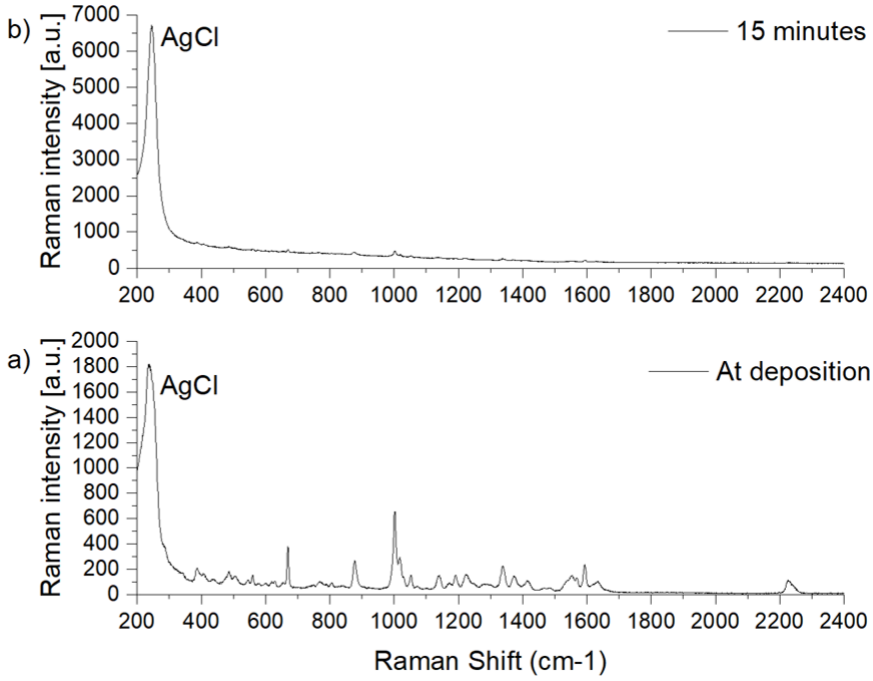

Figure 5.7: SERS spectra of PER deposited from a pH 2 solution, where the acidic condition was achieved with the exclusive use of HCl. *a*) Spectrum obtained at the time of deposition, *b*) spectrum obtained 15 minutes after deposition. The sharp increase in intensity of the AgCl peak is clearly shown, going from about 1800 to almost 7000.

5.2.1 HCl and sulphuric acid mix tests

Experimental setup

Several acid ratios $HCl : H_2SO_4$ have been considered and tested, namely 1/4, 1/9, 1/19 (molar ratios) This has been achieved by mixing the suitable amounts of acids to reach a total of 2,7 mL of acidic solution at pH 2. 0,3 mL of PER in methanol solution ($10^{-3}M$ of PER) was then added to achieve a total concentration of both $10^{-4}M$ and $10^{-5}M$. The spectra were collected using 785 nm excitation, 0,1 mW power, 10 s exposure time (3 averages) and using a 50x objective. The spectra were collected at the surface of a completely dried SERS substrate after the drop casting of the prepared acidic solutions of PER.

Results

The results, reported in Fig. 5.8, 5.9, and 5.10, are positive and confirm our previous considerations. Contrarily from what found when using HCl alone, the SERS spectra can be seen at every acid ratio, when the droplet has fully dried. One notable phenomenon, observed in Fig. 5.11 is that at the 1:19 acid ratio for PER $10^{-4}M$, the SERS signal of PER does not show, leaving in its place a signal similar to sodium citrate, which is used to produce the colloidal silver nanoparticle substrate[34]. Therefore, the use of chlorine ions is crucial not only for the bridging of PER on the NPs, but also thanks to its action on sodium citrate molecules, which are displaced from th metal surface when the ions form their shell around the Ag nanoparticles. It is very likely that when the amount of Cl^- is too low, sodium citrate cannot be displaced from the nanoparticles. This does not happen when the same acid ratio is tested on PER $10^{-5}M$, most probably since the analyte molecules are less than before, more chlorine ions are available to displace citrate.

This finding discussed above raise an interesting further consideration. Depending on PER concentration and the exposed surface of the SERS substrate, two apparently opposite phenomena regulate the SERS action.

1. Chlorine ions should be present in a sufficient amount in order to displace sodium citrate;

2. Chlorine ions cannot exceed a given amount, which should correspond to the formation of a complete shell around the nanoparticles. Exceeding that amount the layer of chlorine ions would hinder the bridging of the PER-H^+-chlorine couples on the nanoparticles.

However, for the concentrations of PER that are expected in human samples, the 1:9 ratio seems the most suitable for a reliable SERS detection. Nevertheless, specific optimal ratios for different concentrations could be considered in future studies to develop a more controlled and optimized technique.

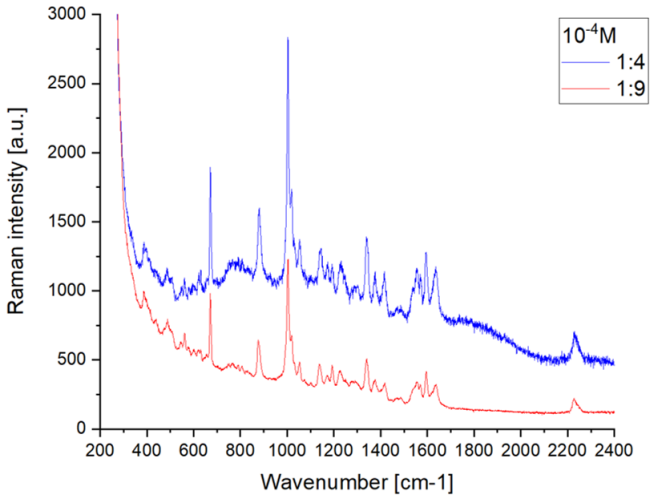

Figure 5.8: SERS spectra of PER $10^{-4}M$ using the hydrochloric and sulphuric acids mix. In red the spectrum obtained using a 1:9 hydrochloric/sulphuric ratio, in blue the spectrum collected using a 1:4 ratio. The spectra were collected using 785 nm excitation, 0,1 mW power, 10 s exposure time (3 averages).

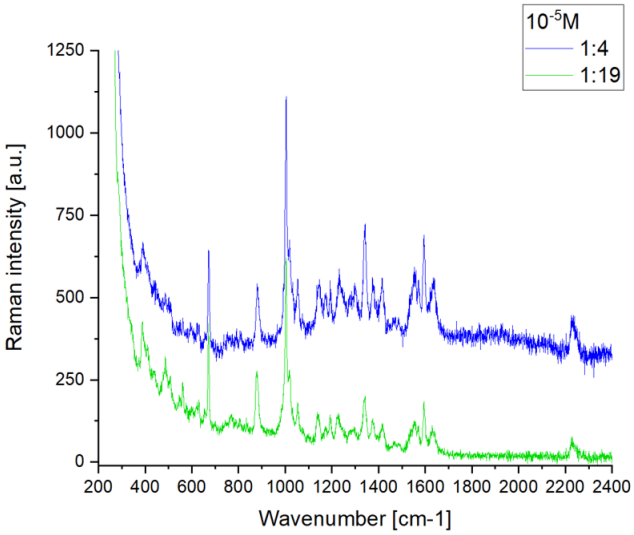

Figure 5.9: SERS spectra of PER $10^{-5}M$ using the hydrochloric and sulphuric acids mix. In green the spectrum obtained using a 1:19 hydrochloric/sulphuric ratio, in blue the spectrum collected using a 1:4 ratio. The spectra were collected using 785 nm excitation, 0,1 mW power, 10 s exposure time (3 averages).

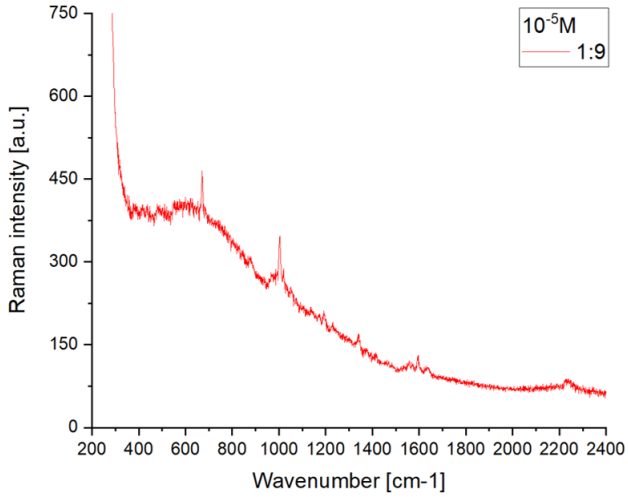

Figure 5.10: SERS spectrum of PER $10^{-5}M$ using the hydrochloric and sulphuric acids mix. In red the spectrum obtained using a 1:9 hydrochloric/sulphuric ratio. The spectrum was collected using 785 nm excitation, 0,1 mW power, 10 s exposure time (3 averages).

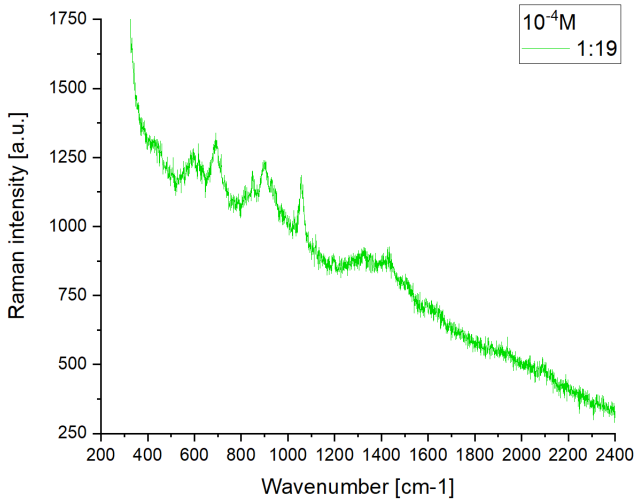

Figure 5.11: SERS spectrum of PER $10^{-4}M$ using the hydrochloric and sulphuric acids mix. In green the spectrum obtained using a 1:19 hydrochloric/sulphuric ratio. the spectrum shows similar features to the spectrum of sodium citrate[34], showing the similar features. The spectrum was collected using 785 nm excitation, 0,1 mW power, 10 s exposure time (3 averages).

Chapter 6

SERS detection of PER on substrates made by PLAL

As discussed in Ch. 3, nanoparticles produced by PLAL lead to substrates which possess many technical and production advantages, namely the absence of stabilizing agents (such as citrate), a better control on particle size and controlled deposition by spraying. The best features of these substrates is their morphological homogeneity and production repeatability. If PLAL reveals to be a technique capable of producing nanostructured surfaces with high electromagnetic enhancement properties, this points combined with the aforementioned advantages, would make PLAL substrates the best candidates for systematic application of SERS in therapeutic drug monitoring. The substrates used in this experiments have been received from a collaboration with E. Fazio from Messina University, Sicily.

The substrates employed in the experiments are the following (one sample for each kind was available.):

1. **nAg**: Ag sample prepared using nanoseconds laser and deposited on a Si support;
2. **pAg**: Ag sample prepared using picoseconds laser and deposited on a Si support;
3. **nAu**: Au sample prepared using nanoseconds laser and deposited on a Si support;
4. **pAu**: Au sample prepared using picoseconds laser and deposited on a *glass* (microscope slide) support;
5. **AgAu 50/50**: Ag and Au alloy sample containing a 50/50 ratio of Ag and Au particles respectively. Made using picoseconds laser and deposited on a Si support.

6. **IrrAgAu 50/50**: Ag and Au alloy sample containing a 50/50 ratio of Ag and Au particles respectively. Made using picoseconds laser, deposited on a Si support and irradiated for 20 minutes with a nanoseconds laser.

7. **AgAu 75/25**: Ag and Au alloy sample containing a 75/25 ratio of Ag and Au particles respectively. Made using picoseconds laser and deposited on a Si support.

8. **IrrAgAu 75/25**: Ag and Au alloy sample containing a 75/25 ratio of Ag and Au particles respectively. Made using picoseconds laser, deposited on a Si support and irradiated for 20 minutes with a nanoseconds laser.

Due to the minimal number of samples available for each kind of SERS substrate, an oculate selection of the procedure and experimental setup organization had to be made. This was possible based on the experience gained working with Ag/Au colloids prepared by chemical methods (see Ch. 5). As for the preparation of the PER solutions, the ratio of 1:9 hydrochloric acid versus sulphuric acid was selected, and concentrations of PER of $3x10^{-4}M$ for the single-metal substrates and $1x10^{-4}M$ for the alloys were considered. Finally, for every substrate the choice of the excitation wavelength is also important. To obtain the electromagnetic enhancement, the radiation wavelength should be as close as possible to the frequency of the plasmon of the substrate. Based on the data provided by E. Fazio and the available instrumentation, a suitable choice has been made, as indicated below.

6.1 SERS of PER on ns-PLAL Ag substrates

Experimental setup

Aqueous solutions were made mixing hydrochloric acid and sulphuric acid in a ratio 1:9 with water to obtain 2,7 mL at pH 2. Subsequently 0,3 mL of a solution of PER ($3x10^{-3}M$) dissolved in methanol was added to obtain a total concentration of $3x10^{-4}M$. A 20 μL droplet was deposited on the substrates. Spectra were collected using a 458 nm excitation (blue) focused with a 50x objective. 1mW laser power was employed with 30 seconds exposition time (2 averages). The spectra were collected at both the solid-liquid interface and at dry droplet at the following times: 0, 8 minutes, 15 minutes and 25 minutes.

Results

Obtaining a satisfactory SERS spectrum on nanosecond PLAL substrate proved to be problematic. By taking a close look at the surface of the substrate shown in Ch.

3, the morphology reveals a rather low density of nanoparticles with respect to the substrates made with the colloids prepared by chemical route. This is likely to be the main reason for the much lower SERS signal observed. Moreover, the thickness of the substrates is most likely fairly thin, as one can deduce from the strong signal coming from the Si support, which is evident in Fig. 6.1. The intensity and quality

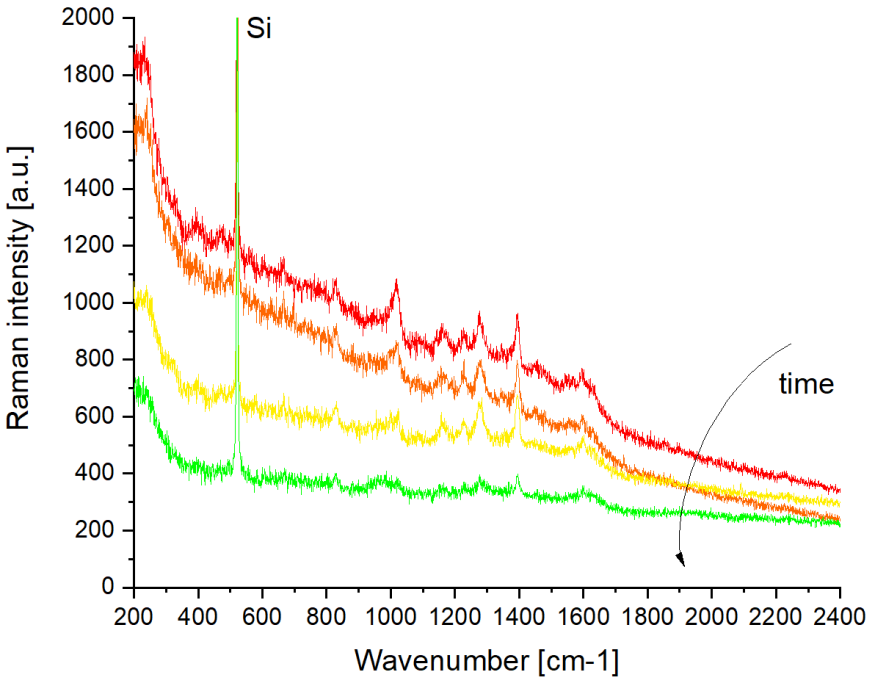

Figure 6.1: SERS spectra of PER on nanosecond-PLAL Ag substrate. Spectra were collected using a 458 nm excitation (blue) focused with a 50x objective. 1mW laser power was employed with 30 seconds exposition time (2 averages). The spectra were collected at both the solid-liquid interface and at dry droplet.

of the signal decreases as the SERS substrate dries, similarly to what is described in Ch. 5 when the acidic solution was made only using hydrochloric acid. A similar phenomenon it is likely what we have here, but the proving analysis with solution made using HCl could not be made due to the unavailability of further substrates. However, when the SERS substrate is still wet, most of the features of PER are slightly detected (Fig. 6.2). Therefore, for the next samples, measurements were performed at the solid-liquid interface, on wet SERS substrates.

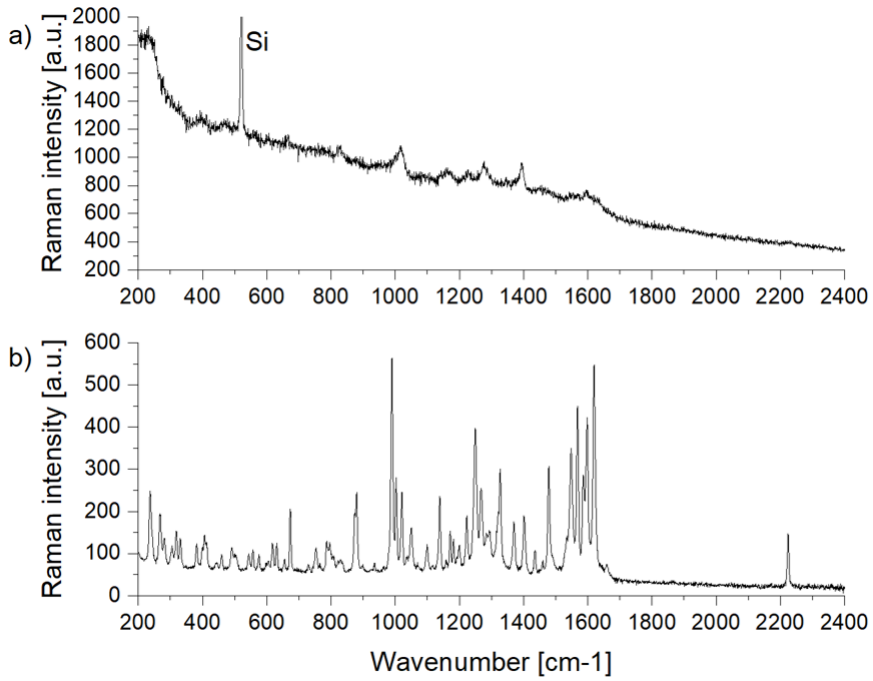

Figure 6.2: a) SERS spectrum of PER on the solid-liquid interface of a nanosecond-PLAL Ag substrate collected using a 458 nm excitation (blue) focused with a 50x objective. 1mW laser power was employed with 30 seconds exposition time (2 averages). b) Raman spectrum of solid PER, collected using 785 nm excitation, 10 mW laser power, 10 s exposure time (3 averages).

6.2 SERS detection on ps-PLAL Ag substrates

Experimental setup

Aqueous solutions were made mixing hydrochloric acid and sulphuric acid in a ratio of 1:9 with water to obtain 2,7 mL at pH 2. Subsequently 0,3 mL of a solution of PER dissolved in methanol was added to obtain a total concentration of $3x10^{-4}M$. A 20 μL droplet was deposited on the substrates. Spectra were collected using a 458 nm excitation (blue) focused with a 50x objective. 0,1mW, 1mW and 10mW laser powers were employed. The spectra were collected at both the solid-liquid interface and at dry droplet in consecutive times, before the complete drying.

Results

The experiment was carried out assuming that a picosecond PLAL substrate would do a better job with SERS due to its more populated and homogeneous surface.

Initially, 0,1 mW laser power was employed and a long measurement was set. However, it revealed a non-satisfactory SERS spectrum. The spectrum, shown in Fig. 6.3, features two large bands from 1100 cm^{-1} to 1700 cm^{-1}, which are similar to the G and D peaks that would be observed in a condition of photo-degraded analyte. Nevertheless, the low laser power employed makes this conclusion rather unlikely. Then the focus was moved to another point and the laser power was increased to 1 mW, decreasing significantly the exposure time from 100 s to 20 s, in order to avoid a possible damage (Fig. 6.4). The signal collected shows a high noise and the anomalous bands were recorded once again.

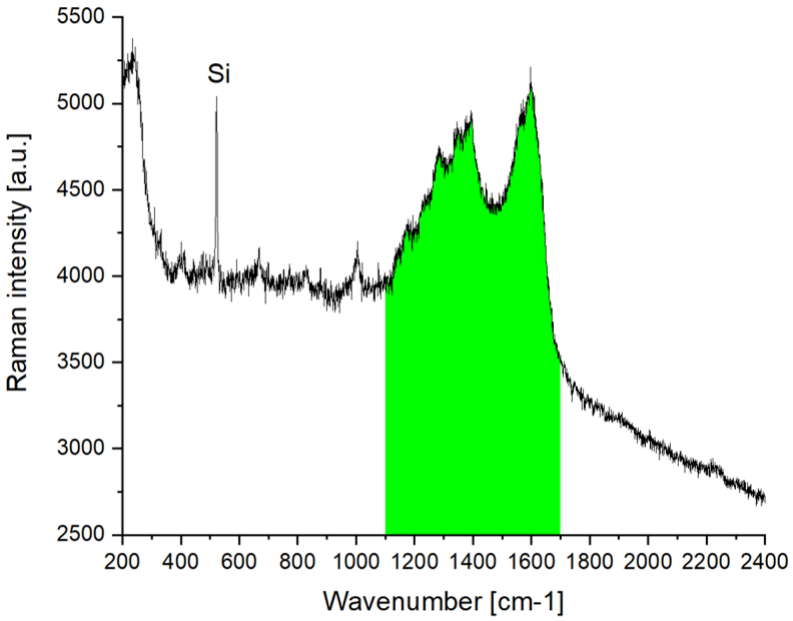

Figure 6.3: SERS spectrum of PER on picosecond-PLAL Ag substrate. 458 nm excitation, 0,1 mW laser power, 100 seconds exposure time (5 averages). In green the two bands suggesting analyte photodamage are highlighted.

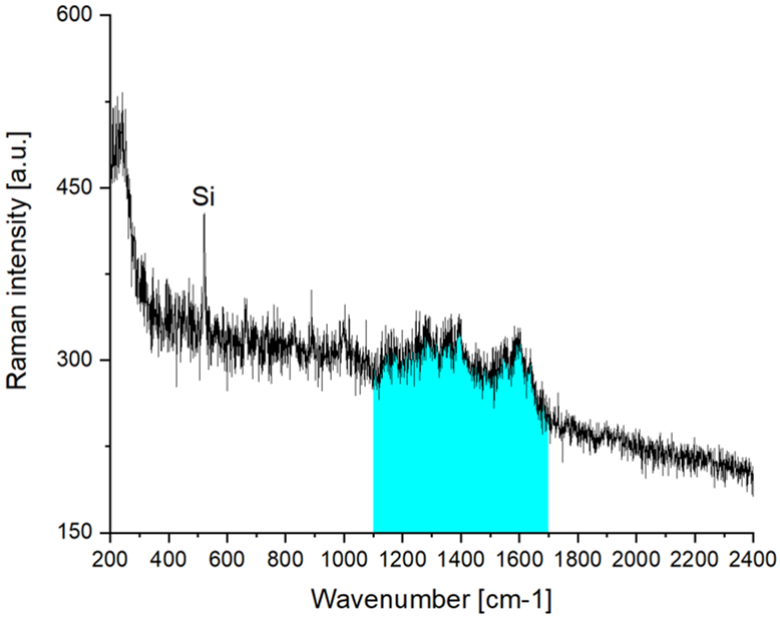

Figure 6.4: SERS spectrum of PER on picosecond-PLAL Ag substrate. 458 nm excitation, 1 mW laser power, 20 seconds exposure time (2 averages). In cian the two bands suggesting analyte photodamage are highlighted.

Finally, the laser power was set to 10 mW and in this case a good SERS spectrum was recorded. Therefore consecutive spectra were collected (fig.6.5) until the droplet dried to check the phenomena observed before for the Ag ns-PLAL. The SERS spectrum reported in Fig. 6.7 shows that the analyte is photo-degraded in the process. Nevertheless the spectra taken at the solid-liquid interface when the droplet was still drying show all the features of PER (Fig.), even showing the CN stretching at around 2250 cm^{-1} (fig.6.8). Therefore, to obtain a satisfactory signal, showing all feature of PER using picoseconds PLAL Ag substrate is necessary to use high laser power with short exposure time to avoid damaging the analyte. Another possible option for further study could be to further lowering the amount of HCl used in the preparation of the solution, as drying effects similar to the case of colloidal substrates are observed (Fig. 5.6).

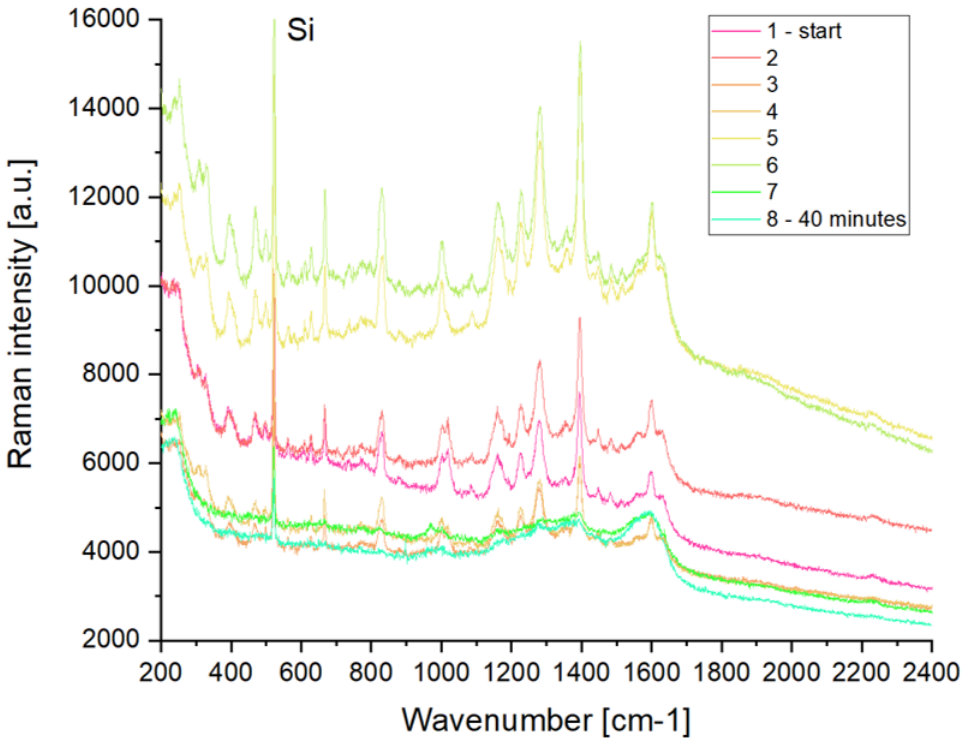

Figure 6.5: SERS spectrum of PER on picosecond-PLAL Ag substrate. 458 nm excitation, 10 mW laser power, 20 seconds exposure time (2 averages). The spectra were collected at increasing times for 40 minutes until the droplet was dry.

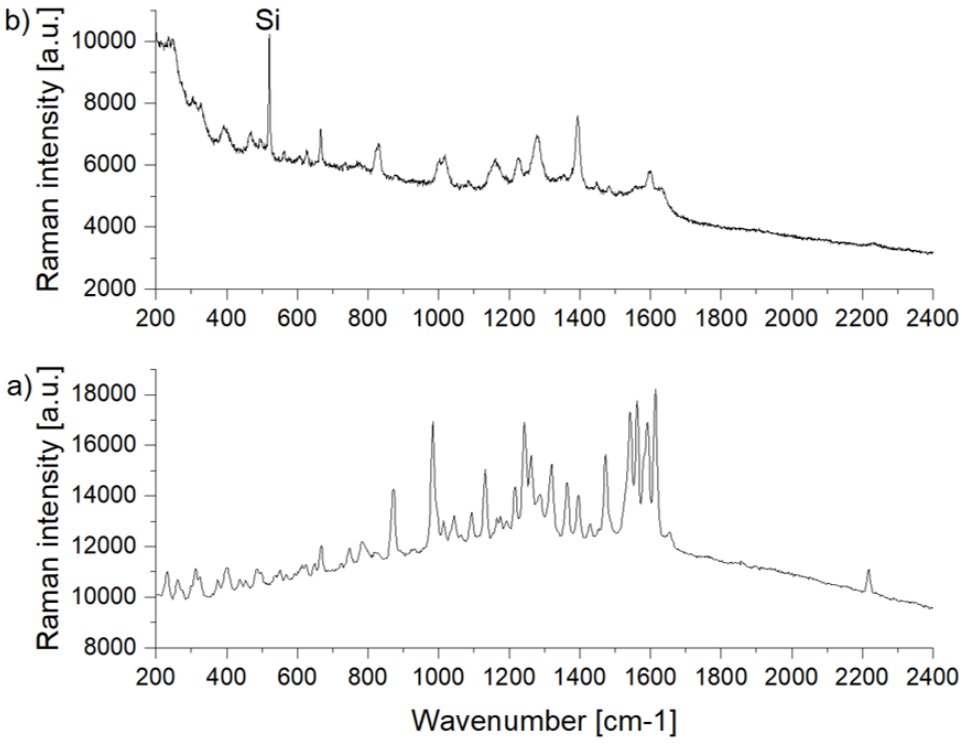

Figure 6.6: b) SERS spectrum of PER on the solid-liquid interface of a nanosecond-PLAL Ag substrate collected using a 458 nm excitation (blue) focused with a 50x objective. 10 mW laser power was employed with 20 seconds exposition time (2 averages). a) Raman spectrum of solid PER, collected using 514 nm excitation, 10 mW laser power, 10 s exposure time (3 averages).

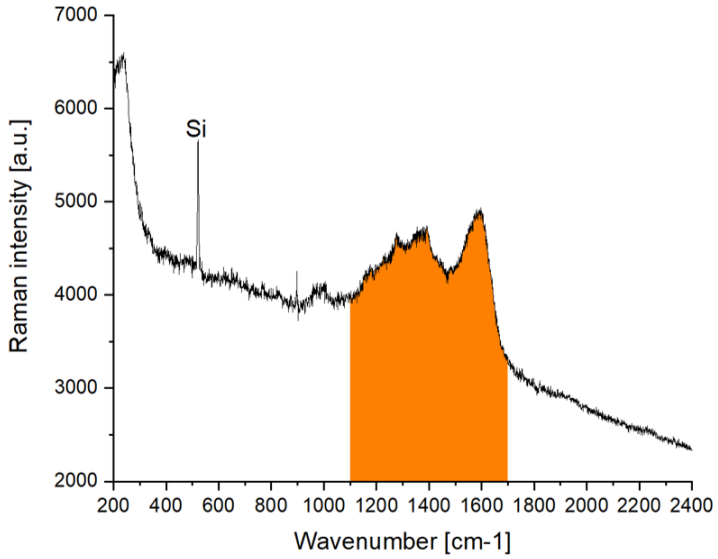

Figure 6.7: SERS spectrum of PER on picosecond-PLAL Ag substrate. 458 nm excitation, 10 mW power, 20 seconds exposure time (2 averages). In orange the two bands suggesting analyte photodamaging are highlighted.

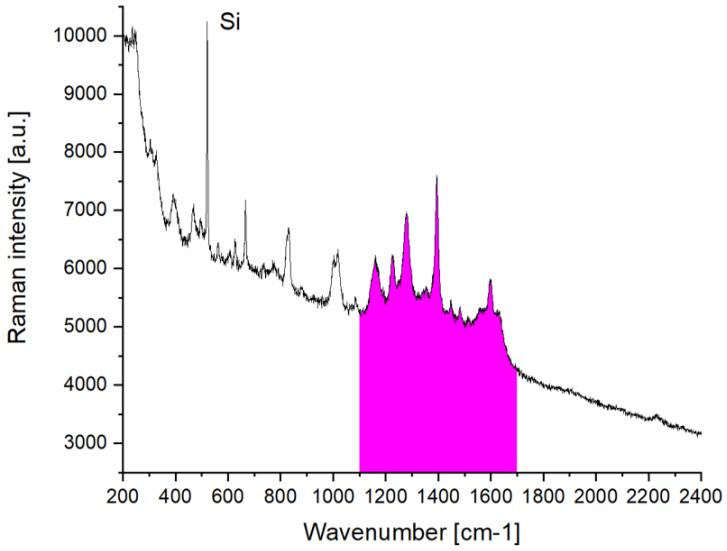

Figure 6.8: SERS spectrum of PER on picosecond-PLAL Ag substrate. 458 nm excitation, 10 mW laser power, 20 seconds exposure time (2 averages). In purple the bands suggesting the start of the analyte photodamaging process are highlighted.

6.3 SERS detection on ns- and ps-PLAL Au substrates

Experimental setup

Aqueous solutions were made mixing hydrochloric acid and sulphuric acid in a ratio of 1:9 with water to obtain 2,7 mL at pH 2. Subsequently 0,3 mL of a solution of PER ($3x10^{-3}M$) dissolved in methanol was added to obtain a total concentration of $3x10^{-4}M$. A 20 μL droplet was deposited on the substrates. Spectra were collected using a 785 nm excitation (red) focused with a 50x objective on the solid-liquid interface.

Results

The ns-Au substrates used for this experiments are characterized by a very thin layer of sprayed nanoparticles, for this reason the spectra feature a very strong Si peak. By zooming, the expected features of PER are mostly visible, although with a low relative intensity (Fig. 6.9). To record a spectrum that can reveal the presence of PER, a power of 10 mW was employed (Fig. 6.10). In this case, no signs of degradation were identified.

As for ps-Au substrates, the nanoparticles were deposited on glass, which brings concerns with respect to the measurements, being glass a fairly good Raman scatterer with 785 nm excitation. Moreover, the nanoparticle layer thickness is the lowest observed so far. Therefore, as expected, at lower laser power the signal of PER could not be spotted whatsoever (Fig. 6.11). By rising the power to 10 mW some features of PER could be detected, although accompanied the strong background signal from glass and, possibly, the onset of the G, D, bands suggesting photo-degradation.

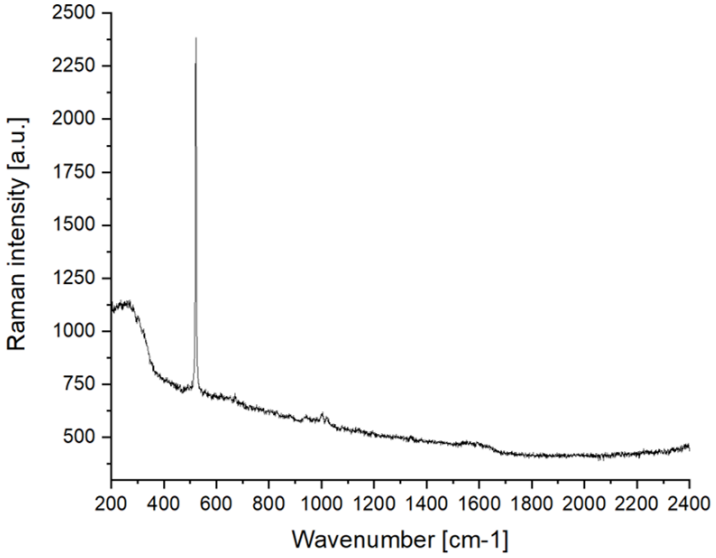

Figure 6.9: SERS spectrum of PER detected on ns-Au substrate. 785 nm excitation, 0,1 mW power, 20 s exposure time (2 averages).

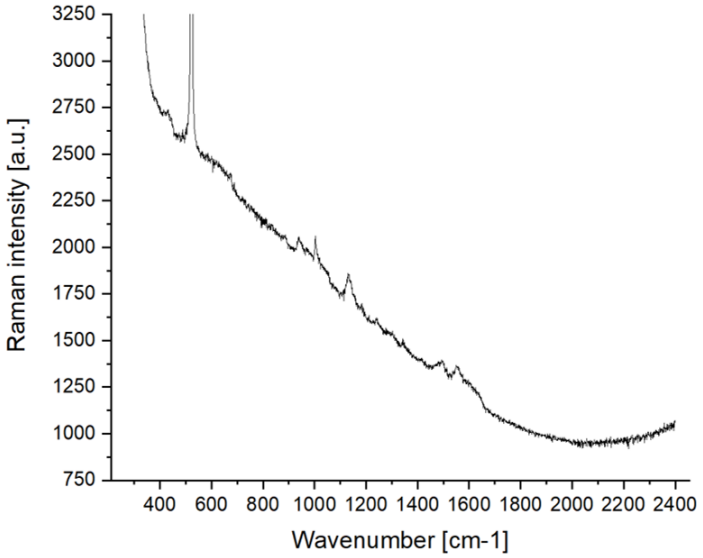

Figure 6.10: SERS spectrum of PER detected on ns-Au substrate. 785 nm excitation, 10 mW power, 20 s exposure time (2 averages).

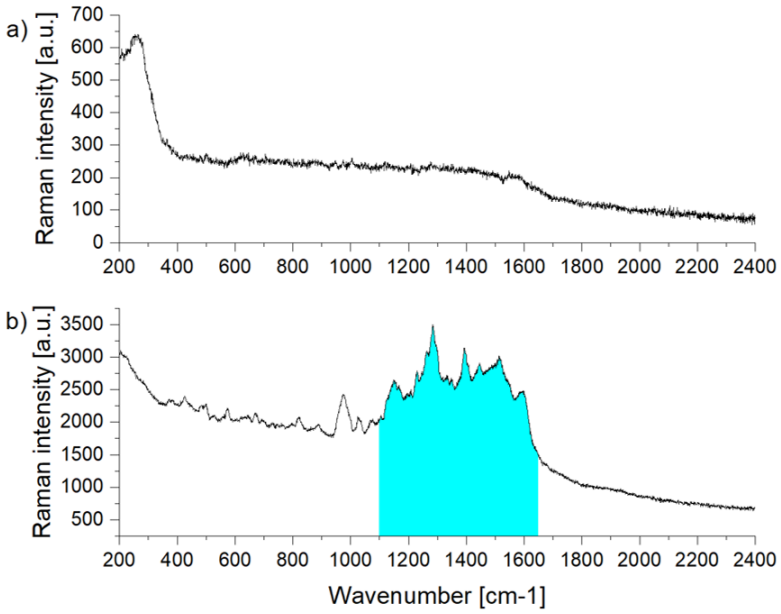

Figure 6.11: SERS spectra of PER detected on ps-Au substrate. 785 nm excitation, 20 s exposure time (2 averages). a) spectrum detected with 1 mW laser power and b) spectrum detected with 10 mW laser power. In cian the fluorescent band is highlighted.

6.4 SERS detection on Ag/Au alloys substrates

Experimental setup

Aqueous solutions were prepared mixing hydrochloric acid and sulphuric acid in a ratio of 1:9 with water to obtain 2,7 mL at pH 2. Subsequently 0,3 mL of a solution of PER ($10^{-3}M$) dissolved in methanol was added to obtain a total concentration of $10^{-4}M$. A 20 μL droplet was deposited on the substrates. Spectra were collected using a 514 nm excitation (green) focused with a 50x objective. The optical settings were fixed to 20 s exposure time (3 averages), with 0,1 mW and 1 mW laser power. The SERS measurement was collected when the droplet was completely dry.

Results - 50:50 Ag/Au alloy

The SERS spectrum collected at 0,1 mW laser power (Fig. 6.12) did not show the spectral features of PER, even though some hints could be spotted in the high noise spectrum. By rising the exposure time and averages the noise could be lowered, but not enough to show the signals of PER in a satisfactory way. At 1 mW laser power (Fig. 6.13) some features are visible, such as the peaks at around 1000 cm^{-1} and the peaks around 1600 cm^{-1}, which in this spectrum are clustered in a large band. At higher power a better spectrum should be recordable, but with a very high risk of photo-degradation.

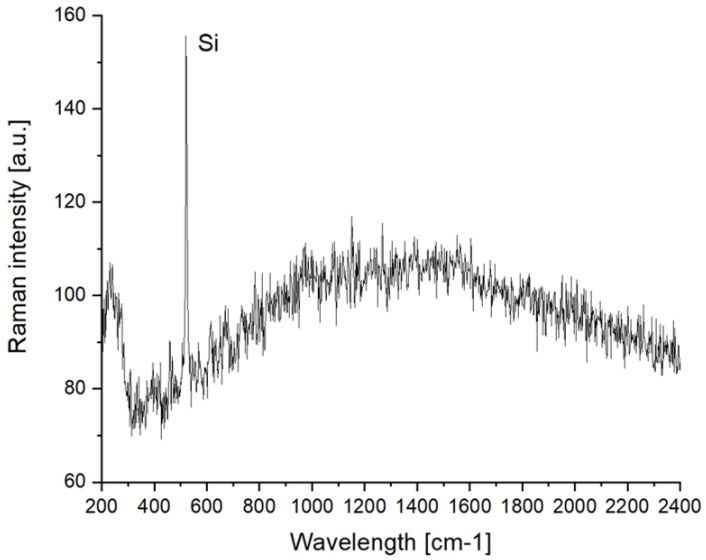

Figure 6.12: SERS spectrum of PER detected on a 50:50 Ag-Au alloy substrate using 514 nm laser excitation, 0,1 mW laser power, 20 seconds exposure time (3 averages).

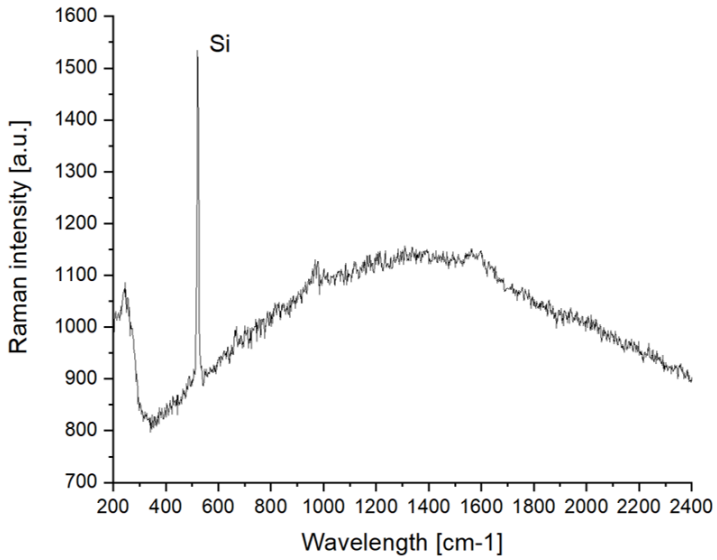

Figure 6.13: SERS spectrum of PER detected on a 50:50 Ag-Au alloy substrate using 514 nm laser excitation, 1 mW laser power, 20 seconds exposure time (3 averages).

Results - 75:25 Ag/Au alloy

For this SERS substrate the situation is analogous to the previous case. At 0,1 mW the signal is dominated by noise, even though the peak at 1000 cm^{-1} is slightly visible (Fig. 6.14). The scenario gets better at 1 mW where the features at 1000 cm^{-1} and 1600 cm^{-1} are better detected (Fig. 6.15). The latter group of peaks appear again clumped in a band due to the low quality of the signal.

It can be noticed how the intensity of the SERS signal for the 75:25 alloy is about 4 times that scattered by the 50:50 alloy. This is most likely due to the fact that the larger presence of Ag nanoparticles in the alloy shifts the plasmonic frequency of the substrate closer to the excitation used for the detection of the spectra.

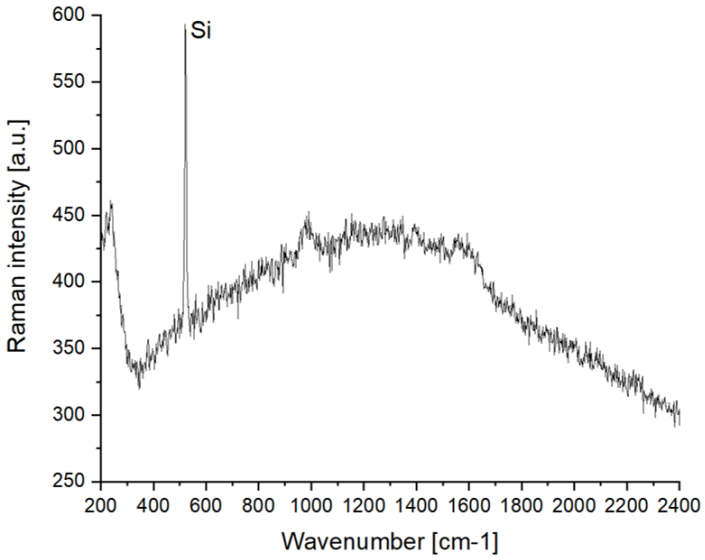

Figure 6.14: SERS spectrum of PER detected on a 75:25 Ag-Au alloy substrate using 514 nm laser excitation, 0,1 mW laser power, 20 seconds exposure time (3 averages).

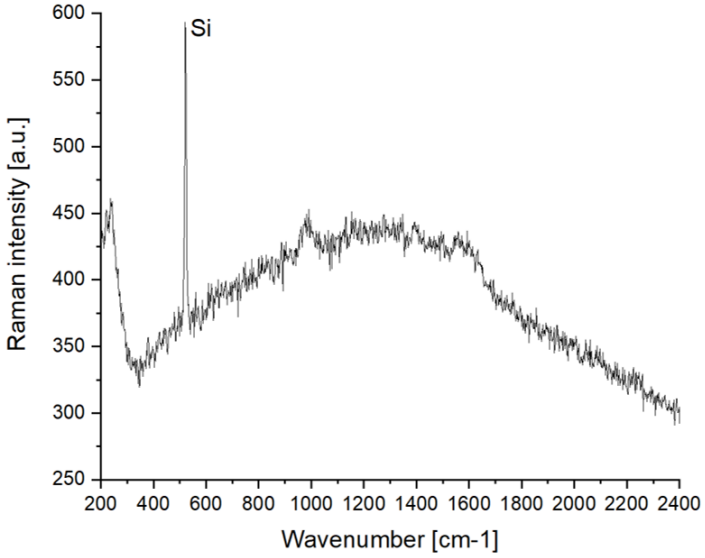

Figure 6.15: SERS spectrum of PER detected on a 75:25 Ag-Au alloy substrate using 514 nm laser excitation, 1 mW laser power, 20 seconds exposure time (3 averages).

6.5 SERS detection on irr-Ag/Au alloys substrates

Experimental setup

Aqueous solutions were prepared mixing hydrochloric acid and sulphuric acid in a ratio of 1:9 with water to obtain 2,7 mL at pH 2. Subsequently 0,3 mL of a solution of PER ($10^{-3}M$) dissolved in methanol was added to obtain a total concentration of $10^{-4}M$. A 20 μL droplet was deposited on the substrates and let dry. Spectra were collected using a 514 nm excitation (green) focused with a 50x objective. For both alloys, a long measurement using 0,1 mW, with 50 seconds exposure time (3 averages) was collected, then 1 mW and 10 mW laser power were used with 10 seconds exposure time (2 averages). For the 75:25 alloy the spectrum at 1 mW was not recorded as it will be shown that the analyte would be damaged.

Results - 50:50 irr-AgAu alloy

The SERS spectrum collected at 0,1 mW (Fig. 6.16) can show most of the spectral features of PER, although with a high noise. The peak at 1000 cm^{-1} is defined and comparing with the experiments done on non-irradiated substrates, the peaks at around 1600 cm^{-1} are more resolved. Interestingly, at 1 mW (Fig. 6.17) the spectral features of PER are less visible and at 10 mW the analyte was ultimately photodegraded (Fig. 6.18).

Results - 75:25 irr-AgAu alloy

The results obtained in this case are clearly similar those obtained with the 50:50 alloy substrate. At 0,1 mW (Fig. 6.19) with a long measurement, most of the PER features are visible, while at 1 mW (Fig. 6.20) they become less visible. Compared with the case of the 50:50 alloy substrate, the noise is considerably reduced, most likely due to the plasmonic resonance frequency being closer to the laser excitation.

For both irradiated alloy substrates, the results has proven to be more satisfactory than the ones obtained using non-irradiated alloy samples.

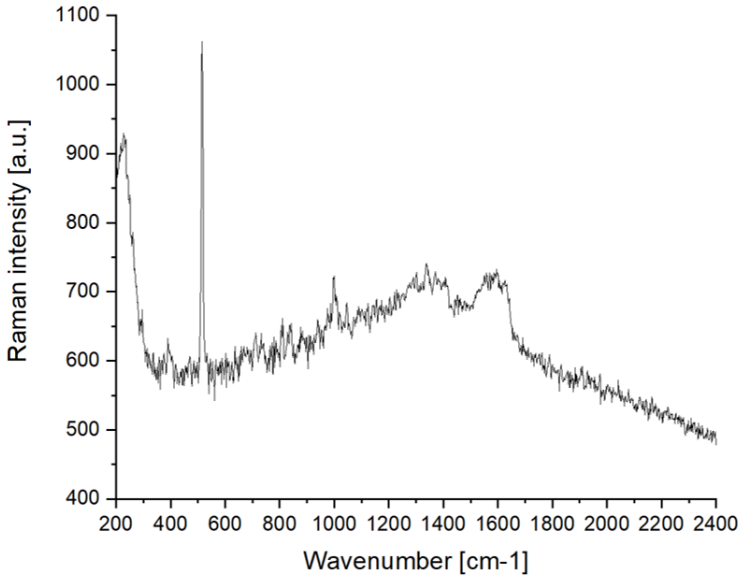

Figure 6.16: SERS spectrum of PER detected on an irradiated 50:50 Ag-Au alloy substrate using 514 nm laser excitation, 0,1 mW laser power, 50 seconds exposure time (3 averages).

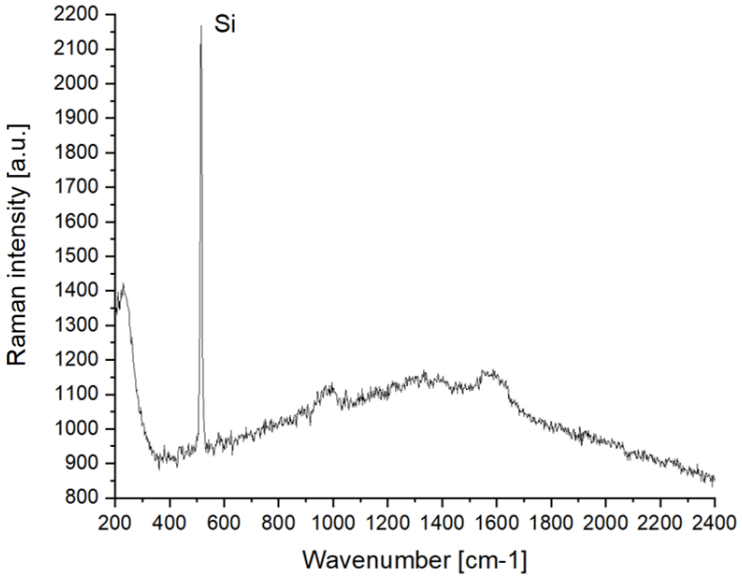

Figure 6.17: SERS spectrum of PER detected on an irradiated 50:50 Ag-Au alloy substrate using 514 nm laser excitation, 1 mW laser power, 10 seconds exposure time (2 averages).

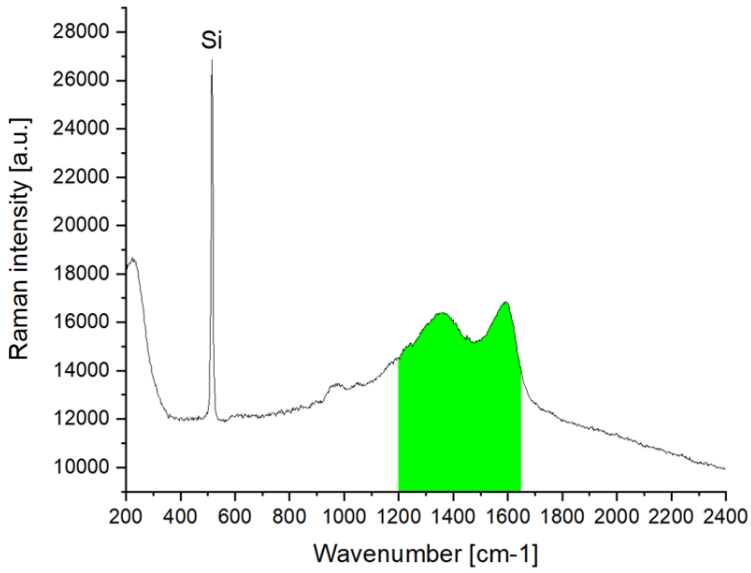

Figure 6.18: SERS spectrum of PER detected on an irradiated 50:50 alloy substrate using 514 nm laser excitation, 10 mW laser power, 10 seconds exposure time (2 averages). In green the bands suggesting analyte damaging are highlighted.

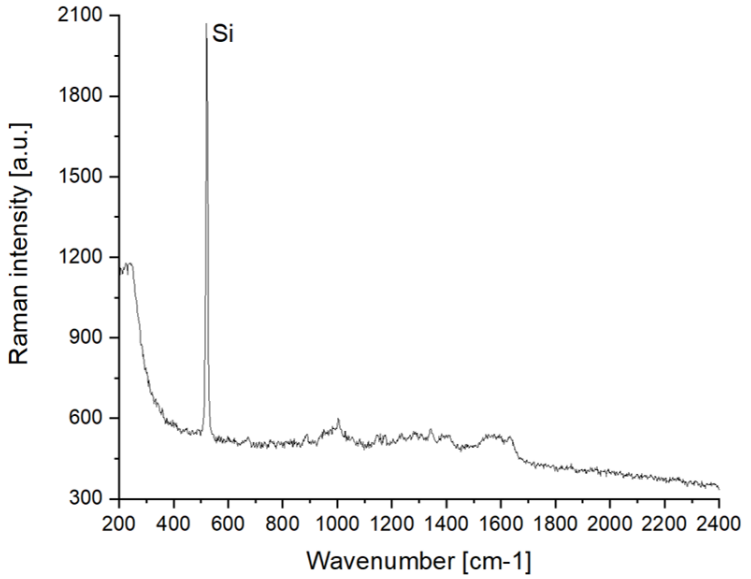

Figure 6.19: SERS spectrum of PER detected on an irradiated 75:25 Ag-Au alloy substrate using 514 nm laser excitation, 0,1 mW laser power, 50 seconds exposure time (3 averages).

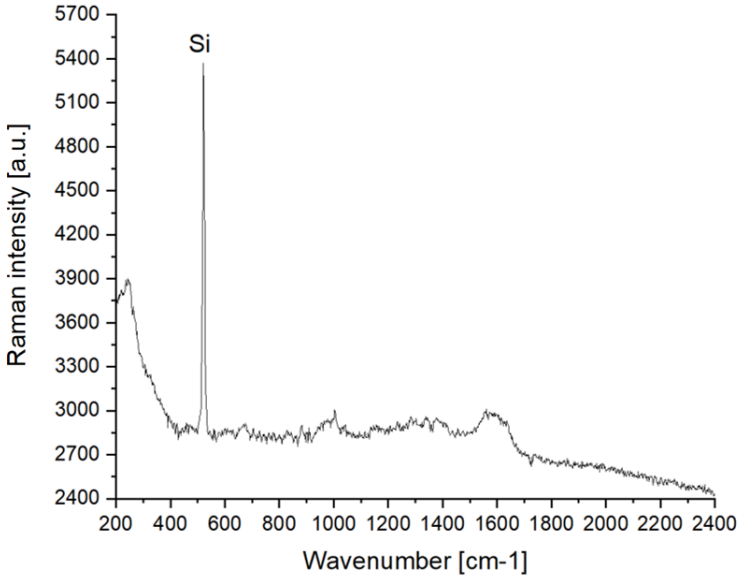

Figure 6.20: SERS spectrum of PER detected on an irradiated 75:25 Ag-Au alloy substrate using 514 nm laser excitation, 1 mW laser power, 10 seconds exposure time (2 averages).

6.6 Concluding remarks

As far as the experiments that could be carried out show, the SERS substrates made of nanoparticles produced by PLAL are a very promising research path that is worth further consideration. Nevertheless, these first-generation PLAL-SERS substrates still cannot match the SERS efficiency displayed by chemically produced colloidal SERS substrates, but there is definitely room to improve the production of the substrates. Moreover, the procedure for the preparation of the analyte solution and deposition can be specifically optimized for PLAL substrates. Suggested research lines are:

1. More alloys can be produced, with different ratios between the metals, to match the plasmonic frequency with the radiation that is intended to employ for the detection.

2. It was shown that the SERS measurements seriously degrade in intensity and quality after the deposited droplet is completely dried. This is an analogous scenario to what already observed for colloidal substrates. Therefore, a specific optimization of the acids ratio in the analyte solution should be investigated also in this case.

Optimizing these aspects, along with the already numerous advantages of PLAL, would most likely establish PLAL as the best production method for SERS detection through controlled and reproducible metallic nanostructures. Another advantage that was noticed during the experiments, is the possibility of using the Si peak as a reference for the statistical analysis and assessment of the data collected. This introduces a very valuable intensity reference that does not depend on variables associated with the analyte solution preparation.

Chapter 7

Spinning Cell (SC) for improving SERS

As shown in chapter 3, the substrates produced by chemical route, are not homogeneous all over their surface. For this reason, SERS spectra collected at different spots will most likely show different intensities, determined by the morphological features of the measured spot and the amount of locally adsorbed analyte, which is rather homogeneous. Nevertheless, it has been shown that these substrates show a much greater signal enhancement, so a way to make reliable and repeatable measurements should be found. In principle, when many measurements are made by scanning the whole substrate and an average is taken, this quantity should be almost invariant among different substrates, assuming all the preparation steps are exactly the same. Although this can be a good way to address the issue, practically it can be very problematic. Scanning a substrate to collect SERS spectra at all points would require a long time, which would make the procedure impractical for clinical applications. To address both the experimental and practical issues, a different approach is proposed here, involving the mechanical rotation of the SERS substrates. In this way the moving part of the setup is not anymore the objective, but the nanostructured metal surface are. This can be done rather easily: Here we used a simple Hard Disk Drive (HDD) to spin the deposited SERS substrates. The objective will be fixed during the whole measurement. SERS signals are collected from different spots while the substrates are in rotation, so the net result will be an spatially averaged spectrum. As an added important feature of this technique, it will be shown that in this configuration, due to the reduced time of residence of the laser on one spot, the intensity of the radiation can be increased by orders of magnitude without damaging the samples. For this application chemically-produced Au nanoparticles substrates have been employed, which can be easily deposited by drop casting on the surface of the rotating disk. For this tests I will consider a PER concentration of $10^{-4}M$, for which Au can show a good SERS signal.

7.1 Multiple-drops spinning cell (MDSC)

Experimental setup

In the first configuration, 24 droplets of Au colloid have been deposited along a circumference with a measured radius of $3,4$ cm from the axis of rotation of the disk (see Fig. 7.1). An $HCl : H_2SO_4$ molar concentration ratio of 1:9 was used. This has been achieved by mixing the suitable amounts of acids to reach a total of 2,7 mL of acidic solution. 0,3 mL of PER $10^{-3}M$ in methanol solution was then added to achieve a total concentration of $10^{-4}M$. 5 μL were deposited on each substrate, then left drying on the substrates. The spectra were recorded using a 785 nm excitation, starting from the center of the substrate and moving by roughly 5 μm for each step, in both radial directions. The objective scans over all the 24

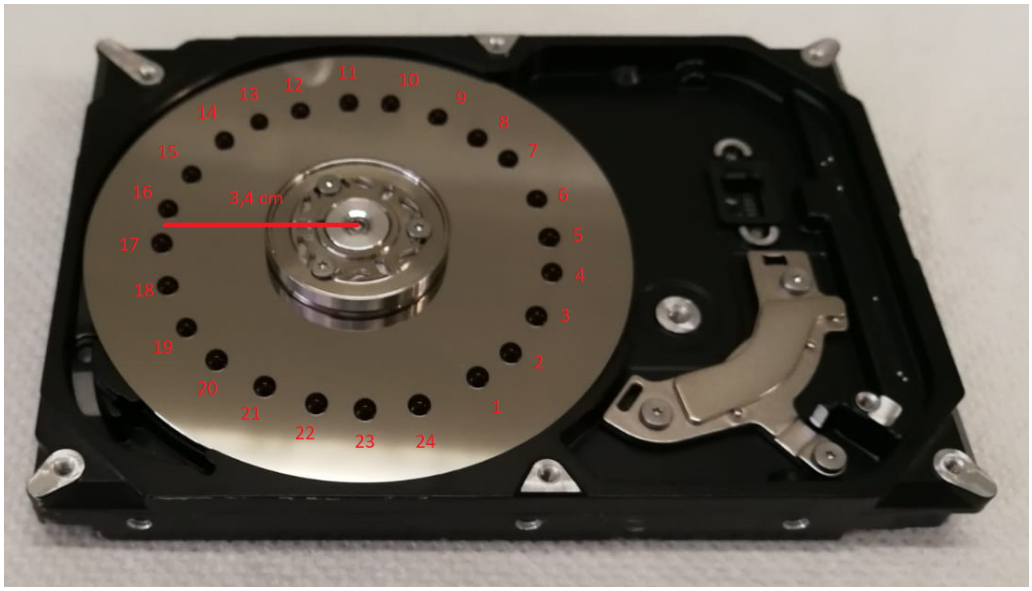

Figure 7.1: Au colloids deposited on the surface of the rotating disk. 24 droplets were deposited along a circumference 3,4 cm distant from the rotation axis.

SERS substrates during the measurements, collecting the SERS spectra averaging them. It should be noticed that this configuration is not yet optimal, due to the many gaps between the SERS substrate surfaces. Moreover, the spot-size of the laser will change with time, being the disk subjected to vertical micro-oscillations due to the added non-uniform weight given by the SERS substrates. First, static measurements on one spot were collected, to figure out at which laser power photodegradation occurs. For this test, the laser power was set in the range from 0,1 mW to 100 mW, with steps differing by one order of magnitude each. I used 10 seconds exposure time (2 averages). Thereafter, SERS spectra were recorded with

the spinning disk. 8 measurements at different radial distance from the central axis have been collected. The device was kept rotating throughout all the experiment. The power was fixed at 25 mW, adopting 20 seconds exposure time (2 averages), which is above the degrading threshold recorded for the static configuration. In all cases, to focus the radiation on the substrates a 50x microscope objective with $NA = 0,75$ was used.

Results

As shown in Fig. 7.2, photodegradation is observed at high powers through the characteristic broad G and D peaks. Comparing with the spectrum of Fig. 7.3, it can be noticed that the D peak is entirely given by the degradation of the analyte, while the G peak results from a combination of the analyte degradation and spectral contributes from the disk surface.

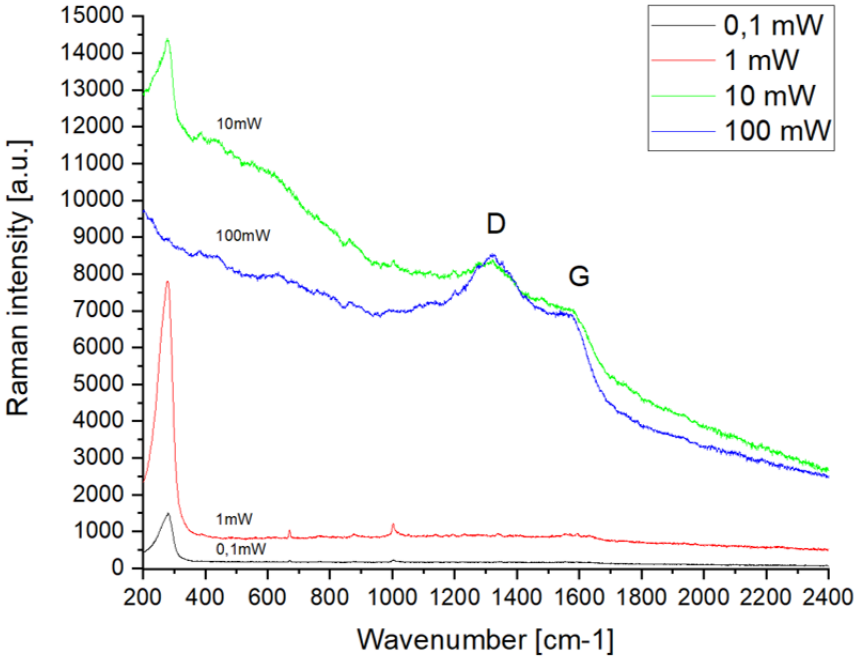

Figure 7.2: SERS spectra of PER aquired in static mode using laser powers of increasing value from 0,1 mW to 100 mW. 10 s exposure time (2 averages).

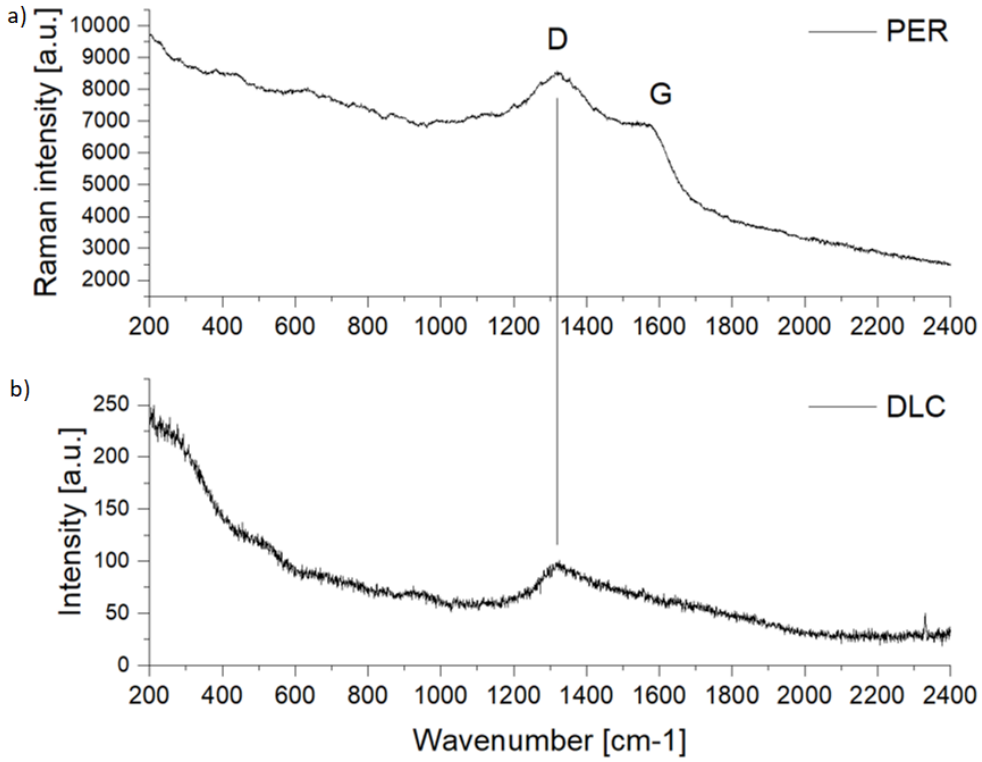

Figure 7.3: Comparison between a) SERS sectrum of PER on Au aquired in static mode with 100 mW laser power, 10 s exposure time (2 averages) and b) spectrum of the DLC coating of the rotating disk.

The photodamaging hypothesis is also confirmed by looking at the local morphology of the substrate after the high power measurement (in static mode). In Fig. 7.4, a closeup of the substrate after the laser exposition at 100 mw is shown, confirming the damaging.

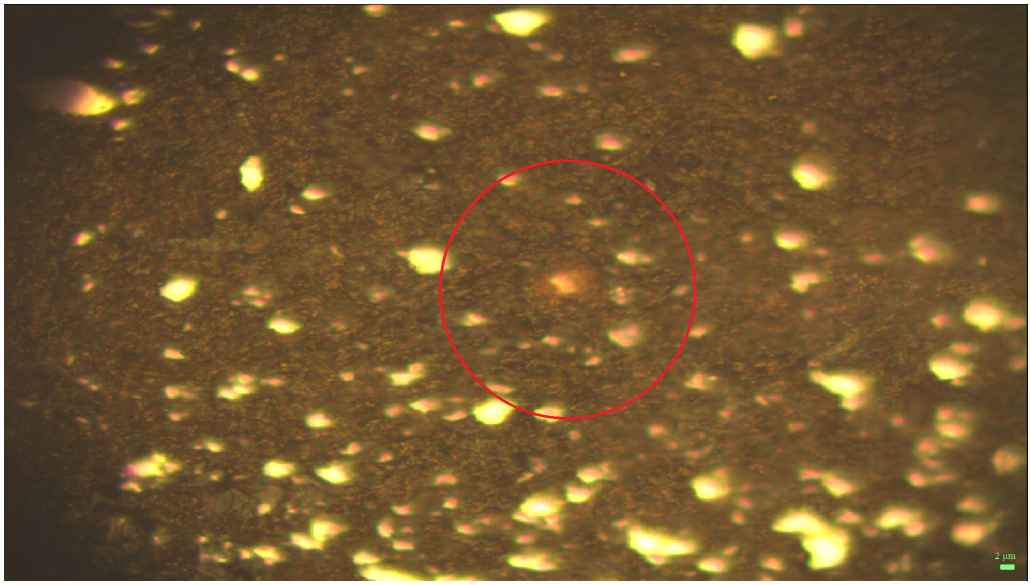

Figure 7.4: Microscope image of the Au substrate after irradiation with a 785 nm excitation at 100 mW incident power.

I report, in Fig. 7.5, the SERS spectra collected with the rotating disk. With a laser power of 25 mW, no degradation signs are shown. Furthermore, when normalized with respect to the AgCl peak, the spectra show a promising close resemblance with each other. In section 10.3 I will analyze these data to seek out signs of repeatability for this procedure. All the relevant features of PER are nicely detected. Finally, to better understand how the rotating disk reduces significantly the photodamage even at high laser power, I introduce the following simple model. Considering a circular focus spot and knowing the Numerical Aperture (NA) of the objective, its diameter D is given by the relation[35]:

$$D = \frac{1.22\lambda}{NA} \tag{7.1}$$

By knowing that the incoming radiation has $\lambda = 785nm$, the diameter is $D = 1277nm$. Then the energy deposited per unit surface, in a static measurement of duration T_{meas} is given by:

$$E_{stat} = \frac{P}{A_{spot}} T_{meas} \tag{7.2}$$

Where P is the incoming laser power and $A_{spot} = \pi D^2/4$ is the area of the focused laser spot (calculated approximating its shape to a disk of diameter D).

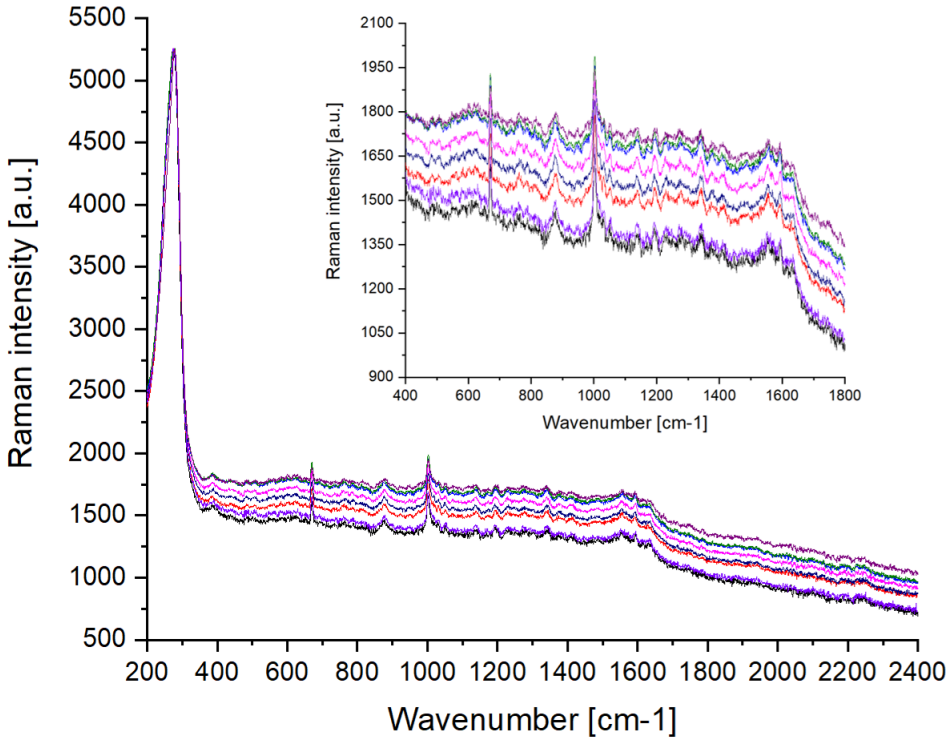

Figure 7.5: SERS spectra obtained in rotation mode using the MDSC configuration. 785 nm laser excitation, 25 mW power, 20 seconds exposure time (2 averages).

In the static case, the analyte starts to show signs of degradation at an incoming power of 10 mW, corresponding to $E_{stat} = 7.8x10^{10}\frac{J}{m^2}$ (with 10 s measurement time). The deposited energy increases by an order of magnitude at 100 mW, and it is sufficient to photodegrade the analyte in 10 s. When the setup is in rotation mode, the deposited energy is distributed during the time of measurement throughout the annular area of radius R and thickness D. Due to the high rotation speed of the disk, there will be a small permanence time of the laser on a given circular spot along the annular area. Approximating the total scanned area of a deposited substrate as a rectangle with sides ϕ (diameter of the SERS substrate active pad) and D (diameter of the laser spot), the total scanned area is:

$$A_{scan} \simeq N\phi D \tag{7.3}$$

where N is the number of deposited SERS substrates (SERS pads), which in my case is 24. By considering that $\phi = 3$ mm on the average, the total active area scanned during the measurement is $A_{scan} \simeq 92\ nm^2$. The residence time of the

laser on a single spot of diameter D can be calculated by knowing that the rotation angular frequency of the device is $\omega = 7200RPM$ (or 754 rad/s):

$$T_{res} = \frac{D}{R\omega} \tag{7.4}$$

which can be numerically evaluated and gives $T_{res} \simeq 50ns$. The total energy deposited per unit surface in the spinning mode is then given by the energy deposited on the laser spot during the time of residence, multiplied by the number of disk rounds during the time of measurement ($N_{rounds} = \omega T_{meas}/2\pi = 1200$):

$$E_{spin} = \frac{P}{A_{spot}} T_{res} N_{rounds} \tag{7.5}$$

Which is equal to $4,7x10^5 \frac{J}{m^2}$. This clearly shows that the energy deposited in static mode is about five orders of magnitude larger than the energy deposited in spinning mode. I therefore demonstrated that the rotation mode allows to employ a greater laser power without damaging the analyte, which in turn gives higher signal intensities, which implies spectra of higher quality.

7.2 Single-centered drop spinning cell (SCDSC)

The previous spinning disk configuration, whilst representing a step forward to solve the issues of the static SERS measurements, also brings up other issues: the spot-size of the focused laser on the SERS substrate cannot be kept constant; the configuration requires the deposition of several drops, which needs more time, increasing the risk of contamination of the substrate. Finally, the deposition inevitably leaves many gaps between substrates. Therefore, a considerable signal from the lower material is also detected[1] and contributes to the averaged spectrum. To address these new issues, another configuration has been tested, which involves the deposition of a single colloidal drop at the center of the rotation axis of the device. The laser is then on a slightly eccentric spot with respect to it. This should solve all issues related with the positioning of the substrate. Moreover, it requires less material and time. Therefore, there's a lower risk of contamination on the substrate. The only drawback is a lower tangential speed of the rotating SERS substrate, which implies longer residence times of the laser on the focused spots.

[1] This could also be solved via the implementation of a guide where the Au colloid could be deposited throughout all the circumference.

Experimental setup

In this configuration, one droplet of Au colloid has been deposited on the axis of rotation of the disk, as shown in Fig. 7.6. An $HCl : H_2SO_4$ molar concentration ratio of 1/9 was used. This has been achieved by mixing the suitable amounts of acids to reach a total of 2,7 mL of acidic solution. 0,3 mL of PER $10^{-3}M$ in methanol solution was then added to achieve a total concentration of $10^{-4}M$. 5 μL were deposited, and left drying on the substrate.

Figure 7.6: Au colloid droplet deposited on the axis of rotation of the device.

The objective was set to focus the laser on a slightly eccentric distance from the center of rotation, in a way that allows the objective hindrance to not interfere with the functioning of the HDD. Static and spinning mode measurements were compared. For both cases, 12 spectra were recorded, using 1 mW laser power and 10 s exposure time (2 averages), starting from the external countour of the substrate and moving towards the center by roughly 5 μm for each step. The laser power has been decreased due to the fact that in this case T_{res} would be considerably higher. 10 mW was set to be a reasonable power in order to not damage the analyte and confirmed so by the good quality SERS spectra obtained.

Results

Both static and spinning mode SERS measurements have been carried out in order to compare the data obtained. In Fig. 7.7 the spectra relative to the static mode are shown. The spectral features of PER are all well-detected, although there is an evident fluctuation of the relative peaks among all the spectra. In Fig. 7.8 the data relative to the rotation mode are then presented. As expected, by effective space-averaging of the spinning mode, the relative intensities of the SERS peak heights

are in this case considerably closer to each other. This shows the better reliability of the recorded SERS spectra in the spinning mode. It is also evident that in both cases the analyte has not been photodegraded by the laser. Therefore, with the selected optical characteristics well-resolved SERS spectrum can be recorded.

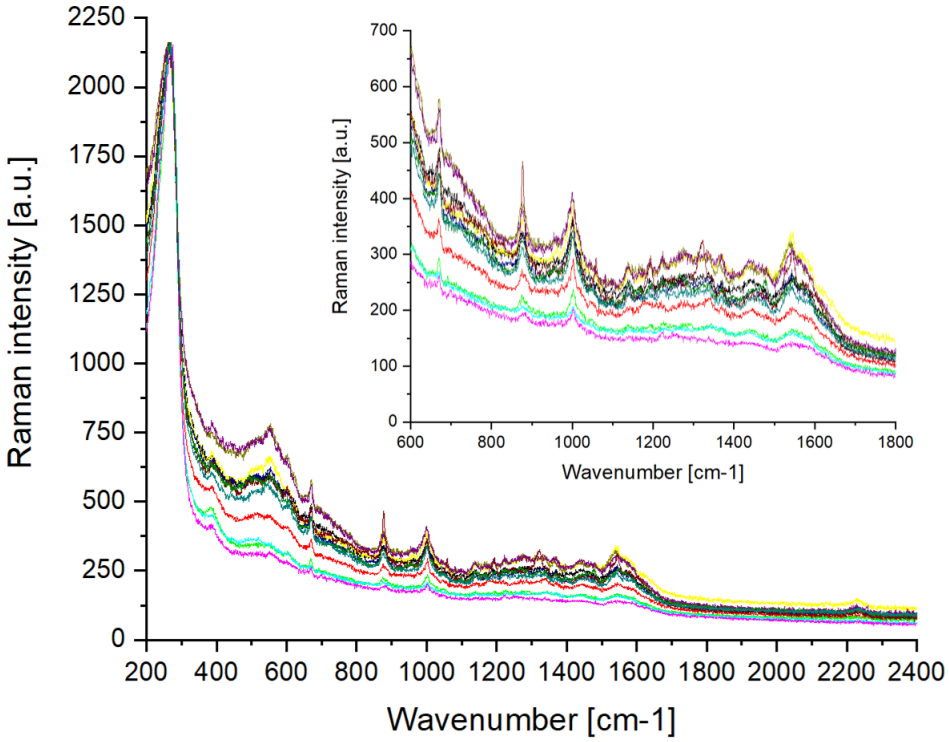

Figure 7.7: Static mode SERS spectra. 785 nm laser excitation, 1 mW power, 10 s exposure time (2 averages).

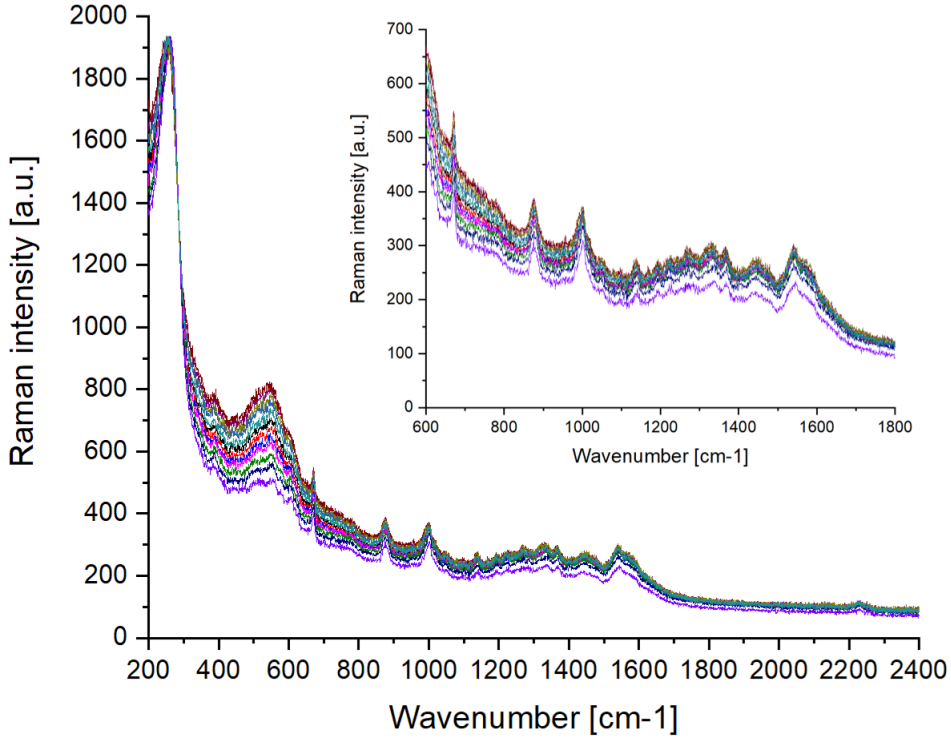

Figure 7.8: Rotation mode SERS spectra using the SCDSC configuration. 785 nm laser excitation, 1 mW power, 10 s exposure time (2 averages).

7.3 Statistical analysis

After the functionality test of the proposed spinning cell techniques, simple statistical data analysis is performed to check the repeatability and the possible quantitative value. Therefore, a comparison between the two spinning cell approaches will give an assessment of these SERS measurements. The analysis will be performed with the following methodology:

1. Individuation of two peaks which are most visible on the spectra and suitable for the analysis. The peaks chosen are located at about 670 cm^{-1} and 1001 cm^{-1}.

2. Collection of the baseline-corrected peak height values for every spectrum; calculation of the average values and standard deviations assuming that a Gaussian distribution of the values is applicable.

3. Peak height normalization by dividing the height of the analyzed peak by the height of the AgCl peak. These values were then analyzed in the same way as in the previous point (2). This analysis is done under the assumption that the AgCl peak could be used as internal reference for quantitative SERS analysis.

Results

Static mode

The statistical analysis in the static case (Fig. 7.9) gives the expected results: The standard deviations for the non-normalized values are corresponding to a shift of 31,7% and 21,5,% from the average, for the 670 cm^{-1} and 1001 cm^{-1} peaks, respectively. The standard deviations for the normalized values are corresponding to a shift of 47,6% and 38% from the average, for the 670 cm^{-1} and 1001 cm^{-1} peaks, respectively. The dispersion of the peak height values is very large, with the values distributed around the average at range that in the best scenario is more than a 21,5%, shift from the average, which is the corresponding height difference at the first standard deviation. The values non-normalized to the AgCl peak show a better behavior. Although the values are confined in the second standard deviation, the dimensions of it clearly tell that this mode cannot be employed for quantitative SERS analysis.

MDSC - rotation mode

The standard deviations (Fig. 7.10) for the non-normalized values are corresponding to a shift of 55,8% and 51,6% from the average, for the 670 cm^{-1} and 1001

cm^{-1} peaks, respectively. The standard deviations for the normalized values are corresponding to a shift of 11,6% from the average, for both peaks. For the non-normalized case, the values are even worse than the static mode. The standard deviation is very large and the values cannot be confined inside it. The normalized case, though, gives much better values for the standard deviation, which is more constrained, but the values still cannot be confined in one and even two standard deviations.

SCDSC - rotation mode

This modality is the one with the best results (Fig. 7.11). The standard deviations for the non-normalized values are corresponding to a shift of 13,8% and 13,2% from the average, for the 670 cm^{-1} and 1001 cm^{-1} peaks, respectively. These are not extremely satisfactory numbers, but when the peaks are referenced to the AgCl peak, the scenario is totally different: the standard deviations for this case are equal to a 3,4% and 2,6% shift from the standard deviation for the the 670 cm^{-1} and 1001 cm^{-1} peaks, respectively. Moreover, the values are mostly confined in the first standard deviation. These results tell us that a quantitative analysis of SERS employing this methodology has a high chance to give reliable results.

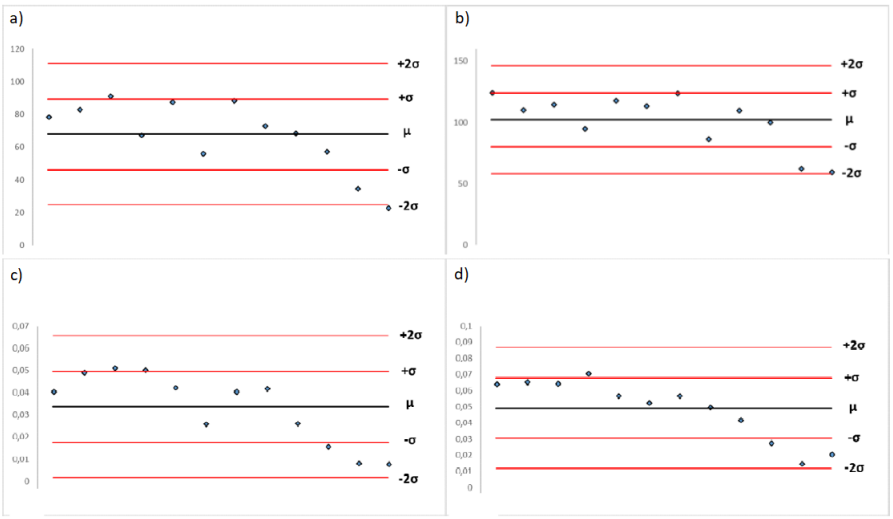

Figure 7.9: Static mode standard deviation graphs for the a-b) unreferenced values and c-d) AgCl-peak-referenced values

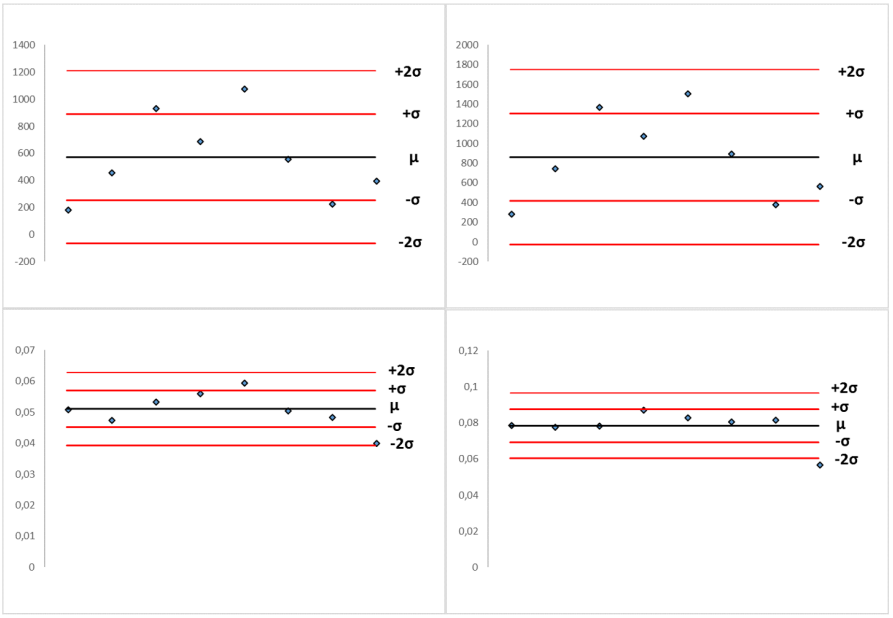

Figure 7.10: MDSC rotation mode standard deviation graphs for the a-b) unreferenced values and c-d) AgCl-peak-referenced values

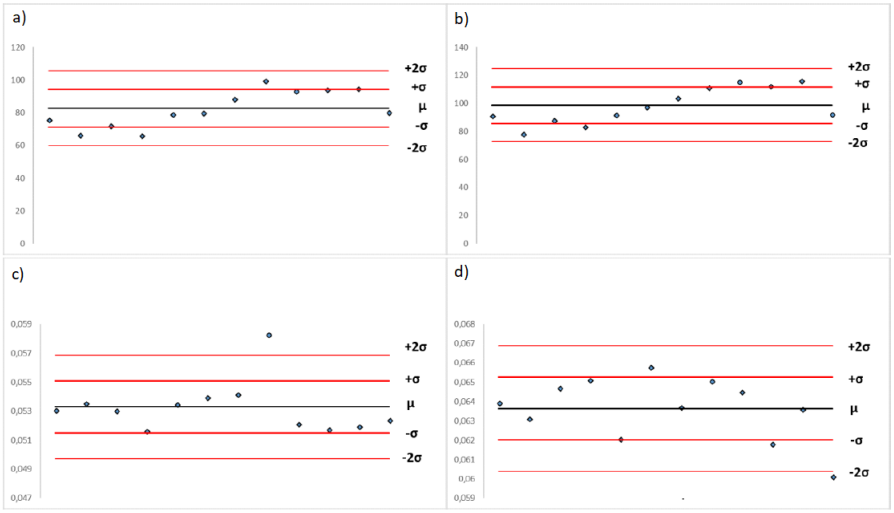

Figure 7.11: SCDSC rotation mode standard deviation graphs for the a-b) unreferenced values and c-d) AgCl-peak-referenced values

7.4 Concluding remarks

At the end of this experimental activity, it is possible to propose a procedure for the SERS detection of PER, which could be later extended to other drugs. This procedure involves the use of colloidal Ag and Au nanoparticles produced by chemical methods and can be schematized as follows:

1. Preparation of colloidal suspensions of Au or Ag nanoparticles.
2. Dissolution of PER in methanol.
3. Preparation of an aqueous solution of hydrochloric and sulphuric acid in a 1:9 molar concentration ratio, achieving pH 2.
4. Mixing a suitable amount of PER dissolved in methanol in the acidic solution.
5. Deposition of the Au or Ag nanoparticles on a spinning device (see section 7.2).
6. Deposition of a suitable amount of analyte solution made at step 4 onto the Ag or Au substrate.
7. Alignment of the device with the objective of a Raman spectrometer.
8. The spinning device is switched on.
9. SERS measurement.[2]

The procedure described shows to be promising. Its costs are limited and the time required for an analysis is very low. Detection of PER was achieved without damaging the analyte even at high laser power and the measurement proved to be repeatable, provided a reference that is stable within the experiments. Further research steps in order to improve and consolidate the technique are:

1. Calibration of the setup and determination of the SERS intensity dependence with the concentration of the analyte.
2. Tailoring the steps and variables of the procedure to suit all possible analytes (the settings to look for are pH of the acidic solution, molar concentration ratio between acids and which species to employ, as well as excitation wavelength).

[2]The UV-vis spectrum of the nanoparticles should be collected first to determine the plasmon resonance of the substrate and select the most suitable excitation wavelength.

3. Improvement of the PLAL substrates. If the same detection quality can be achieved, their repeatability and ease of manufacturing can improve the technique up on a production standpoint.

This procedure sets a starting point towards the development of a more complete technique which can be extended to a vast range of drug families and be applied in a clinical environment, making TDM a routine and impactful practice.

Conclusions

In my thesis, I extensively investigated the SERS activity of Perampanel, an antiepileptic drug which is of great interest for therapeutic drug monitoring applications. UV-Vis spectroscopy was carried out to verify its protonation and stability in acidic solutions.

Then, I verified that acidification improves the quality of the SERS spectroscopy on colloidal Ag/Au substrates produced by chemical methods, which are covered by stabilizing agents. I found that a solution obtained by mixing hydrochloric and sulphuric acid in a ratio 1:9 at pH 2 leads to very good quality SERS spectra. In these conditions it is possible to detect concentrations of Perampanel in the range of $10^{-4} \div 10^{-5} M$. Given the high quality of the recorded SERS spectra at $10^{-5} M$, it is reasonable to think that also a $10^{-6} M$ concentration could be handled.

The same methods have been successfully tested also on Ag/Au SERS substrates produced by PLAL. SERS spectra were obtained which can be compared to the spectra collected on the SERS substrates produced by chemical methods.

Finally, it was possible to develop a technique for dynamic SERS measurements on a spinning cell setup, utilizing spare material from hard disk drives. By this method, I addressed and solved two crucial problems of static SERS measurement. Photodegradation could be avoided even at higher laser powers and the device was able to counter the spatial non-homogeneity of the SERS substrates, which in a static setup, would give SERS spectra with differences depending on the probed spot.

The aspects investigated in this thesis can be further analyzed to achieve SERS detection of Perampanel at lower concentrations and to extend the technique to other drugs, bringing SERS closer to being an established method for therapeutic drug monitoring.

Bibliography

[1] J. Robertson; C. Hatton; E. Emerson; S. Baines. "Prevalence of epilepsy among people with intellectual disabilities: a systematic review". In: *Seizure* (2015).

[2] D. Goldsmith; B. A. Minassian. "Efficacy and tolerability of perampanel in ten patients with Lafora disease". In: *Epilepsy & Behavior* (2016).

[3] F.M. Snoeijen-Schouwenaars; J.S. van Ool; I.Y. Tan; H.J. Schelhaas; M.H.J.M. Majoie. "Evolution of perampanel in patients with intellectual disability and epilepsy". In: *Epilepsy & Behavior* (2017).

[4] J.A. French; G.L. Krauss; V. Biton; D. Squillacote; H. Yang; A. Laurenza et al. "Adjunctive perampanel for refractory partial-onset seizures: randomized phase III studies". In: *Neurology* (2012).

[5] J.A. French; G.L. Krauss; D. Squillacote; H. Yang; D. Kumar et al. "Adjunctive perampanel for refractory partial-onset seizures: results of randomized global phase III study 305". In: *Epilepsia* (2013).

[6] G.L. Krauss; J.M. Serratosa; V. Villanueva; M. Endziniene; Z. Hong; J. French et al. "Randomized phase III study 306: adjunctive perampanel for refractory partial-onset seizures". In: *Neurology* (2012).

[7] B.J. Steinhoff; E. Ben-Manachem; P. Ryvlin; S. Shorvon; I. Kramer; A. Satlin; et al. "Efficacy and safety of adjunctive perampanel for the treatment of refractory partial seizures: a pooled analysis of three phase III studies". In: *Epilepsia* (2013).

[8] J.S. Kang; M.H. Lee. "Overview of therapeutic drug monitoring". In: *The Korean Journal of Internal Medicine* (2009).

[9] M.D. Krasowski; G.A. McMillin. "Advances in anti-epileptic drug testing". In: *Clinica Chimica Acta* (2014).

[10] D.J. Birkett. "Pharmacokinetics made easy: therapeutic drug monitoring". In: *Aust Prescr* (1997).

[11] G.T. McInnes. “The value of therapeutic drug monitoring to the practising physician- an hypothesis in need of testing.” In: *British Journal of Clinical Pharmacology* (1989).

[12] J.F. Kennedy; Z.S. Rivera and C.A. White. “The use of HPLC in biotechnology”. In: *Journal of Biotechnology* (1989).

[13] N. Kostić; Y. Dotsikas; A. Malenović; B.J. Stojanović; T. Rakić; D. Ivanović; M. Medenica. “Stepwise optimization approach for improving LC-MS/MS analysis of zwitterionic antiepileptic drugs with implementation of experimental design”. In: *J. Mass. Spectrom* (2013).

[14] C. Zanchi; A. Lucotti; M. Tommasini; S. Trusso; U. de Grazia; E. Ciusani; P.M. Ossi. “Laser tailored nanoparticle arrays to detect molecules at dilute concentration”. In: *Appl. Surf. Sci.* (2017).

[15] I.J. Hidi et al. “"LOC-SERS": towards point-of-care diagnostic of methotrexate”. In: *Anal. Methods* (2014).

[16] S. Fornasaro; V. Sergo; A. Bonifacio A. Jaworska. “Potential of surface enhanced raman spectroscopy (SERS) in therapeutic drug monitoring (TDM). A critical review”. In: *Biosensors* (2016).

[17] P.M. Ossi; M. Tommasini; A. Lucotti; C. Zanchi; A. Bombelli; C. Pedrini; N. S. Villa; E. Fazio; F. Neri; S. Trusso. “Nanoparticle-based SERS substrates for therapeutic drug monitoring”. In: *IEEE JSTQE* (2018).

[18] N.J. Halas and M.Moskovits. “Surface-enhanced Raman spectroscopy: Substrates and materials for research and applications”. In: *MRS Bull.* (2013).

[19] S. Barcikowski; A. Hahn; A.V. Kabashin; B.N. Chichkov. “Properties of nanoparticles generated during femtosecond laser machining in air and water”. In: *Appl. Phys. A* (2007).

[20] E. Fazio; F. Neri. “Nonlinear optical effects from Au nanoparticles prepared by laser plasmas in water”. In: *Appl. Surf. Sci.* (2013).

[21] Efremov Evtim V.; Ariese Freek; Gooijer Cees. “Achievements in resonance Raman spectroscopy: Review of a technique with a distinct analytical chemistry potential”. In: *Analytica Chimica Acta* (2008).

[22] M.T. Alula; Z.T. Mengesha and E. Mwenesongole. “Advances in Raman spectroscopy for analysis of pharmaceuticals: A review”. In: *Vibrational Spectroscopy* (2018).

[23] P.J. Hendra M. Fleischmann and A.J. McQuillan. “Raman Spectra of Pyridine Adsorbed at a Silver Electrode”. In: *Chemical Physics Letters* (1974).

[24] A.M. Grant; J.A. Creighton. "Anomalously Intense Raman Spectra of Pyridine at a Silver Electrode". In: *Journal of the American Chemical Society* (1977).

[25] P. C. Lee; D. Meisel. "Adsorption and Surface-Enhanced Raman of Dyes on Silver and Gold Sols." In: *The Journal of Physical Chemistry* (1982).

[26] J. Turkevich; P. C. Stevenson; J. Hillier. "A Study of the Nucleation and Growth Process in the Synthesis of Colloidal Gold". In: *Discussions of the Faraday Society* (1951).

[27] E. Fazio. "Private communications".

[28] F. Mafune; J. Kohno; Y. Takeda; T. Kondow. "Formation and size control of silver nanoparticles by laser ablation in aqueous solution". In: *J. Phys. Chem. B* (2000).

[29] M. Santoro; E. Fazio; S. Trusso; M. Tommasini; A. Lucotti; R. Saija; M. Casazza; F. Neri; P.M. Ossi. "SERS sensing of Perampanel with nanostructured arrays of gold particles produced by pulsed laser ablation in water". In: *MEDICAL DEVICES & SENSORS* (2018).

[30] A. Satlin; L.D. Kramer; A. Laurenza. "Development of perampanel in epilepsy". In: *Acta Neurol. Scand.* (2013).

[31] MAPI PHARMA LTD. "Polymorphs of Perampanel". US 20140371273A1.

[32] G. Socrates. "Infrared and Raman Characteristic Group Frequencies: Tables and Charts". In: *Wiley* (2001).

[33] J.V. Crookes; A.A. Woolf. "Hydrogensulphates of Silver(r) and some Transition-metal Cations". In: *Dalton Transactions* (1975).

[34] Yanwei Zhang; Fangli Wang; Handong Yin; Min Hong. "Nonuniform Distribution of Capping Ligands Promoting Aggregation of Silver Nanoparticles for Use as a Substrate for SERS". In: *Advances in Nanoparticles* (2013).

[35] E. Abbe. "VII.—On the Estimation of Aperture in the Microscope". In: *Journal of the Royal Microscopical Society* (1881).